Laboratoire Léon Brillouin

Annual report 2016

LABORATOIRE LEON BRILLOUIN

ANNUAL REPORT 2016

Table of contents

DIRECTOR'S FOREWORD

SCIENTIFIC HIGHLIGHTS

New frontier in quantum materials

Material and nanosciences, fundamental studies and applications

Soft complex matter and biophysics

PUBLICATIONS

SONATE COMPACT NEUTRON SOURCE

ESS PROJECTS

SOFTWARE DEVELOPMENT

TEACHING AND EDUCATION

BEAM TIME ACCESS

Director's foreword

2016, the LLB is facing its fate

After a particularly troubled 2015, the laboratoire Léon Brillouin (LLB) was able to react in 2016 in a constructive and proactive way for his future and that of the neutron scattering in France. The LLB is a research unit with a service responsibility for the French community; It is one of the main neutrons scattering centres at the international level, and it is part of the European network of European facilities for several H2020 projects (NFFA, SINE2020, Sondes, and other projects for 2017). For illustration, the attached figure, from 2016 Brightness report (INFRADEV-3-2015) funded by the European Union, gives the current situation of the use of neutron scattering centres, in the frame of the arrival of ESS.

	Facility	Number of unique users	Number of instruments	Number of experiments/year	Power	Thermal neutron flux (neutron/cm²s)	Operational days/year
Big-Sized Facilities	ISIS	1580	31/31	850	200 kW	4.5×10^{15} (peak)	150
	ILL	1433	32/37	848	58.3 MW	1.5×10^{15}	200
	MLZ FRM II	965	26/26	832	20 MW	8×10^{14}	240
	LLB	637	20/23	403	14 MW	3×10^{14}	120
	SINQ	477	13/20	485	1 MW	4.1×10^{14}	195
Medium-Sized Facilities	BER II	302	13/13	201	10 MW	2×10^{14}	200
	BNC	145	15/15	127	10 MW	2.1×10^{14}	120
	NPL	54	8/8	30	10 MW	1×10^{14}	189
Small-Sized Facilities	TRIGA JGU	44	4/4	9	100 kW	1×10^{12}	200
	JEEP II	43	5/6	65	2 MW	3×10^{13}	200
	TRIGA JSI	41	8/8	**	250 kW	5.107×10^{12}	150
	RPI	28	0/1	10	1 MW	1×10^{13}	150
	ATI	15	5/5	6	250 kW	5×10^{12}	200
	MARIA	13	4/6	46	30 MW	1×10^{14}	180
	RID	0	9/9	**	2 MW	3×10^{12}	200

The LLB is part of A category of sources having the greatest number of distinct users per year in recent years.

The LLB responded to its research, hosting and training missions: production of scientific articles, with an average impact factor greater than 5, training of PhD students, young (and not so young) researchers, students in master or engineering school and finally with instruments with increased performance and an average rate of overload around 1.7, despite growing concerns of users. Despite the encountered difficulties, the technical and scientific staff of the LLB has not given up. However, we must remain extremely vigilant to ensure the proper functioning of infrastructure and the optimal exploitation of the neutrons produced until the end of 2019.

We actively worked on a possible French strategy for the coming years and the maintenance of the current position of European leader of the scientific and technical French community. We participated in a very large number of meetings to support the need for a national source and for a probe such as the neutron diffusion to get unambiguous correlation functions essential to the understanding of properties of condensed matter. We organized various workshops with French Neutron Society (SFN) and supported the creation of a French Federation of neutron scattering, bringing together all the actors directly involved in associated instrumentation. Thus the LLB staff set up and managed the first selection committees taking into account the availability of French instruments of LLB and of ILL (CRG) in June 2016. An internet portal (Phoenix) was established to bring users of the Federation all the useful information and the management of their experiment proposal demands.

The Scientific and Instrumental Council met in October to reflect on the scientific and technology areas for which the use of neutrons as a probe of the material is unique and indispensable. Such a document is under development but not yet available.

Leading French and foreign, academic and industrial, scientists, coming from the College of France or INRA, not affiliates of neutron centres, came for two days doing the state of affairs and needs. The main addressed topics, combining basic research and engineering with direct applications, were electrochemistry and materials for energy, new quantum objects, issues on surface adhesion and friction, or oil extraction.

We have reassessed our projects in the context of Orphée shutdown and directed our actions according to three axes:

- Transfer of instruments: FA# at the ILL who will become a CRG-A category instrument (the instrument that we will develop will be up to the ILL) with 50% of access time for the French researchers and their collaborators; PA20 inaugurated in February 2016, which will be transferred to PSI in Switzerland against beam time (contracts under negotiation). These operations directly affect the commitments made in December 2010 in the French-Swedish contract (14 M€ in full cost); these were approved by our Swedish colleagues and an extension of this contract until 2019 has been announced at the last Committee Dec 16. 2016 in Stockholm. In 2017 other perspectives of transfer will be considered and a full assessment of the instrumentation will be made.

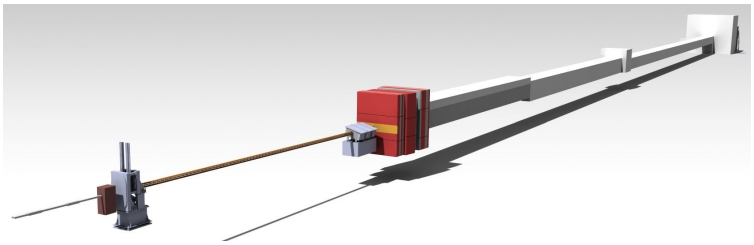

- First ESS instruments at 2021 horizon: the LLB was designated as the Coordinator of French instrumental contributions for future spallation source ESS located south of the Sweden (35 M€ in full cost). For this reason several instruments projects have been proposed recently with our German, Swiss, or Danish partners. All the projects have been selected by the Scientific Council and the Board of Directors of ESS (17 partners). It is a very great success for the LLB teams, which proves once again the technical skills of the teams supported by promising scientific themes for the future. Currently, these projects have passed Phase I and we now have a clearer idea of their schedule and cost. It is likely that all of these instruments will be part of the first wave that will be open to users in 2023, but whose construction will begin on-site in 2020 requiring right now a setting up of special status.

- Finally, the LLB must offer an alternative to the Orphée shutdown, by developing the compact neutron source project SONATE for “Source cOmpacte de Neutrons s’Appuyant sur la Technologie des accélératEurs”. Over the past years, significant technological progress have been made in different areas such as: proton accelerator, neutron optics, calculations codes, thanks especially to the ESS developments and its first scientific returns on investment. Benefiting from these technical advances and optimizing the target/moderator settings, it will be possible to produce and to extract flexible neutron beams dedicated to a specific application, with performances comparable to the instruments of the LLB.

Scientific Highlights

nature COMMUNICATIONS

ARTICLE

Received 20 Jul 2015 | Accepted 22 Jan 2016 | Published 4 Mar 2016 DOI: 10.1038/ncomms10819 OPEN

Commensurate antiferromagnetic excitations as a signature of the pseudogap in the tetragonal high-T_c cuprate $HgBa_2CuO_{4+\delta}$

M.K. Chan[1,2], C.J. Dorow[1,3], L. Mangin-Thro[3], Y. Tang[1], Y. Ge[1,4], M.J. Veit[1,5], G. Yu[1], X. Zhao[1,4], A.D. Christianson[5], J.T. Park[6], Y. Sidis[3], P. Steffens[7], D.L. Abernathy[5], P. Bourges[3] & M. Greven[1]

Antiferromagnetic correlations have been argued to be the cause of the d-wave superconductivity and the pseudogap phenomena exhibited by the cuprates. Although the antiferromagnetic response in the pseudogap state has been reported for a number of compounds, there exists no information for structurally simple $HgBa_2CuO_{4+\delta}$. Here we report neutron-scattering results for $HgBa_2CuO_{4+\delta}$ (superconducting transition temperature $T_c \cong 71$ K, pseudogap temperature $T^* \cong 305$ K) that demonstrate the absence of the two most prominent features of the magnetic excitation spectrum of the cuprates: the X-shaped 'hourglass' response and the resonance mode in the superconducting state. Instead, the response is Y-shaped, gapped and significantly enhanced below T^*, and hence a prominent signature of the pseudogap state.

[1] School of Physics and Astronomy, University of Minnesota, Minneapolis, Minnesota 55455, USA. [2] Pulsed Field Facility, National High Magnetic Field Laboratory, Los Alamos National Laboratory, Los Alamos, New Mexico 87545, USA. [3] Laboratoire Léon Brillouin, LLB/IRAMIS, UMR12, CEA-CNRS, CEA-Saclay, Gif-sur-Yvette 91191, France. [4] State Key Lab of Inorganic Synthesis and Preparative Chemistry, College of Chemistry, Jilin University, Changchun 130012, China. [5] Quantum Condensed Matter Division, Oak Ridge National Laboratory, Oak Ridge, Tennessee 37831, USA. [6] Forschungsneutronenquelle Heinz Maier-Leibnitz, Garching 85747, Germany. [7] Institute Laue-Langevin, Grenoble 38042 CEDEX 9, France. † Present address: Department of Physics, University of California, San Diego, 9500 Gilman Drive La Jolla, California 92093, USA (C.J.D.); Department of Physics, Penn State University, University Park, Pennsylvania 16802, USA (Y.G.); Department of Applied Physics, Stanford University, Stanford, California 94305, USA (M.J.V.). Correspondence and requests for materials should be addressed to M.K.C. (email: mkchan@lanl.gov) or to M.G. (email: greven@physics.umn.edu).

NATURE COMMUNICATIONS | 7:10819 | DOI: 10.1038/ncomms10819 | www.nature.com/naturecommunications 1

CHEMISTRY A European Journal

ChemPubSoc Europe

DOI: 10.1002/chem.201503400

Magnetism Studies [Hot Paper]

Polarized Neutron Diffraction as a Tool for Mapping Molecular Magnetic Anisotropy: Local Susceptibility Tensors in Co^{II} Complexes

Karl Ridier,[a, b] Béatrice Gillon,[a,c] Arsen Gukasov,[a] Grégory Chaboussant,[a] Alain Cousson,[a] Dominique Luneau,[d,e] Ana Borta,[f,g] Jean-François Jacquot,[d] Ruben Checa,[h] Yukako Chiba,[i] Hiroshi Sakiyama,[j] and Masahiro Mikuriya[k]

Abstract: Polarized neutron diffraction (PND) experiments were carried out at low temperature to characterize with high precision the local magnetic anisotropy in two paramagnetic high-spin cobalt(II) complexes, namely [Co(dmf)$_2$(BPh$_4$)$_2$] (1) and [Co(μ-bmp)$_2$(BPh$_4$)$_2$] (2), in which dmf = N,N-dimethylformamide, μ-bmp = 2,6-bis[(2-hydroxyethyl)methylaminomethyl]-4-methylphenolate, and BPh$_4$ = tetraphenylborate. This allowed a unique and direct determination of the local magnetic susceptibility tensor on each individual Co^{II} site. In compound 1, this approach reveals the correlation between the single-ion easy magnetization direction and a trigonal elongation axis of the Co^{II} coordination octahedron. In exchange-coupled dimer 2, the determination of the individual Co^{II} magnetic susceptibility tensors provides a clear outlook of how the local magnetic properties on both Co^{II} sites deviate from the single-ion behavior because of antiferromagnetic exchange coupling.

Introduction

Since their discovery, single-molecule magnets (SMMs) have attracted intense research by both chemists and physicists.[1,2] This is due to their exceptional ability to exhibit slow relaxation of magnetization and then an intrinsic magnetic hysteresis loop below the so-called blocking temperature (T_B).[3,4] This phenomenon essentially originates from the existence of a negative axial magnetic anisotropy ($|D|<0$) in the ground spin state S, which gives an energy barrier ($U=|D|S^2$ and $|D|(S^2-1/4)$ for integer and half-integer S, respectively) to magnetization reversal between the two zero-field split (ZFS) lowest-lying $M_S=\pm S$ states. SMMs provide a new frontier in the race for extreme miniaturization of the elementary bits for use in high-density data storage devices or for quantum computing.[5,6] However, the blocking temperatures (proportional to the energy barrier $T_B \propto U$) remain too low at present for practical applications. At first sight, to enhance the energy barrier and consequently the operating temperature, we can increase either the spin eigenvalue S of the molecular ground state or the axial anisotropy term |D|. Most of the early works have aimed at increasing the ground-state spin (S). This has resulted in the synthesis of numerous high-spin clusters with d or and f metal ions.[7–12] However, it was observed that the energy barriers did not increase accordingly because the molecular anisotropy term |D| is not independent of S but decreases with it. It was later shown[13] that |D| actually varies as S^{-2}, such that the blocking temperature seems to be independent from S for a given complex formed from building blocks with a given local anisotropy. Now, most efforts focus on the synthesis of low-nuclearity complexes in which magnetic anisotropy takes

Chem. Eur. J. 2016, 22, 724 – 730 Wiley Online Library 724 © 2016 Wiley-VCH Verlag GmbH & Co. KGaA, Weinheim

Macromolecules Article

pubs.acs.org/Macromolecules

Thermoresponsive Toughening in LCST-Type Hydrogels with Opposite Topology: From Structure to Fracture Properties

Hui Gao,[1,2] Cécile Mussault,[1,3] Annie Brûlet,[3] Alba Marcellan,*[1,2] Dominique Hourdet,*[1,2] and Nicolas Sanson*[1,2]

[1]École Supérieure de Physique et de Chimie Industrielles de la Ville de Paris (ESPCI), ParisTech, PSL-Research University, Sciences et Ingénierie de la Matière Molle, CNRS UMR 7615, 10 rue Vauquelin, F-75231, Paris cedex 05, France
[2]Sorbonne-Universités, UPMC Université Paris 06, SIMM, 10 rue Vauquelin, F-75231 Paris cedex 05, France
[3]Laboratoire Léon Brillouin (UMR 12 CEA CNRS), CEA Saclay, F-91191 Gif-sur-Yvette Cedex, France

Supporting Information

ABSTRACT: The challenge of this work was to investigate the role of topology in LCST hydrogels that strongly and reversibly thermo-reinforce their mechanical strength under isochoric conditions. To achieve this, two different hydrogels with opposite topologies were designed on the basis of grafted architectures using equal amounts of water-soluble chains (poly(N,N-dimethylacrylamide) = PDMA) and LCST polymer chains (poly(N-isopropylacrylamide) = PNIPAA). By working under isochoric conditions, with almost 85 wt % of water in the whole temperature range (20−60 °C), we were able to clearly highlight the impact of the phase transition of PNIPA on the mechanical reinforcement of the gel without any interference of the volume transition. These graft hydrogels, designed with PNIPA in the backbone (GPN-D) or as pendant chains (GPD-N), have been studied more specifically by tensile tests and 2D neutron scattering at rest and under deformation. From these complementary techniques, we show that PNIPA side-chains in GPD-N self-assemble above their transition temperature into a micellar network greatly interfering with the covalent PDMA frame. While the elastic modulus increases reversibly more than ten times throughout the phase transition, other properties like elongation at break and fracture resistance are greatly enhanced with temperature. At high temperature and under extension, SANS data highlight the affine deformation of PNIPA domains. By comparison, the opposite topology with PNIPA forming the cross-linked backbone undergoes a similar phase separation with temperature and gives rise to a bicontinuous structure that aligns under loading. The collapsed phase being topologically defined as the load-bearing phase, GPN-D displays remarkable fracture toughening with crack bifurcation at high temperature whereas GPD-N gels fracture in a more conventional way.

Thermo-Toughening of Hydrogels under Isochoric Condition

INTRODUCTION

During the last few decades, covalent hydrogels have received considerable attention due to their important potential as biological contrasters or mechanical transducers. They are actually used in many bioapplications[1−3] such as super-absorbents, contact lenses, drug delivery systems, or scaffolds for tissue engineering, but they intrinsically suffer from their poor mechanical strength. More recently, new challenges have emerged in this field such as the reinforcement of the mechanical properties in order to elaborate smart and innovative polymer-based materials. On one hand, one can find original covalent architectures like double networks,[4] slide-ring gels,[5] or tetra-PEG gels,[6] which have been shown to strongly improve the mechanical properties in terms of stiffness, fracture toughness or stretchability. On the other hand, a more ventile approach consists in introducing physical interactions into the covalent network. In this case, the reinforcement of mechanical properties has been nicely demonstrated with nanocomposite[7] and hybrid networks,[8] which develop reversible interactions between the polymer matrix and inorganic nanofillers like clay platelets or silica nanoparticles. In these examples, hybrid hydrogels showed improved mechanical response with an increase of modulus, dissipation, and fracture properties. This also to mix both reversible and covalent cross-links within the same structure to get tough hydrogels has been extended afterward to either physical interactions. We can mention for instance hydrophobically modified hydrogels,[9−12] which show a large increase of their extensibility and resistance to crack propagation due to a "cooly" deformation of hydrophobic associations under stress, or other mixed systems involving complex formation like calcium alginates embedded in a cross-linked polyacrylamide network[13] or polyvinylidyle hydrogels.[14] With these examples, it is clearly shown that the mechanical

Received: April 16, 2014
Revised: May 18, 2014
Published: May 20, 2014

ACS Publications © 2014 American Chemical Society 4286 DOI: 10.1021/ma5007458 Macromolecules 2014, 47, 4286−4300

New frontier in quantum materials

Material and Nanosciences,

Fundamental Studies and Applications

Soft complex matter and biophysics

nature COMMUNICATIONS

ARTICLE

Received 20 Jul 2015 | Accepted 22 Jan 2016 | Published 4 Mar 2016 DOI: 10.1038/ncomms10819 OPEN

Commensurate antiferromagnetic excitations as a signature of the pseudogap in the tetragonal high-T_c cuprate $HgBa_2CuO_{4+\delta}$

M.K. Chan[1,2], C.J. Dorow[1,†], L. Mangin-Thro[3], Y. Tang[1], Y. Ge[1,†], M.J. Veit[1,†], G. Yu[1], X. Zhao[1,4], A.D. Christianson[5], J.T. Park[6], Y. Sidis[3], P. Steffens[7], D.L. Abernathy[5], P. Bourges[3] & M. Greven[1]

Antiferromagnetic correlations have been argued to be the cause of the *d*-wave superconductivity and the pseudogap phenomena exhibited by the cuprates. Although the antiferromagnetic response in the pseudogap state has been reported for a number of compounds, there exists no information for structurally simple $HgBa_2CuO_{4+\delta}$. Here we report neutron-scattering results for $HgBa_2CuO_{4+\delta}$ (superconducting transition temperature $T_c \approx 71$ K, pseudogap temperature $T^* \approx 305$ K) that demonstrate the absence of the two most prominent features of the magnetic excitation spectrum of the cuprates: the X-shaped 'hourglass' response and the resonance mode in the superconducting state. Instead, the response is Y-shaped, gapped and significantly enhanced below T^*, and hence a prominent signature of the pseudogap state.

[1] School of Physics and Astronomy, University of Minnesota, Minneapolis, Minnesota 55455, USA. [2] Pulsed Field Facility, National High Magnetic Field Laboratory, Los Alamos National Laboratory, Los Alamos, New Mexico 87545, USA. [3] Laboratoire Léon Brillouin, LLB/IRAMIS, UMR12, CEA-CNRS, CEA-Saclay, Gif sur Yvette 91191, France. [4] State Key Lab of Inorganic Synthesis and Preparative Chemistry, College of Chemistry, Jilin University, Changchun 130012, China. [5] Quantum Condensed Matter Division, Oak Ridge National Laboratory, Oak Ridge, Tennessee 37831, USA. [6] Forschungsneutronenquelle Heinz Maier-Leibnitz, Garching 85747, Germany. [7] Institute Laue Langevin, Grenoble 38042 CEDEX 9, France. † Present address: Department of Physics, University of California, San Diego, 9500 Gilman Drive La Jolla, California 92093, USA (C.J.D.); Department of Physics, Penn State University, University Park, Pennsylvania 16802, USA (Y.G.); Department of Applied Physics, Stanford University, Stanford, California 94305, USA (M.J.V.). Correspondence and requests for materials should be addressed to M.K.C. (email: mkchan@lanl.gov) or to M.G. (email: greven@physics.umn.edu).

New frontier in quantum materials

The last decades in solid state physics have seen the emergence of new concepts, going beyond the traditional Fermi liquid theory and the Landau theory of phase transitions. Recent discoveries, such as those made on the magnetic properties of low dimensional systems or on high-T_c superconductors, have shown indeed the reality of a rich, novel physics, escaping conventional descriptions. These new systems are primarily characterized by subtle correlations, in which the concept of effective charge carriers with a renormalized mass seems inappropriate, and interactions between electrons need to be re-considered. New kinds of phase transition have also emerged, which do not involve symmetry breaking necessarily, but are rather described by the confinement / de-confinement of topological objects. As a gateway towards the development of new physical concepts, the exploration of "quantum matter and materials" is the subject of intensive research nowadays, all the more so that its applications in novel technologies also offer promising perspectives in the years to come.

LLB scientists are fully involved in these new trends. Their research fields cover quantum materials, such as unconventional superconductors or frustrated magnets, anomalous states of matters induced by coupling magnetism with orbital or lattice degrees of freedom, and functional materials. The extraordinary tool that is neutron scattering is used to directly probe the atom and spin correlation functions in space and time in these systems, and to reveal the microscopic origin of their unusual properties. The unique properties of neutrons also allow one to carry out experiments in extreme conditions, like high pressure, very low temperatures, or very high magnetic fields, to probe the properties of quantum matter even deeper.

The examples selected below highlight the power of neutron scattering techniques, especially when combined with other probes, to disentangle the various mechanisms at the origin of the complex states under study. These examples range from the model Hg-based superconducting cuprates to hybrid perovskites, chiral magnets, and quantum spin ice.

- **Spin dynamics of the model cuprate $HgBa_2CuO_{4+d}$**

  M.K. Chan, C.J. Dorow, Y. Tang, Y.Ge, M.J. Veit, G. Yu, X. Zhao, M. Greven, A.D. Christianson, D.L. Abernathy, J.T. Park, P. Steffens, L. Mangin-Thro, J. Jeong, Y. Sidis, P. Bourges', F. Onufrieva

- **Elastic Constants, Optical Phonons, and Molecular Relaxations in the High Temperature Plastic Phase of the $CH_3NH_3PbBr_3$ Hybrid Perovskite**

  Antoine Létoublon, Serge Paofai, Benoît Rufflé, Afonso Ferreira, Philippe Bourges, Bernard Hehlen, Thierry Michel, Claude Ecolivet, Olivier Durand, Stéphane Cordier, Claudine Katan, Jacky Even

- **Exploring the meta-magnetism of $EuNiGe_3$**

  X. Fabrèges, A. Gukasov, P. Bonville, A. Maurya, A. Thamizhavel, S. K. Dhar

- **A chiral magnet with 'invar' properties**

  N. Marti[1], M. Deutsch, J.-P. Itié, J.-P. Rueff, U.K. Rössler, K. Koepernik, L.N. Fomicheva, A.V. Tsvyashchenko, I. Mirebeau

- **Antiferro-quadrupolar correlations in the quantum spin ice candidate $Pr_2Zr_2O_7$**

  Sylvain Petit, Elsa Lhotel, Solène Guitteny, Ovidiu Florea, Julien Robert, Pierre Bonville, Isabelle Mirebeau, Jacques Ollivier, Hanu Mutka, Eric Ressouche, Claudia Decorse, Monica Ciomaga-Hatnean and Geetha Balakrishnan

Spin dynamics of the model cuprate $HgBa_2CuO_{4+\delta}$

The cuprates exhibit strong antiferromagnetic (AF) correlations even in the superconducting doping range. The prominence of these correlations has motivated suggestions that they may drive both the pseudogap phenomenon and superconductivity in these quantum materials. Hence extensive studies have been carried out in $La_{2-x}Sr_xCuO_4$ (LSCO) and $YBa_2Cu_3O_{6+x}$ (YBCO), which revealed (i) an AF excitation gap that is often associated with the opening of the superconducting gap, (ii) an hourglass-shaped dispersion, and (iii) a related resonance upon cooling into the superconducting state. In our recent study of the model cuprate $HgBa_2CuO_{4+\delta}$ (Hg1201), we observed several features that are distinct from YBCO and/or LSCO and that exhibit a strong doping dependence. A recently developed theoretical model, which features a dual localized-itinerant character of the spin response and the emergence of spiral spin correlations, provides an appealing conceptual framework to capture the underlying phenomenology of the spin excitations in cuprates that is most clearly revealed in Hg1201.

M.K. Chan[1,2], C.J. Dorow[1], Y. Tang[1], Y.Ge[1], M.J. Veit[1], G. Yu[1], X. Zhao[1,3], M. Greven[1], A.D. Christianson[4], D.L. Abernathy[4], J.T. Park[5], P. Steffens[6], L. Mangin-Thro[7], J. Jeong[7] Y. Sidis[7], P. Bourges[7], F. Onufrieva [7]

[1] School of Physics and Astronomy, University of Minnesota, Minneapolis, Minnesota 55455, USA.
[2] Pulsed Field Facility, NHMFL, Los Alamos National Laboratory, Los Alamos, New Mexico 87545, USA.
[3] State Key Lab of Inorganic Synthesis and Preparative Chemistry, Jilin University, Changchun 130012, China.
[4] Quantum Condensed Matter Division, Oak Ridge National Laboratory, Oak Ridge, Tennessee 37831, USA.
[5] Forschungsneutronenquelle Heinz Maier-Leibnitz, Garching 85747, Germany.
[6] Institute Laue Langevin, Grenoble 38042 CEDEX 9, France.
[7] Laboratoire Léon Brillouin, CEA, CNRS, Université Paris-Saclay, CEA Saclay, 91191 Gif-sur-Yvette, France

yvan.sidis@cea.fr

The prevalence of prominent antiferromagnetic (AF) excitations in the cuprates has motivated considerable theoretical efforts to describe not only the superconducting (SC) state, but also the pseudogap (PG) phenomenon and charge-density-wave (CDW) order as a result of AF correlations. Neutron scattering studies of $La_{2-x}Sr_xCuO_4$ (LSCO) and $YBa_2Cu_3O_{6+x}$ (YBCO) have revealed a seemingly universal X-shaped "hourglass" magnetic dispersion centered at the AF wave vector ($\mathbf{q}_{AF}$=(1/2,1/2) r.l.u.). A related feature is the magnetic resonance, a collective excitation in the superconducting state with well-defined energy at the neck of the hourglass, which is prominent in YBCO but not seen in LSCO.

$HgBa_2CuO_{4+\delta}$ (Hg1201) exhibits a particularly simple crystal structure (one copper-oxygen layer per primitive cell and high tetragonal P4/mmm crystal symmetry) and an optimal T_c of 97 K that is the highest among single-layer cuprates. We have begun to conduct a detailed study of the AF response in Hg1201 using both time-of-flight and triple-axis instruments [1-2]. As shown in Fig. 1 (*right panel*), for sample UD88 (T_c=88 K, hole doping p≈0.13), the imaginary part of the dynamical magnetic susceptibility $\chi''(\mathbf{Q},\omega)$ an X-shaped dispersion at 5 K in the SC state, but upon warming to 100 K, just above T_c, the response remains commensurate up to about 60 meV, eventually disperses outward, resulting in a Y-shaped spectrum [2]. The response exhibits a prominent peak at near 60 meV at 5 K, and falls off significantly above T_c, which is the hallmark of the so-called magnetic resonance peak. On the other hand, as shown in Fig. 1 (*left panel*) [1], for sample UD71 (labeled UD71, T_c=71 K, hole doping p≈0.09), $\chi''(\mathbf{Q},\omega)$ maintains a Y-shaped magnetic dispersion spectrum even above T_c. Moreover, the magnitude and overall shape of χ'' remain rather similar upon warming across T_c, which suggests the absence of a magnetic resonance. The lack of the proto-

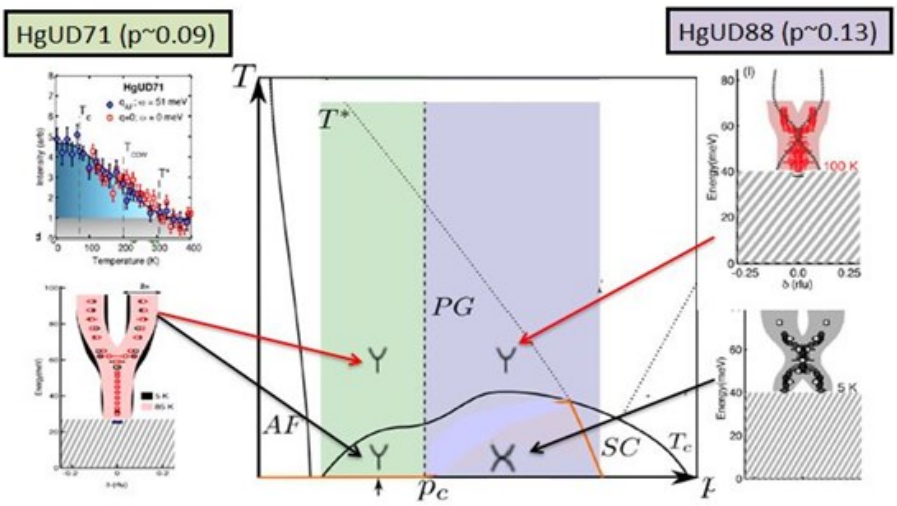

Figure 1: Schematic phase diagram of Hg1201. As a function of the hole doping (p), the system evolves from an insulating antiferromagnetic phase (AF) to a metallic and superconducting state (SC) below T_c. The metallic state is characterized by the mysterious pseudo-gap below T. Above about p_c=0.11, the spin excitation spectrum undergoes a transformation from a Y-like to a X-like dispersion across T_c. Below p_c, the Y-like dispersion remains unchanged across T_c.*

typical hourglass response and resonance in UD71 constitutes a surprising departure from the presumed universal AF magnetic spectrum of the cuprates, and it correlates with prominent CDW order at this doping level [9]. However, a similar Y-shaped response is also observed for another sample at lower doping (T_c = 55 K, not shown here), where the CDW order is weak.

For both UD71 and UD88, χ" displays a remarkable order-parameter-like temperature dependence that ends at T^* and, for UD71, that matches the known T-dependence of the intra-unit-cell magnetic order (q=0) probed by polarized neutron diffraction in the PG state. This observation highlights a strong interplay between the PG physics and the spin dynamics.

Changes of electronic properties have a direct impact on the two-particle functions in the spin and charge sectors probed, respectively, by inelastic neutron scattering (INS) and electronic Raman scattering (ERS). As noticed in [2], above a critical hole doping level of about p_c=0.11, the transition towards the d-wave SC state is accompanied in ERS measurements by the appearance of a peak in the B_{1g} channel, whereas this peak is absent below p_c. As a consequence, the so-called anti-nodal portions of the Fermi surface (probed in the B_{1g} channel, and connected by AF fluctuations) are subject to a strong competition between PG and SC physics, and when the PG dominates, the spin excitation spectrum only displays a characteristic Y-like dispersion.

Interestingly, the excitation gap Δ_{AF} at the AF wave vector is often seen to disappear above T_c, and thus usually thought to be connected with the SC gap. However, Δ_{AF} remains very robust even above T_c for all SC Hg1201 samples that we have measured. Its magnitude decreases with decreasing doping and should extrapolate to zero upon approaching the non-SC AF state at low doping. The evolution of the spin gap and the dispersive part of the excitation spectrum (reminiscent of spin waves in the AF state) suggest the presence of correlations inherited from the undoped Mott-insulating state that involve localized spins.

Qualitatively, the spin excitation spectrum in YBCO as probed by INS also displays an evolution from a X-like dispersion to Y-like as a function temperature and/or hole doping (see [3] and references therein), as shown in Fig. 2. However, whereas in tetragonal Hg1201 the bottom (low-energy) part of the Y-like dispersion remains commensurate at $\mathbf{q}_{AF}$, in weakly orthorhombic YBCO (with a net uniaxial anisotropy) it is found to be incommensurate.

Starting from the t-t'-J model, which is the minimum model to address the physics of cuprates, it is found that both localized and itinerant degrees of freedom are always present throughout the entire phase diagram and cannot be disentangled. In a recent theoretical study [3], it was shown that a weak planar magnetic anisotropy favors the appearance of an incommensurate spiral spin state in the lightly-doped cuprates. The hybridization of spiral spin waves with the

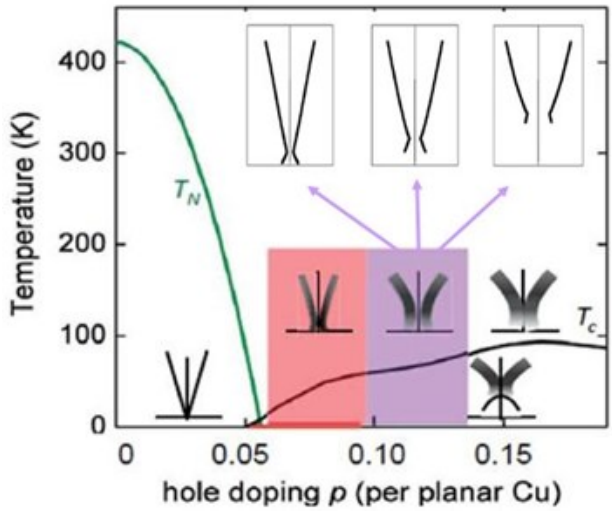

Figure 2: Phase diagram of YBCO with a schematic evolution of the spin excitation spectra as a function the hole doping (reproduced from B. Keimer et al., see [3]). The upper insert gives a schematic description of the theoretically proposed renormalized short-range spiral dynamic correlations [3].

continuum of elementary two-fermion excitations strongly renormalizes the spin excitation spectrum, producing an effective Y-like dispersion (see insert in Fig. 2). With increasing hole doping, the spiral long-range order vanishes, but in the paramagnetic phase, short-range spiral correlations remain. Whereas the high-energy part of magnetic excitation spectrum should be hardly affected, a spin gap develops at low energy and growths as the spiral correlations become shorter. In this model, the primary difference between Hg1201 and YBCO is their spiral pitch.

At large hole doping, the low-energy part of the spin excitation spectrum is fully determined by itinerant degrees of freedom, and a spin exciton with a characteristic downward dispersion appears in the SC state, as observed experimentally.

References

[1] M.K. Chan *et al., Nat. Comm.* **7**, 10819 (2016).

[2] M.K. Chan *et al., Phys. Rev. Lett.* **117**, 277002 (2016).

[3] F. Onufrieva, *Phys. Rev. B* **95**, 125110 (2017).

Elastic Constants, Optical Phonons, and Molecular Relaxations in the High Temperature Plastic Phase of the $CH_3NH_3PbBr_3$ Hybrid

Low frequency dynamics have been studied in a $CH_3NH_3PbBr_3$ hybrid perovskite single crystal, by using four different spectroscopy techniques: coherent inelastic neutron, Raman and Brillouin scatterings and ultrasound measurements. Sound velocities of transverse and longitudinal acoustic waves were measured for the first time to yield the complete set of elastic constants in a hybrid halide perovskite crystal in the pseudo cubic plastic phase. The crystal structure exhibits a very small shear C_{44} elastic constant, leading to a particularly low resistance to shear stress. Near the cubic to tetragonal phase transition reported at T_c≈230K, no soft phonons were found. The critical dynamics at T_c≈230K is thus compatible with an order-disorder character, dominated by relaxational motions of methylammonium (MA=CH_3NH_3) molecules as well as translation-rotation coupling as evidenced by Brillouin light scattering. Overall, this experimental study shows that the spectrum of low energy structural excitations in $MAPbX_3$ hybrid perovskites is dominated by anharmonicity of optical phonons, stochastic disordered reorientational motion of the MA cations and strong translation-rotation coupling leading to mechanical softening.

[1] UMR FOTON, CNRS, INSA-Rennes, F- 35708, Rennes, France

[2] Institut des Sciences Chimiques de Rennes, UMR 6226, CNRS, Université de Rennes 1, France

[3] Laboratoire Charles Coulomb, UMR 5221, Université de Montpellier, France

[4] Laboratoire Léon Brillouin, CEA, CNRS, Université Paris-Saclay, CEA Saclay, 91191 Gif-sur-Yvette, France

[5] Institut de Physique de Rennes, UMR 6251, Université de Rennes 1, France

Jacky.Even@insa-rennes.fr, philippe.bourges@cea.fr

There is an ever-growing need to address both energy and environmental issues, product of generations of over-exploitation of fossil fuel sources and the increased associated industries, which represent one of the most beneficial and, at the same time, injurious aspects of modern times. Solar energy offers the advantages of being renewable and clean, thus making photovoltaic cells attractive as a prospective alternative energy source. During the past few years, hybrid organic perovskites have been intensively studied as promising materials for not only photovoltaics [1,2], but also optoelectronic applications in general. Hybrid perovskites enabled the first low-cost photovoltaic components to be fabricated with photoconversion efficiencies in excess of 25%, achieving almost the same output as silicon in just five years of research [3], although photostability and long life performances are still open issues [4].

These materials are "organohalides of lead", composed of organic ions including carbon, hydrogen and nitrogen within a regular mineral network formed of halogen and lead atoms. An illustration of their AMX_3 crystal structure can be seen in Figure 1. The organic cation is located at the center of the cube with an averaged position sketched by the brown ball. These hybrid organic perovskite compounds typically exhibit a primitive cubic structure at high temperature but they all undergo a cubic (Pm-3m) to tetragonal (I4/mcm) antiferro-distorsive phase transition [5], near room temperature. Understanding the role of lattice dynamics is then essential for the optical and carrier transport properties at room temperature and for the photovoltaics phenomenon. What is the effect at the microscopic level of structural excitations for inelastic carrier scattering [6] or the exciton screening? The lattice dynamics concerns acoustic and polar optical modes, involving both inorganic and organic sublattices. This prompts also the question: to which extent the hybrid character is important for the intended applications? Despite the importance of the macroscopic mechanical properties for material processing, thermal and photo-stabilities, no experimental study has been reported so far on the complete set of elastic constants.

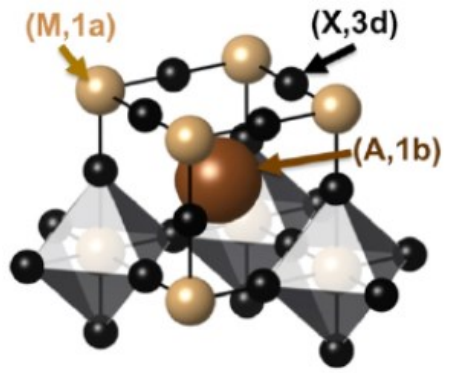

Figure 1: Real space 3D view of the Pm-3m reference cubic crystal structure ofmetal-halide of general formulae AMX_3 where A is an organic cation such as methylammonium, *(MA=CH_3NH_3), M a metal (here Pb) and X an halogen (from [7]).*

We have then studied the low frequency dynamics in a $CH_3NH_3PbBr_3$ hybrid perovskite single crystal by using four different spectroscopy techniques [7]: coherent inelastic neutron, Raman and Brillouin light scatterings, and ultrasound measurements. Sound velocities were measured over five decades in energy to yield the complete set of elastic constants in hybrid halide perovskites in its pseudo-cubic plastic phase. Dispersions of the acoustic phonons have been measured with coherent inelastic neutron scattering using the triple axis spectrometer 4F1 at LLB at room temperature and down to 245K.

The figure 2 reports the transverse acoustic modes around the (200) Bragg reflection as well as transverse and longitudinal sound velocities. The LA sound velocity agrees with the ones determined using ultrasonic technique and Brillouin light scattering. Further, Brillouin scattering has been used to study the angular dispersion of transverse acoustic phonons in the (110) basal plane. The three different cubic elastic constant of a system were then determined (C_{11} = 32, C_{44} = 4 and C_{12} = 12 GPa) and reveal anisotropic crystal properties that are comparable than the ones predicted by DFT predictions but the observed values are all significantly lower. The C_{44} shear elastic constant is very small, leading to a particularly low resistance to shear stress. Broad quasi-elastic excitations and low energy optical phonons were also observed using coherent inelastic neutron scattering and Raman scattering [6], confirming the large anharmonicity of the perovskite lattice modes. However, these optical modes do not exhibit a displacive behavior, as no soft phonons were observed near the antiferro-distorsive phase transition located at $T_c \approx 230K$ for $CH_3NH_3PbBr_3$.Further, Brillouin scattering has been used to study the relaxation dynamics of the methylammonium, $CH_3NH_3^+$, cations and to evidence a translation−rotation coupling associated with the phase transition. When lowering the temperature, the LA phonon mode actually exhibits an anomalous increase of its damping concomitant with the appearance of a large quasi-elastic central component (CP) [7]. This behavior is interpreted as a coupling between acoustic modes and low energy relaxational modes. The CP is attributed to a relaxation mode of the $CH_3NH_3^+$ molecule (tumbling around the C-N axis). Moreover, the LA phonon mode at T=238K displays an asymmetric shape which can only be explained by a coupling to a relaxational mode. The critical dynamics at $T_c \approx 230$ K is then compatible with an order−disorder character, dominated by the stochastic relaxational motions of the MA^+ cations.

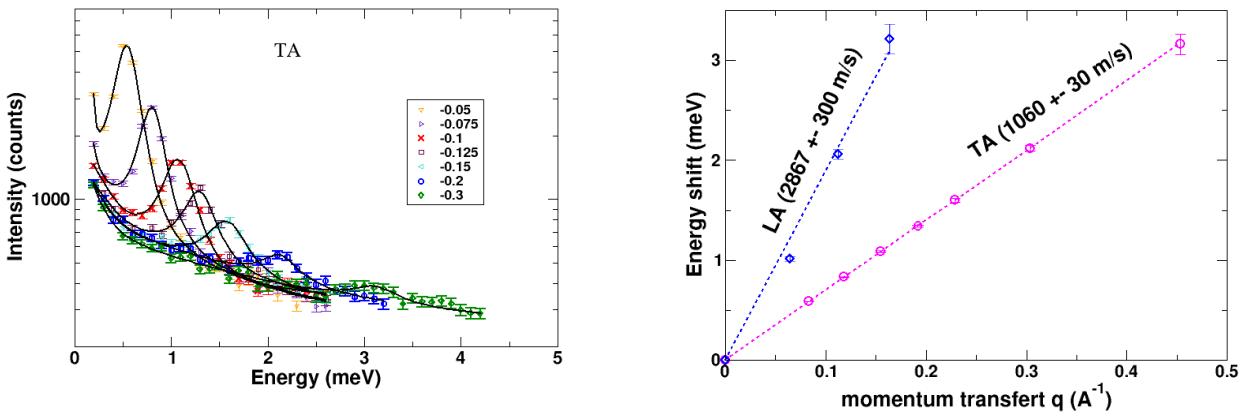

*Figure 2: (a) Low energy transverse acoustic (TA) phonon spectra measured by inelastic neutron scattering in the cubic phase of $CH_3NH_3PbBr_3$ (T=280K) for different **Q** positions going away from the (200) Bragg peak, along the [011] direction. The experimental spectra are described by a sum of a damped harmonic oscillator to describe the phonon mode and a quasi -elastic peak centered at zero energy, further convolved with the spectrometer resolution function. (b) Dispersion curves of the TA and Longitudinal Acoustic (LA) phonon branches close to the (200) Bragg peak (from [7]).*

References

[1] B. Romney, *La Recherche* **495**, 30-33 (2015) .

[2] M.M. Lee *et al., Science* **338**, 643–647 (2012) .

[3] National Renewable Energy Laboratory chart at https://www.nrel.gov/pv/assets/images/efficiency_chart.jpg.

[4] Wanyi Nie *et al., Nat. Comm.* **7**, (2016), 11574.

[5] I.P. Swainson *et al.,* J. *Solid State Chem.* **176**, 97 (2003).

[6] J. Even *et al.* , J. *Phys. Chem. C* **118**, 11566 (2014).

[7] A. Létoublon *et al.,* J. *Phys. Chem. Lett.* **7**, 3776 (2016).

Exploring the meta-magnetism of $EuNiGe_3$

We present here a neutron diffraction study, both in zero field and as a function of magnetic field, of the magnetic structure of the tetragonal intermetallic $EuNiGe_3$ on a single crystalline sample. A cascade of transitions is observed and we show that the low temperature phase presents a spiral moment arrangement with wave-vector k = (1/4 δ 0). Applying a magnetic field in the ab-plane revealed two additional transitions towards a fully polarized state.

X. Fabrèges[1], A. Gukasov[1], P. Bonville[2], A. Maurya[3], A. Thamizhavel[3], S. K. Dhar[3]

[1] Laboratoire Léon Brillouin, CEA, CNRS, Université Paris-Saclay, CEA Saclay, 91191 Gif-sur-Yvette, France

[2] Service Physique de l'Etat Condensée, CEA, CNRS, Université Paris-Saclay, CEA Saclay, 91191 Gif-sur-Yvette, France

[3] Department of Condensed Matter Physics and Materials Science, Tata institute of Fundamental Research, Homi Bhabha Road, Colaba, Mumbai 400 005, India

Xavier.fabreges@cea.fr

Studies of Eu compounds magnetic properties were carried out a few decades ago in $EuAs_3$ and in $EuCo_2P_2$. Interestingly, antiferromagnetic $EuAs_3$ presents a feature which was to be found in many Eu intermetallics studied later: a first transition to a modulated incommensurate phase, extending only over a few K, followed by a transition to an equal moment phase [1]. In these compounds, most of the information has been obtained through macroscopic measurements such as Mössbauer spectroscopy and magnetization. The modulated magnetic ground state and the associated anisotropy are therefore still a mystery as Eu^{2+} ions carry a zero-orbital moment leading to a vanishing crystalline anisotropy at first order. As a result, the deduction of their magnetic structure from solely macroscopic measurements is often impossible and diffraction of thermal neutrons is mandatory.

Neutron diffraction on Eu materials is inherently difficult because of the very strong absorption of natural europium. The absorption corrections were made with an absorption coefficient μ=1.05 mm^{-1} improving R_{int} for nuclear reflections from 0.32 to 0.07. The extinction and absorption parameters obtained were used as input in further magnetic structure refinements. The corresponding zero-field magnetic structure of $EuNiGe_3$ was first studied using a PSD. Eight magnetic satellites are observed around the nuclear reflections and indexed using a k=(±1/4 δ 0) propagation vector, with δ=0.05, and its tetragonal permutations. The four possible k domains are labelled k_1=±(1/4 δ 0), k_2=±(1/4 -δ 0), k_3=±(δ 1/4 0) and k_4=±(-δ 1/4 0). It is not possible to decide whether k is incommensurate with the lattice spacing or not although, generally, such a small δ value points to an incommensurate structure. The temperature evolution of k_3=(δ 1/4 0) magnetic reflection was followed showing a stable δ=0.05 value up to 11K above which it shifts to 0.066 at 12K (fig. 1). Up to 11K, the thermal variation of the scattering intensity is well fitted to the S=7/2 Brillouin function. Above 11K, the intensity deviates from the mean field function, and vanishes above 13.5K. This temperature range corresponds to the intermediate modulated phase reported in previous Mössbauer investigation [2]. The weakness of the magnetic signal in this phase prevented us from determining its detailed structure. At 1.6K the tetrag-

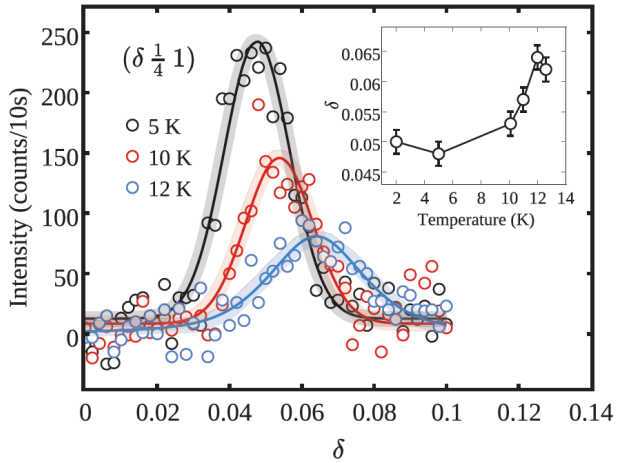

Figure 1: Position of the magnetic satellite at 5, 10 and 12 K. Inset: fitted δ value versus temperature. A clear shift is observed above 10K.

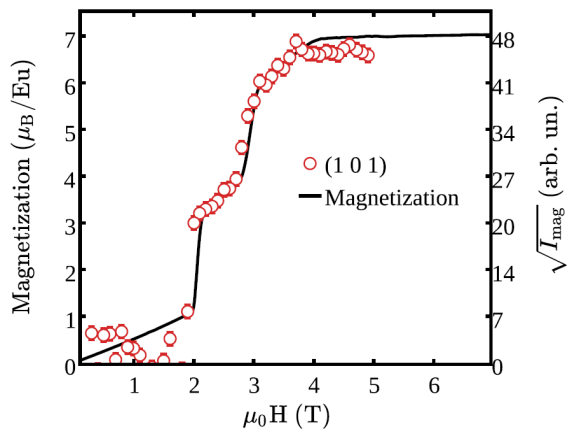

Figure 2: magnetization at 1.8 K (black line) and square root of the (1 0 1) magnetic scattered intensity at 1.6K (red circles)

onal symmetry and the (0 0 z) Wyckoff position of Eu^{2+} ion limits possible magnetic structures to amplitude modulated and helical ones. The best fit was obtained with the helix envelope with the major axes lying in the (b,c) plane for $k_{1,2}$, and (a,c) plane for $k_{3,4}$.

Adding ``ellipticity'' to the helix yields a similar agreement factor. Both the circular and elliptic solutions are valid candidates.

With the magnetic field applied along *c* we monitored the scattering intensity of the (1 0 1) reflection versus field. Figure 2 shows the field evolution of its magnetic contribution compared with the magnetization data. The two probes perfectly match, with two well defined jumps at respectively 2 and 3T, followed by the spin-flip transition at H=4T with the fully saturated Eu^{2+} moment of 7µB. As seen on fig. 3, the two peaks at δ=±0.05 are observed in zero field. A 1st order transition occurs at 2T with the appearance of two new satellites with δ^*=0.072 coexisting with those at δ=0.05. The new satellites correspond to a smaller magnetic unit cell in the b^* direction. At 2.5T, the zero field δ satellites completely vanish. In turn, the δ^*=0.072 satellites disappear at H=3T. In this case, the AF contribution is well described by a similar helical structure with reduced ordered magnetic moment of *m*=5.5µB.

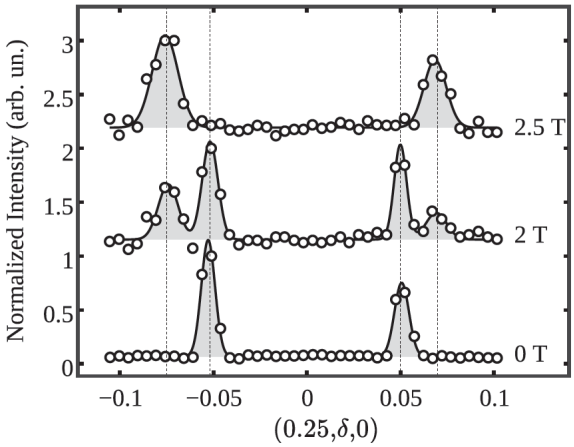

Figure 3: normalized (1/4 δ 0) scans at 0, 2 and 2.5 T

With the magnetic field applied along *b*, no anomaly was observed on the magnetization curve [2]. On the neutron diffraction pattern, applying a field at 8K will first select the $k_{3,4}$ domain over the $k_{1,2}$ ones up to 2.5T where the opposite process occurs. Finally, all domains vanish above 4.5T. The first anomaly corresponds to a spin-flop like transition selecting domains for which the ordered moments are orthogonal to the applied field. The second transition is well described by a transition to a collinear AF order with moment ordered along the *c*-axis. The corresponding phase diagram extracted from neutron diffraction data is presented in fig. 4.

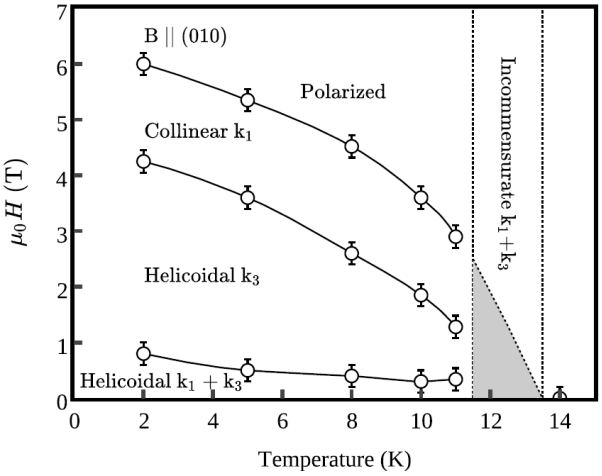

Figure 4 : (H,T) phase diagram. The shaded area corresponds to the transition observed in [2] above T_{N2}

A numerical model composed of 4 exchange paths and an anisotropy has been used to reproduce most of the (H,T) diagram features. In particular, the k=(1/4 0 0) modulation as well as the 2 transitions observed with the field applied along the c-axis are induced by the frustrated J_a/J_{2a} interactions in the (a,b) plane. With the field along the b-axis, the non-linearity of the magnetization curve at low field is attributed to the superposition of the 4 domains susceptibilities and is in perfect agreement with the macroscopic observations [3].

The microscopic origin of the δ modulation remains unexplained at this stage as it breaks the well-established tetragonal symmetry. A numerical effort is mandatory to look at the DM and/or dipolar interactions effect on the magnetic and nuclear structures. Additionally, a clear anisotropy in the (a,c) plane is observed which contradicts the vanishing crystalline anisotropy of Eu^{2+} ions. The crystal field interaction is known to mix the excited states of rare-earth compounds, yielding a strong anisotropy. The study of magnetic excitations coupled to diffraction is the next step to reveal the true nature of the magnetic ground state of Eu based compounds.

References

[1] P. Bonville *et al., Eur. Phys. J. B* **21**, 349 (2001).

[2] A. Maurya *et al., J. Phys.: Condens. Matter* **26**, 216001 (2014).

[3] X. Fabrèges *et al*, Phys. Rev. B **93,** 214414 (2016)

A chiral magnet with 'invar' properties

Magnetism in electronic systems is fundamentally unstable with respect to lattice compression. Spin state instabilities cause thermodynamic anomalies under temperature or pressure changes. One of the most notorious is the 'invar' effect, yielding a paused thermal expansion around room temperature in Fe-Ni alloys and having many industrial applications. Besides thermal expansion, several physical quantities can be affected, such as atomic volume, bulk modulus or magnetic moment. The 'invar' effect is usually observed in strong ferromagnets. Using neutron and X-ray scattering, we show that the helimagnet MnGe exhibitss the main fingerprints of the 'invar' behavior. We namely observe a pressure-induced HS-LS transition at low and room temperature and monitor the magnetic collapse, where Mn moments vanish. Our observations set the stage for an improved understanding of the 'invar' effect and the physics of partially-ordered state in general.

N. Martin[1], M. Deutsch[2,3], J.-P. Itié[3], J.-P. Rueff[3,4], U.K. Rössler[5], K. Koepernik[5], L.N. Fomicheva[6], A.V. Tsvyashchenko[6,7], I. Mirebeau[1]

[1] Laboratoire Léon Brillouin, CEA, CNRS, Université Paris-Saclay, CEA Saclay, 91191 Gif-sur-Yvette, France

[2] Université de Lorraine, CRM2, UMR UL-CNRS 7036, BP 70239, 54506 Vandœuvre-lès-Nancy, France

[3] Synchrotron SOLEIL, L'Orme des Merisiers, Saint-Aubin, 91192 Gif-sur-Yvette, France

[4] Sorbonne Universités, UPMC Université Paris 06, CNRS, Laboratoire de Chimie Physique-Matière et Rayonnement, 75005 Paris, France

[5] IFW Dresden, P.O. Box 270116, 01171 Dresden, Germany

[6] Vereshchagin Institute for High Pressure Physics, Russian Academy of Science, 142190 Troitsk, Moscow, Russia

[7] Skobeltsyn Institute of Nuclear Physics, MSU, Vorobevy Gory 1/2, 119991 Moscow, Russia

nicolas.martin@cea.fr

The study of non-centrosymmetric magnets hosting long-wavelength spin helices has become a cornerstone of experimental and theoretical condensed matter physics. Especially interesting are the so-called B20 magnets which crystallize within the $P2_13$ chiral space group. They display a variety of unconventional phenomena, such as the breakdown of Fermi liquid behavior under applied pressure [1] and the stabilization of a skyrmion lattice in the critical temperature region under applied magnetic field [2]. MnGe is the most recently studied member of this family. At ambient pressure, it is characterized by a relatively high Néel temperature ($T_N \approx 170$ K), below which a helimagnetic order with a short spatial period ($\lambda_H \approx 30$ Å) sets in. Both features reveal strong magnetic interactions and a high degree of frustration, arising from the competition between symmetric ferro- and antiferromagnetic exchange terms, balanced by a weak Dzyaloshinskii-Moriya anisotropy.

Following *ab initio* (DFT) band structure calculations [3], a pressure-induced spin transition from the initial Mn high-spin (HS) state ($\approx 2\ \mu_B$) to a low-spin (LS) state ($\approx 1\ \mu_B$) is expected to take place in MnGe. In order to verify this prediction, neutron powder diffraction experiments have been jointly performed at LLB and ILL, monitoring the pressure-dependence of the ordered Mn spin moment [4]. As shown in Figure 1a, the HS-LS transition is clearly observed and takes place at $p_{C1} \approx 5$ GPa for $T << T_N$, in agreement with calculations. Additionally, T_N is found to decrease linearly as a function of pressure until its suppression at $p_0 \approx 13$ GPa (black symbols in Figure 1b). We note that this set of results provide the first example of spin state instability in a metallic chiral helimagnet.

However, according to theory [3], the *local* moment should

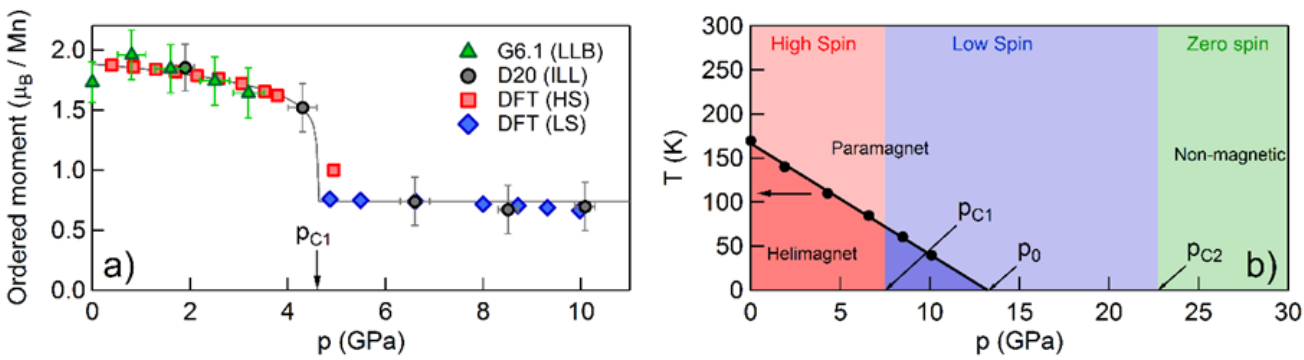

Figure 1: (a) Pressure-dependence of the low-temperature ordered magnetic moment of MnGe as determined by neutron diffraction and ab initio (DFT) calculations (from [4]). Solid line is a guide to the eye. (b) Phase diagram of MnGe inferred from our study. One can distinguish long-range ordered ('helimagnet'), disordered ('paramagnet') and non-magnetic (green shading) phases.

remain finite above p_0. In order to provide us with a more complete check of the model, we have carried out a new series of measurements at room temperature (*i.e.* in the paramagnetic state of MnGe), using synchrotron-based X-ray techniques. We have monitored the HS-LS transition by measuring the (p,V) equation of state of MnGe using powder diffraction at the PSICHÉ beamline (SOLEIL synchrotron). As depicted in Figure 2a, we observe the opening of a huge hysteresis loop upon pressure cycling. The latter implies coexistence of HS and LS states and can be explained as a cooperative effect between local strains, induced by the volume mismatch due nucleation of LS droplets (with small volume) surrounded by the dominant HS matrix (with larger volume). We have developed a thermodynamical approach to this problem, treating MnGe as an open system tuned by pressure as an external potential. We showed that the progressive replacement of HS by LS unit cells comes along with a macroscopic energy barrier which is overcome at difference pressure values, depending on the initially dominant spin state [5]. The coexistence of HS and LS unit cells in an extended pressure range demonstrate the 'invar' character of MnGe, since such configuration promotes *e.g.* thermal expansion anomalies in Fe-Ni alloys.

Using hard X-ray emission spectroscopy (GALAXIES beamline, SOLEIL synchrotron), we have also followed the evolution of the local moment upon pressure increase. The intensity δ of the low energy shoulder of the Mn-Kβ emission line (inset of Figure 2b) is known to be sensitive to the amplitude of spin polarization of the 3d band. As shown in Figure 2b, δ progressively decreases until it saturates at pressures larger than ≈ 25 GPa. A fit of a power law to the data yields a critical pressure for magnetic collapse p_{C2} ≈ 23 GPa and a critical exponent β ≈ 0.38, meaning that the transition falls into the 3D Ising universality class as expected for a fluctuation-dominated disappearance of a scalar order parameter [5]. This reveals a precious analogy between the LS state observed here and the topologically non-trivial partial ordered phases observed in isostructural compounds such as MnSi [7] and FeGe [8], the formation of which being supposedly linked with an abundance of thermal or quantum spin fluctuations.

Taken together, our results underscore the prominent role of spin-state instabilities in the exotic properties of the intensively studied family of B20 magnets. We have shown that MnGe represents one of the finest playground to study such physics, given its large magnetic moment and strong magneto-elastic coupling.

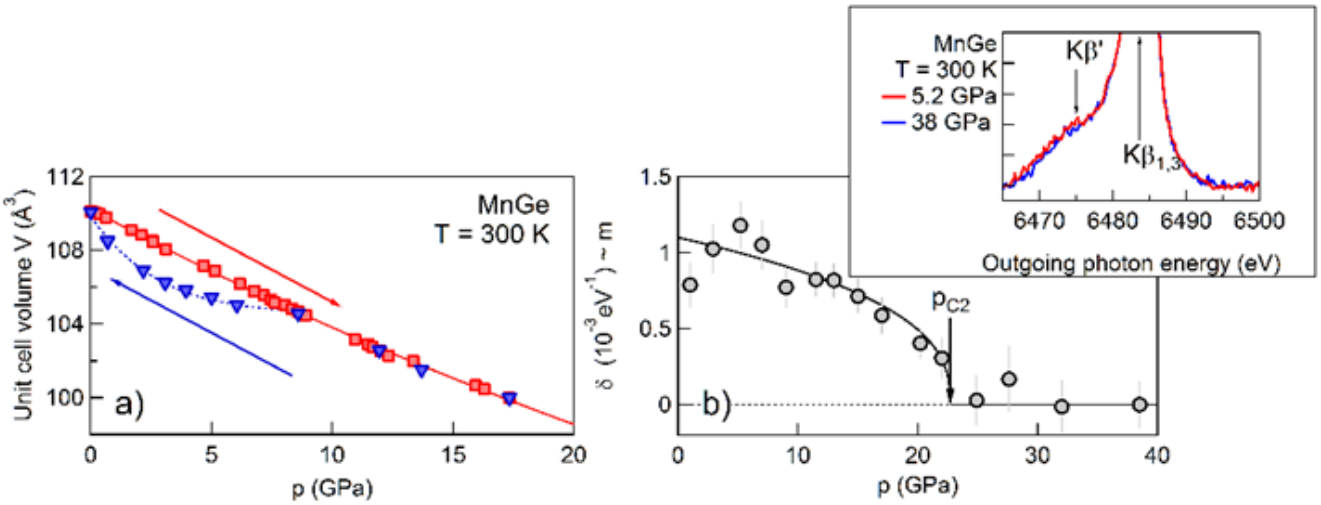

Figure 2: Pressure-dependence of the cubic unit cell parameter (a) and local Mn spin moment (b) (from [5]). In panel (b), solid line is a fit of a critical law to the data. Inset shows emission spectra recorded at different pressures

References

[1] C. Pfleiderer et *al., Nature* **414**, 427 (2001).

[2] S. Mühlbauer *et al., Science* **323**, 915 (2009).

[3] U.K. Rössler, *J. Phys.: Conf. Series* **391**, 012104 (2012).

[4] M. Deutsch et al., Phys. Rev. B **89**, 180407(R) (2014).

[5] N. Martin *et al., Phys. Rev. B* **93**, 214404 (2016).

[6] C. Pfleiderer *et al., Nature* **427**, 227 (2004).

[7] A. Barla *et al., Phys. Rev. Lett.* **114**, 016803 (2015).

Antiferro-quadrupolar correlations in the quantum spin ice candidate $Pr_2Zr_2O_7$

We present an experimental study of the quantum spin ice candidate pyrochlore compound $Pr_2Zr_2O_7$ by means of magnetization measurements, specific heat and neutron scattering up to 12 T and down to 60 mK. We discuss these results in the light of mean field calculations and propose an interpretation where quadrupolar interactions play a major role, overcoming the magnetic exchange. We propose a range of acceptable coupling parameters that allow to reproduce several experimental features observed under field. With these parameters, it is proposed that the actual ground state of this material supports antiferroquadrupolar short range correlations from which emerge spin-ice like excitations.

S. Petit[1], E. Lhotel[2], S. Guitteny[1], O. Florea[2], J. Robert[2], P. Bonville[3], I. Mirebeau[1], J. Ollivier[4], H. Mutka[4], Eric Ressouche[5], C. Decorse[6], M. Ciomaga-Hatnean[7], G. Balakrishnan[7]

[1] Laboratoire Léon Brillouin, CEA, CNRS, Université Paris-Saclay, CEA Saclay, 91191 Gif-sur-Yvette, France

[2] Institut Néel, CNRS and Université Grenoble Alpes, F-38042 Grenoble, France

[3] Service Physique de l'Etat Condensée, CEA, CNRS, Université Paris-Saclay, CEA Saclay, 91191 Gif-sur-Yvette, France

[4] Institut Laue Langevin, F-38042 Grenoble, France,

[5] Institut Nanosciences et Cryogénie, CEA et Université Grenoble Alpes, CEA Grenoble, F-38054 Grenoble

[6] Institut de Chimie Moléculaire et des Matériaux d'Orsay, Université Paris-Sud et Université Paris-Saclay, F-91405 Orsay,

[7] Department of Physics, University of Warwick, Coventry, CV4 7AL, United Kingdom

sylvain.petit@cea.fr, isabelle.mirebeau@cea.fr

In the last decades, condensed matter physicists have tried to describe and observe new phenomena that would lie beyond the Néel paradigm of classical ordered phases. In this quest, the frustrated pyrochlore magnets have attracted much attention.

Frustration covers a wide variety of situations where a local configuration, stabilized by a given scheme of interactions, cannot extend simply over the whole system. Numerous examples can be found as for instance in pentagonal or icosahedral lattices, metallic binary alloys, liquid crystals, the bi-stable states of metal organic networks, the packing of molecules on triangular lattices, among others. In condensed matter physics, the archetype of magnetic geometrical frustration in three dimensions is the problem of Ising spins residing on the vertices of the pyrochlore lattice [1]. If the spins are constrained to lie along the local crystal field axes which link the center of a tetrahedron to its summits and experience ferromagnetic interactions, as it is the case in $Ho_2Ti_2O_7$ and $Dy_2Ti_2O_7$ for instance (see Figure 1), a highly degenerate and disordered ground state so-called spin ice, develops at low temperature. The nearest-neighbor ferromagnetic coupling indeed favors local configurations where in each tetrahedron, two spins point into and two out of the center ("2-in 2-out" configurations), forming a magnetic analog of the water ice. One of the clear proofs of this physics came with the observation of a peculiar magnetic diffuse scattering characterized by arm-like features in reciprocal space along (hhh) directions together with specific bow tie singularities also called pinch points [2].

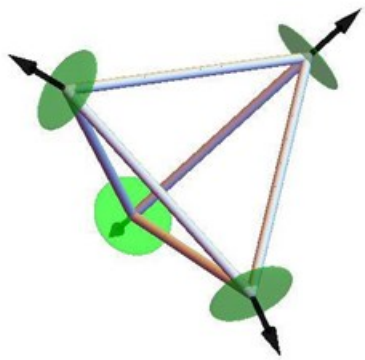

Figure 1: sketch of a tetrahedron in the pyrochlore structure. The green disks show the local XY planes and the black arrows the local CEF "z" axis

While temperature naturally melts the spin ice, the possibility that quantum fluctuations might also melt spin ice is a topical and fascinating issue. According to several theoretical works, this may happen for moderate transverse terms compared to the "classical" ferromagnetic interaction between Ising spins. Different arguments advocate that $Pr_2Zr_2O_7$ could be a good candidate in this research. As in spin ice, the Pr moment has a strong Ising character and no magnetic long range ordering is observed down to a few mK. The magnetic specific heat shows a broad peak at about 2 K [3], similar to what is observed in the classical spin ice $Dy_2Ti_2O_7$. Finally, $Pr_2Zr_2O_7$ hosts a very peculiar magnetic excitation spectrum. As revealed by inelastic neutron scattering, it consists of a broad inelastic response centered around 0.4 meV with a structure factor that strongly resembles the spin-ice pattern observed in spin ice

[3]. For this reason, it has been described as a dynamical spin ice mode.

In this context, we have further explored the ground state and magnetic excitations spectrum in $Pr_2Zr_2O_7$, by means of magnetization, specific heat, neutron diffraction and inelastic neutron scattering [4,5]. In particular, we have confirmed the existence of the dynamical spin ice mode (Figure 2). In addition, we have determined how it evolves

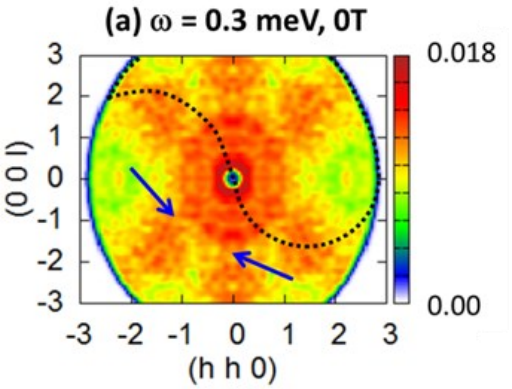

Figure 2: broad inelastic response centered around 0.4 meV in $Pr_2Zr_2O_7$. Its structure factor strongly resembles the spin-ice pattern.

with the field, and characterized the associated field induced magnetic structures. For a field H parallel to [1-10] (at least up to 2.5 T), we find that a well-defined mode forms from this broad response, whose energy increases with H, in the same way as the temperature of the specific heat anomaly. When the field is applied along the [111] and [1-10] directions, **k**=0 field induced structures settle in. We find that the ordered moment rises slowly, even at very low temperature, in agreement with macroscopic magnetization. This behavior is quite different from the Ising spin ice case and supports the idea that some hidden force competes and tends to oppose to the magnetization process.

Using a mean field treatment of the minimal Hamiltonian widely accepted in the literature for these materials, it emerges that these observations can be qualitatively understood by considering that the transverse terms are indeed relevant and all the more dominate the "classical" interaction of spin ice. Since Pr is a non-Kramers ion, these transverse terms correspond physically to effective antiferro-quadrupolar interactions. In this interpretation, an "all-in all-out" quadrupolar phase is stabilized, for moderate positive or negative values of the interactions between Ising spins. The dynamical ice-like mode then naturally emerges from this peculiar ground state

In addition, recent results show that the chemical disorder, revealed by lattice diffuse scattering, plays a key role in $Pr_2Zr_2O_7$ [6]. Indeed, the non-Kramers nature of the Pr ion makes it extremely sensitive to defects or lattice strain perturbing the 4f electronic density. This disorder limits the development of the quadrupolar phase, which is long range ordered in the above mean field approximation only. In this picture, $Pr_2Zr_2O_7$ would not be a "quantum spin ice" but a new state of matter supporting short range antiferro-quadrupolar correlations and from which emerge spin-ice correlations.

References

[1] M. J. P. Gingras and P. A. McClarty, *Rep. Prog. Phys.* **77**, 056501 (2014).

[2] T. Fennell et *al., Science* **326**, 415 (2009).

[3] K. Kimura *et al., Nature Comm*. **4**, 1934 (2013).

[4] P. Bonville *et al., Phys. Rev. B* **94** 134428 (2016).

[5] S. Petit *et al., Phys. Rev. B* **94** 165153 (2016).

[6] N. Martin *et al., Phys. Rev. X* **7**, 041028 (2017).

CHEMISTRY
A European Journal

ChemPubSoc Europe

ChemPubSoc Europe

DOI: 10.1002/chem.201503400

CHEMISTRY
A European Journal
Full Paper

Magnetism Studies |*Hot Paper*|

Polarized Neutron Diffraction as a Tool for Mapping Molecular Magnetic Anisotropy: Local Susceptibility Tensors in Co^{II} Complexes

Karl Ridier,[a, f] Béatrice Gillon,*[a] Arsen Gukasov,[a] Grégory Chaboussant,[a] Alain Cousson,[a] Dominique Luneau,*[b] Ana Borta,[b, g] Jean-François Jacquot,[c] Ruben Checa,[b] Yukako Chiba,[d] Hiroshi Sakiyama,[d] and Masahiro Mikuriya[e]

Abstract: Polarized neutron diffraction (PND) experiments were carried out at low temperature to characterize with high precision the local magnetic anisotropy in two paramagnetic high-spin cobalt(II) complexes, namely $[Co^{II}(dmf)_6](BPh_4)_2$ (**1**) and $[Co^{II}_2(sym\text{-}hmp)_2](BPh_4)_2$ (**2**), in which dmf = *N,N*-dimethylformamide; sym-hmp = 2,6-bis[(2-hydroxyethyl)methylaminomethyl]-4-methylphenolate, and BPh_4^- = tetraphenylborate. This allowed a unique and direct determination of the local magnetic susceptibility tensor on each individual Co^{II} site. In compound **1**, this approach reveals the correlation between the single-ion easy magnetization direction and a trigonal elongation axis of the Co^{II} coordination octahedron. In exchange-coupled dimer **2**, the determination of the individual Co^{II} magnetic susceptibility tensors provides a clear outlook of how the local magnetic properties on both Co^{II} sites deviate from the single-ion behavior because of antiferromagnetic exchange coupling.

[a] Dr. K. Ridier, Dr. B. Gillon, Dr. A. Gukasov, Dr. G. Chaboussant, Dr. A. Cousson
Laboratoire Léon Brillouin (UMR12), CEA-CNRS
CEA Saclay, 91191 Gif-sur-Yvette (France)
E-mail: beatrice.gillon@cea.fr

[b] Prof. D. Luneau, Dr. A. Borta, Dr. R. Checa
Laboratoire des Multimatériaux et Interfaces (UMR5615)
Université Claude Bernard Lyon 1
69622 Villeurbanne (France)
E-mail: dominique.luneau@univ-lyon1.fr

[c] Dr. J.-F. Jacquot
SCIB, UMR-E 3 CEA/UJF-Grenoble 1, INAC, CEA-UJF
38054 Grenoble (France)

[d] Y. Chiba, Prof. H. Sakiyama
Faculty of Science, Yamagata University
Yamagata 990-8560 (Japan)

[e] Prof. M. Mikuriya
School of Science and Technology, Kwansei Gakuin University
Sanda 669-1337 (Japan)

[f] Dr. K. Ridier
Present address: GEMaC, UMR8635
Université Versailles St-Quentin-en-Yvelines
45, avenue des Etats-Unis, 78035 Versailles Cedex (France)

[g] Dr. A. Borta
Present address: Service Photons Atoms & Molecules, IRAMIS, CEA Saclay, 91191 Gif Sur Yvette (France)

Supporting information for this article is available on the WWW under http://dx.doi.org/10.1002/chem.201503400 and contains crystallographic data (excluding structure factors) and structure at 10 K (Tables S1 and S2), magnetic susceptibility from SQUID measurements on powder (Figure S1), eigenvectors of the Co^{II} susceptibility tensor (Table S3), and Co^{II} magnetic susceptibility ellipsoid with different viewing directions for one molecule and in the cell (Figures S2, S3) for complex **1**; and a definition of the local molecular axes (Figure S4), magnetic susceptibility ellipsoid of the molecule with different viewing directions for one molecule and in the cell (Figures S5, S6), eigenvectors of the Co1 and Co2 local susceptibility tensors (Table S4), and a representation of the Co^{II} local induced moments at 2 K under a field of 1 T in perspective view (Figure S7) for complex **2**.

Introduction

Since their discovery, single-molecule magnets (SMMs) have attracted intense research by both chemists and physicists.[1,2] This is due to their exceptional ability to exhibit slow relaxation of magnetization and then an intrinsic magnetic hysteresis loop below the so-called blocking temperature (T_B).[3,4] This phenomenon essentially originates from the existence of a negative axial magnetic anisotropy ($D<0$) in the ground spin state S, which gives an energy barrier ($U=|D|S^2$ and $|D|(S^2-1/4)$ for integer and half-integer S, respectively) to magnetization reversal between the two zero-field split (ZFS) lowest-lying $M_S=\pm S$ states. SMMs provide a new frontier in the race for extreme miniaturization of the elementary bits for use in high-density data storage devices or for quantum computing.[5–8] However, the blocking temperatures (proportional to the energy barrier $T_B \propto U$) remain too low at present for practical applications. At first sight, to enhance the energy barrier and consequently the operating temperature, we can increase either the spin eigenvalue S of the molecular ground state or the axial anisotropy term $|D|$. Most of the early works have aimed at increasing the ground-state spin (S). This has resulted in the synthesis of numerous high-spin clusters with d or/and f metal ions.[9–12] However, it was observed that the energy barriers did not increase accordingly because the molecular anisotropy term $|D|$ is not independent of S but decreases with it. It was later shown[13] that $|D|$ actually varies as S^{-2}, such that the blocking temperature seems to be independent from S for a given complex formed from building blocks with a given local anisotropy. Now, most efforts focus on the synthesis of low-nuclearity complexes in which magnetic anisotropy takes

Material and nanosciences, fundamental studies and applications

Materials Science activity at the LLB covers a variety of research fields including metals, alloys, polymers, geological materials, nanocomposites, organic materials, thin films... They are at the frontier of chemistry, physics and engineering sciences. The objectives of these studies are to understand and predict how parameters such as the chemical composition, the atomic structure and the microstructure determine the properties measured in materials at the macroscopic scale. Most of these studies have direct applications in technology and industry. Neutron scattering provides a wide range of tools, unique to perform such studies:

Coupling neutron diffraction with complementary techniques (electron and synchrotron powder diffraction, solid-state NMR) and with first-principles calculations allows a complete characterization of compounds structure as illustrated in the first paper.

Monitoring and visualizing building materials by neutron radiography and imaging give possibility to describe the time dependence of particular phenomena that could influence the behaviour of such materials. This is illustrated in the case of the effect of capillary water uptake in stone.

For organometallic compounds with promising magnetic anisotropy properties, the use of polarized neutron diffraction (PND) tackle the question of the influence of a magnetic field on these properties. It opens the way towards the optimization of magnet molecules to develop ultra-high storage density devices.

Another way to deeply understand intrinsic mechanisms of structural changes in physical processes is the use of time-resolved neutron diffraction. In the last article, the crystallization processes in a super cooled liquid has been observed by this mean for about three days.

- **Structure determination of Ba5AlF13 by coupling electron, synchrotron and neutron powder diffraction, solid-state NMR and ab initio calculations**

  C. Martineau, M. Allix, M. R. Suchomel, F. Porcher, F. Vivet, C. Legein, M. Body, D. Massiot, F. Taulelle, F. Fayon·

- **Weathering effects on capillary water uptake of natural building stones by using neutron imaging**

  Simona Raneri, Germana Barone, Paolo Mazzoleni, Eva Rabot

- **When the magnetic anisotropy of molecules reveals its forms to neutrons**

  K. Ridier, B. Gillon, A. Gukasov, G. Chaboussant, A. Cousson, D. Luneau, A. Borta, R. Checa, J.-F. Jacquot, Y. Chiba, H. Sakiyama, M. Mikuriya

- **Real-time observation of the isothermal crystallization kinetics in a deeply super cooled liquid**

  M. Zanatta, L. Cormier, L. Hennet, C. Petrillo, F. Sacchetti

Structure determination of Ba_5AlF_{13} by coupling electron, synchrotron and neutron powder diffraction, solid-state NMR and *ab initio* calculations

The room temperature structure of Ba_5AlF_{13} has been investigated by coupling electron, synchrotron and neutron powder diffraction, solid-state high-resolution NMR (^{19}F and ^{27}Al) and first-principles calculations. GIPAW computations of the NMR parameters validate the refined structural model, and indicate a local motional process of one fluorine atom. Visualisation of the dynamic process was obtained from Rietveld refinement of neutron diffraction data using an anharmonic description of the displacement parameters to account for the thermal motion of the mobile fluorine.

C. Martineau,[1,2] M. Allix,[2] M. R. Suchomel,[3,4] F. Porcher,[5] F. Vivet,[2] C. Legein,[6] M. Body,[6] D. Massiot,[2] F. Taulelle,[1] F. Fayon[2]

[1] Tectospin, Institut Lavoisier de Versailles, CNRS UMR 8180, Université de Versailles Saint-Quentin en Yvelines, 45 Avenue des Etats-Unis, 78035 Versailles Cedex, France

[2] CNRS, CEMHTI UPR3079, Université d'Orléans, F-45071 Orléans, France

[3] Argonne National Laboratory, Advanced Photon Source, Argonne, IL 60439, USA

[4] Current address: CNRS, Université Bordeaux, ICMCB, UPR 9048, F-33608 Pessac, France

[5] Laboratoire Léon Brillouin, CEA, CNRS, Université Paris-Saclay, CEA Saclay, 91191 Gif-sur-Yvette, France

[6] Université Bretagne Loire, Université du Maine, CNRS UMR 6283, Institut des Molécules et des Matériaux du Mans, Avenue Olivier Messiaen, 72085 Le Mans Cedex 9, France

charlotte.martineau@uvsq.fr

Ba_5AlF_{13} was reported isostructural [1] to $Sr_{10}Al_2F_{25}Cl$ (space group Fd-3m, a = 16.4209 Å). The whole pattern fit, performed using the Le Bail method, of a synchrotron powder diffraction (SPD) diagram of Ba_5AlF_{13} confirmed the expected cubic system, with a refined unit cell parameter a = 17.3780(1) Å. Reflection extinctions were in good agreement with the Fd-3m space group. To construct the structural model, we used the atomic positions of $Sr_{10}Al_2F_{25}Cl$ as starting point replacing Sr by Ba and Cl by F. These initial atomic positions were refined using the Rietveld method, for which good fit statistics were obtained: Rp = 6.07%, Rwp = 8.93% and RBragg = 4.79%. Analysis of the structural model indicated that one fluorine atom (F3) was not properly located (too long Ba-F distances). Additional contrast was sought by using neutron powder diffraction (NPD) measurements. The room temperature NPD pattern of Ba_5AlF_{13} was collected on the 3T2 high-resolution/high-flux powder diffractometer at the Laboratoire Léon Brillouin (LLB) in Saclay, France. The data were recorded throughout the 4.5°<2θ<120° angular range with a 0.05° step size and a 1.2256 Å wavelength for 22 hours. The SPD refined structural model was used as a starting point for the Rietveld. To get insights into the position of F3, difference Fourier maps were calculated by removing F3 atoms from the model (Fig. 1). The map shows no residual density at the initial 8a position (at 1/8 1/8 1/8) but clearly exhibits four distinct spots around the 8a position, corresponding to a 32e Wyckoff site (x x x). Therefore, each of the eight F3 atoms was considered to occupy one of those four positions (25% occupancy). The Rietveld refinement led to improved reliability factors: goodness of fit = 1.63, Rp = 2.59%, Rwp = 3.30%, with F3 at x = 0.0796(7).

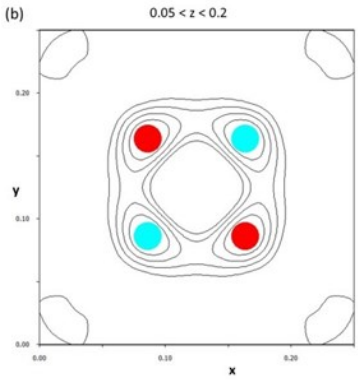

Figure 1. Difference Fourier map obtained from Rietveld refinement. The red and cyan circles represent the 32e site positions respectively at z ~ 0.085 and z ~ 0.170.

GIPAW calculations of the ^{19}F NMR parameters confirmed the inaccurate location of F3 in the initial model, as its calculated ^{19}F shielding (Fig. 2b) significantly differs from the measured value (Fig. 2a). The computations performed assuming a static random disorder of the F3 site predicted a better agreement for the F3 ^{19}F shielding (Fig. 2c), but also a large and bimodal distribution of the F1 isotropic

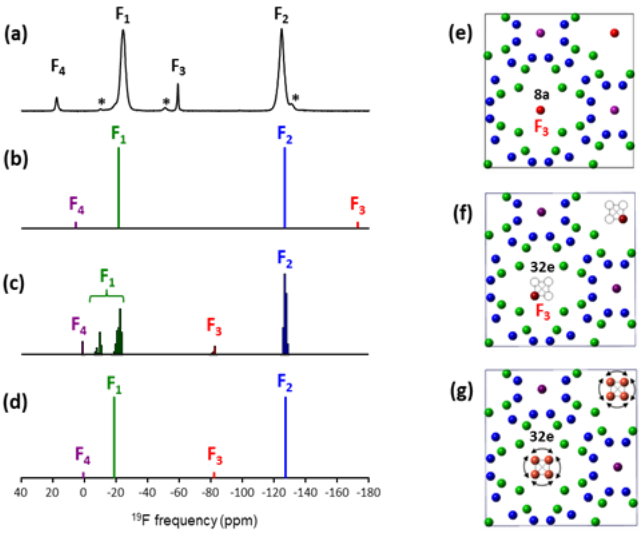

Figure 2. (a) Experimental ^{19}F MAS spectrum of Ba_5AlF_{13}. (b-d) GIPAW-calculated ^{19}F isotropic NMR spectra for the model (b) with F3 atoms in 8a position (e), (c) assuming a static random partial occupancy (25%) of the 32e positions (f), (d) assuming a fast local motion of F3 within the four 32e positions (g).

chemical shifts. Since a single resonance was experimentally observed for F1, a static local disorder of F3 was excluded, suggesting the presence of a local dynamical disorder, i.e., the occurrence of rapid jumps of the F3 ions within the four 32e positions. To account for this local motion, the set of configurations generated previously was used as snapshots of the dynamic in a time-dependent approach. The ^{19}F NMR spectrum was obtained by average of the NMR parameters computed for each of these configurations. The calculated ^{19}F chemical shifts obtained in this way (Fig. 2d) were in better agreement with the experimental values. This supported the NPD structural model and indicated that the occupancy of the F3 site is related to fluorine hopping within the four 32e positions.

In elastic scattering experiments using X-rays or neutrons, the Bragg diffraction peaks are affected by the thermal motions of the atoms in the crystal. These effects can be accounted for using a statistical approach for the treatment of anharmonic motion, for example, with the Gram-Charlier expansion development of the temperature factor as implemented in JANA2006 [2]. Because the Fourier difference map of Ba_5AlF_{13}considering F3 on a 32e site with a simple harmonic approximation for the thermal parameters still showed the presence of residues, anharmonic Rietveld refinements of the NPD data were performed to take into account the F3 hopping motion. Development to the fourth order leads to a much better description of the nuclear density around F3, and to good final reliability factors (Fig. 3a). Finally, a 3D joint probability density function map of the F3 sites was calculated, which provides a visualization of the motion path of F3 (Fig. 3b). The combination of all the complementary data (powder diffraction and NMR), associated to DFT calculations was efficient to provide an accurate description of the Ba_5AlF_{13} [3] structure, including site-specific dynamics of the fluorine sub-network.

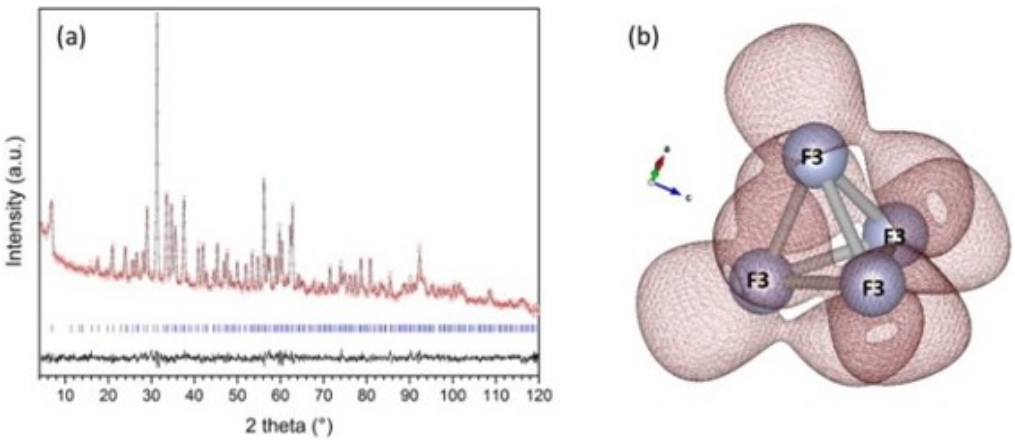

Figure 3. (a) NPD Rietveld refinement of B_o5AlF_{13}. (b) 3D representation of a joint probability density isosurface for the 32e F3 crystallographic site showing its local motion.

References

[1] A. Hémon, PhD Thesis, Université Le Mans, 1991.

[2]. U. H. Zucker, H. Schulz, Acta Crystallogr., 1982, A38, 563; W. F. Kuhs, Acta Crystallogr., 1992, A48, 80; A. Rolle, P. Roussel, N. V. Giridharan, E. Suard, R. N. Vannier, Solid State Ionics, 2008, 179, 1986.

[3]. C. Martineau, M. Allix, M. R. Suchomel, F. Porcher, F. Vivet, C. Legein, M. Body, D. Massiot, F. Taulelle, F. Fayon, Dalton Trans., 2016, 45, 15565.

Weathering effects on capillary water uptake of natural building stones by using neutron imaging

Building stones are frequently subjected to very intense degradation due to salt crystallization, often responsible for strong modifications of their pore network. These effects have a great influence on the mechanical properties and durability of the materials, and on the penetration of water. In this study, neutron radiography has been used to monitor and visualize in two dimensions the capillary water uptake in a Sicilian calcarenite widely used as building and replacement stone (namely Sabucina stone) and to quantify the water content distribution, as a function of time and weathering degree.

Simona Raneri[1] , Germana Barone[1] , Paolo Mazzoleni[1] , Eva Rabot[2]

[1] Department of Biological, Geological and Environment Sciences, University of Catania, Corso Italia 57, 95129 Catania, Italy
[2] Laboratoire Léon Brillouin, CEA, CNRS, Université Paris-Saclay, CEA Saclay, 91191 Gif-sur-Yvette, France

pmazzol@unict.it

Capillary water uptake is one of the main processes driving water penetration in natural building stones, usually described by the capillary absorption coefficient. The capillary absorption coefficient is the amount of water uptake per square meter as a function of the square root of time. It provides useful information on the material properties when liquids spread over solid surfaces. However, this parameter reflects an overall behavior of the material, without providing detailed information on the dynamic chemical and physical processes that occur when aqueous solutions move and react with the material through its pore system. These aspects are of particular interest in heritage engineering and conservation fields, since water is considered to be the main deterioration agent of buildings and monuments. Indeed, the flow of aqueous solutions and the subsequent chemical and physical interactions with porous materials often lead to degradation due to freeze/thaw cycles, solvent action of water and/or salt crystallization. In this context, the visualization and quantification of water absorption into the pore network of stones could provide additional information on these degradation phenomena.

Neutron imaging has been performed using the IMAGINE station at the Laboratoire Léon Brillouin, CEA Saclay, France. The capillary water uptake monitored with neutron radiography is presented in Fig. 1. In detail, radiographs acquired 5, 10, 15, and 20 min after the addition of water for an unweathered sample and for a sample representative of some degradation degrees are shown, as an example. The dry image is formed from the attenuation of neutrons through the solid particles and air, while the wet images are the result of the sum of the attenuations associated with water, solid articles, and air. Therefore, by normalizing a wet image with a dry reference image of a given stone sample, the 2-D distribution of water can be visualized and the position of the wetting front can be determined from the relative water content profiles. The inspection of the raw neutron radiographs clearly suggests that, in the studied samples, the wetting front is not planar. For this reason, the evaluation of its position has been performed by selecting a vertical column of pixels centered in the samples. In this way, lateral and edge effects have been eliminated and the one-dimensional capillary rise of water has been quantified. The resulting wetting front positions have been related to time, and the results are reported in Fig. 2, where the linearity of the relationship between the wetting front position and the square root of time is clearly illustrated. The sorptivity values have been determined by using linear regression.

In order to quantify the water distribution in the stone samples and to better understand the water uptake process, the thickness of water crossed by the neutron beam as a function of time has been estimated. In Fig. 3, examples of contour plots of the water content distribution (WC%) estimated from the neutron radiographs at 5, 10, 15, and 20 min after the water addition are shown. It is worth noting that the contact time labeled as t0 has to be considered as a reference start value for the evaluation of the whole sequence, as it effectively represents the first wet acquisition available after the manual addition of water and the opening of the neutron beam in safe conditions. Contours describing the quantitative distribution of water inside the stone volumes clearly show that the penetration depth of water at the end of the experiment was substantially higher in the unweathered sample than in the weathered ones. Higher amount of water was absorbed by the weathered samples as compared to the unweathered sample. Figure 3 also highlights the heterogeneity of the pore space of the artificially weathered samples. Additionally, the more intense action of the degradation process close to the surface is evidenced by the fast advancement of the wetting front and the high WC% at the edges of the weathered stone samples as compared to the inner part in the early time steps of the experiment.

In order to quantify the water distribution in the stone

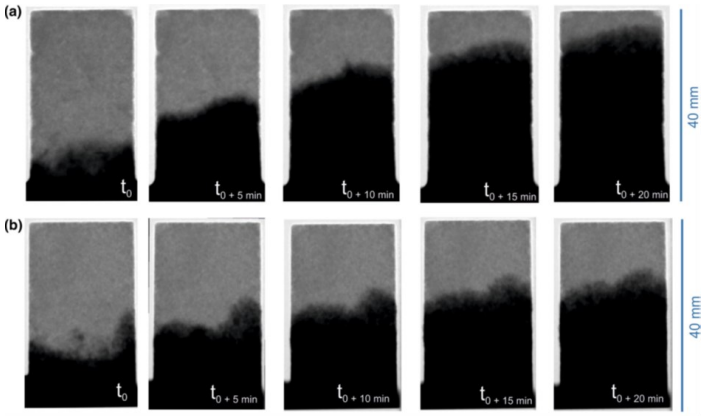

Figure 1: Normalized neutron radiographs at selected time steps during capillary water uptake by Sabucina stones: (a) unweathered sample and samples subjected to (b) 8 artificial weathering cycles. Light gray areas dry conditions, while dark gray areas saturation conditions.

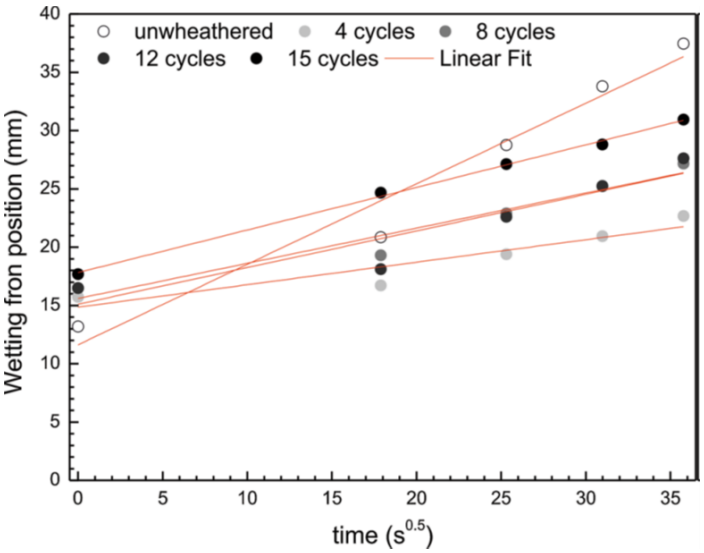

Figure 2 : Wetting front position as a function of the square root of time, for increasing numbers of artificial weathering cycles.

samples and to better understand the water uptake process, the thickness of water crossed by the neutron beam as a function of time has been estimated. In Fig. 3, examples of contour plots of the water content distribution (WC%) estimated from the neutron radiographs at 5, 10, 15, and 20 min after the water addition are shown. It is worth noting that the contact time labeled as t0 has to be considered as a reference start value for the evaluation of the whole sequence, as it effectively represents the first wet acquisition available after the manual addition of water and the opening of the neutron beam in safe conditions. Contours describing the quantitative distribution of water inside the stone volumes clearly show that the penetration depth of water at the end of the experiment was substantially higher in the unweathered sample than in the weathered ones. Higher amount of water was absorbed by the weathered samples as compared to the unweathered sample. Figure 3 also highlights the heterogeneity of the pore space of the artificially weathered samples. Additionally, the more intense action of the degradation process close to the surface is evidenced by the fast advancement of the wetting front and the high WC% at the edges of the weathered stone samples as compared to the inner part in the early time steps of the experiment.

In this study, we used neutron radiography to characterize the effect of weathering on the hydric behavior of a calcarenite used as a building and replace stone in Sicilian monuments, through its capillary water uptake. Neutron imaging allowed monitoring the evolution of the wetting front position and water content as a function of time. Weathering appeared to actually affect the behavior of this stone against water. The water penetration depth at the end of the experiment was substantially higher in the unweathered than in the weathered stones. However, the dynamics of water absorption was faster in the weathered samples, as observed by the sorptivity values derived from the image analysis, and the amount of water absorbed increased with the number of weathering cycles. In the early stages of weathering, the pore network was greatly modified by the crystallization of salts on pore throats, reducing total porosity, mean pore diameter, and connectivity of the pore network. Penetration depth and sorptivity are thus drastically reduced as compared to fresh samples. Then, the weathering process tends to increase the porosity and to enlarge pores, allowing larger amount of water to be retained in weathered samples.

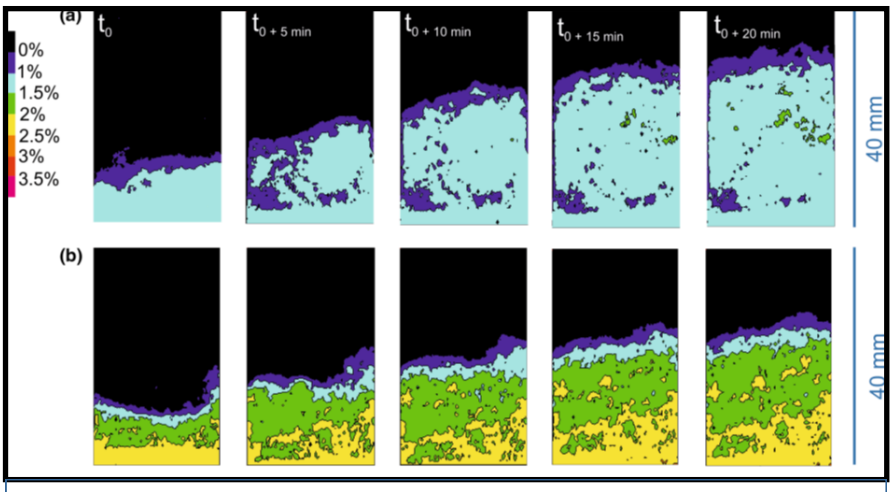

Figure 3: Contour maps of the water content estimated from the neutron radiographs at selected time steps during capillary water uptake by Sabucina stones: an unweathered sample and samples subjected to b 8 and c 15 artificial weathering cycles.

The use of neutron imaging allows us to better understand how salt weathering affects the petrophysical properties of the studied stone and how it influences then the stone response against water, highlighting the role of the pore geometry in the capillary absorption. Additional spatial information on the water absorption process has been gathered. In particular, the depth of water penetration and the heterogeneous distribution of water inside the pore network could affect the depth and intensity of the degradation process during subsequent drying and water absorption cycles.

References

Simona Raneri, Germana Barone, Paolo Mazzoleni, Eva Rabot, Appl. Phys. A (2016) 122:969. DOI 10.1007/s00339-016-0495-8.

When the magnetic anisotropy of molecules reveals its forms to neutrons

We have used polarized neutron diffraction (PND) to determine how the magnetic anisotropy properties of organometallic molecules under magnetic field [1]. These results open new perspectives for the optimization of the magnet molecules to develop ultra-high storage density devices. If successfully implemented, molecular data storage using such materials could store up to 30 terabits of data per square centimeter, about 25000 GBits on a flash drive!

K. Ridier[1], B. Gillon[1], A. Gukasov[1], G. Chaboussant[1], A. Cousson[1], D. Luneau[2], A. Borta[2], R. Checa[2], J.-F. Jacquot[3], Y. Chiba[4], H. Sakiyama[4], M. Mikuriya[5]

[1] Laboratoire Léon Brillouin, CEA/CNRS, F-91191, Gif-sur-Yvette Cedex, France
[2] Laboratoire des Multimatériaux et Interfaces (UMR5615), Université Claude Bernard Lyon 1 (France)
[3] SCIB, UMR-E 3 CEA/UJF-Grenoble 1, INAC (France)
[4] Faculty of Science, Yamagata University Yamagata (Japan)
[5] School of Science and Technology, Kwansei Gakuin University Sanda (Japan)

Gregory.chaboussant@cea.fr

When placed in a magnetic field, some molecular compounds based on magnetic metal ions acquire a remanent magnetization (they stay magnetized when the magnetic field is switched off). This property gives them a behavior analogous to that of the bare magnets but at the molecular scale. They were thus coined "single-molecular magnets". Unlike traditional magnets (metals, alloys and oxides), it is a molecular behavior that opens up prospects for applications in quantum information processing with extremely miniaturized memory units.

To be a "single-molecular magnet" (SMM), the molecule must possess a magnetic moment (S) as well as a strong magnetic anisotropy (D), like a magnet which orients preferentially along some direction under an externa magnetic field. The characteristic time during which the remanent magnetization of the magnet molecules persists is strongly dependent upon D and S. The larger these parameters are, the longer the characteristic time will be. Today, at room temperature, this time is too short for the magnetization to be conserved and this SMM behavior is observed only at temperatures too low to envisage applications but recent progress [2] may quickly open very promising routes towards effective SMM-based devices. The increase in operating temperatures requires to increase in magnetic anisotropy. To do this, it is essential to understand the relations existing between the magnetic anisotropy of the molecule as such, and that of each of the individual metal ions, in relation with the crystalline structure.

To this end, we have used PND, which provides key infor-

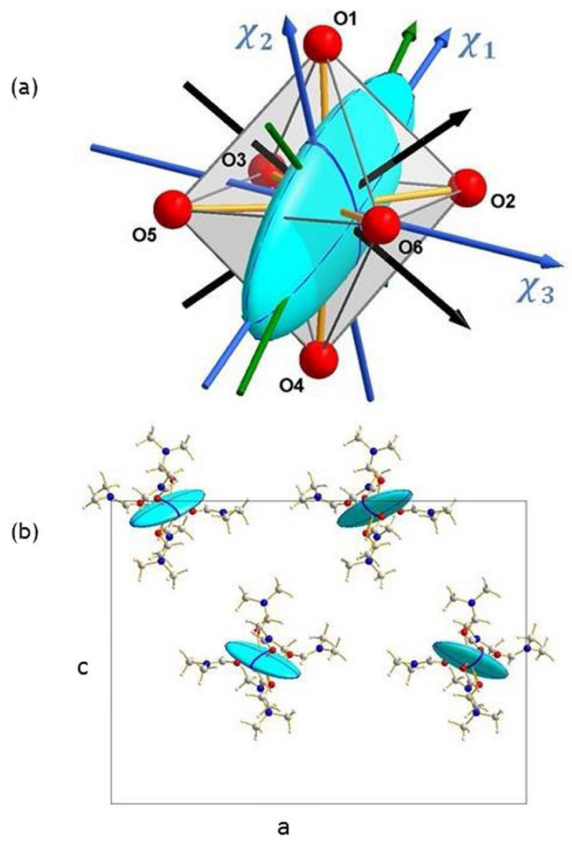

*Figure 1: (a) Representation of the magnetic susceptibility ellipsoid of the Co^{II} ion within its coordination octahedron in complex 1 at 2 K. The C_3 axes of the coordination octahedron are reported: compression in black and elongation in green. The local magnetic principal directions (in blue) are c_1, c_2, and c_3. (b) Projection of the unit cell along the **b** crystallographic direction and representation of the four local magnetic susceptibility tensors.*

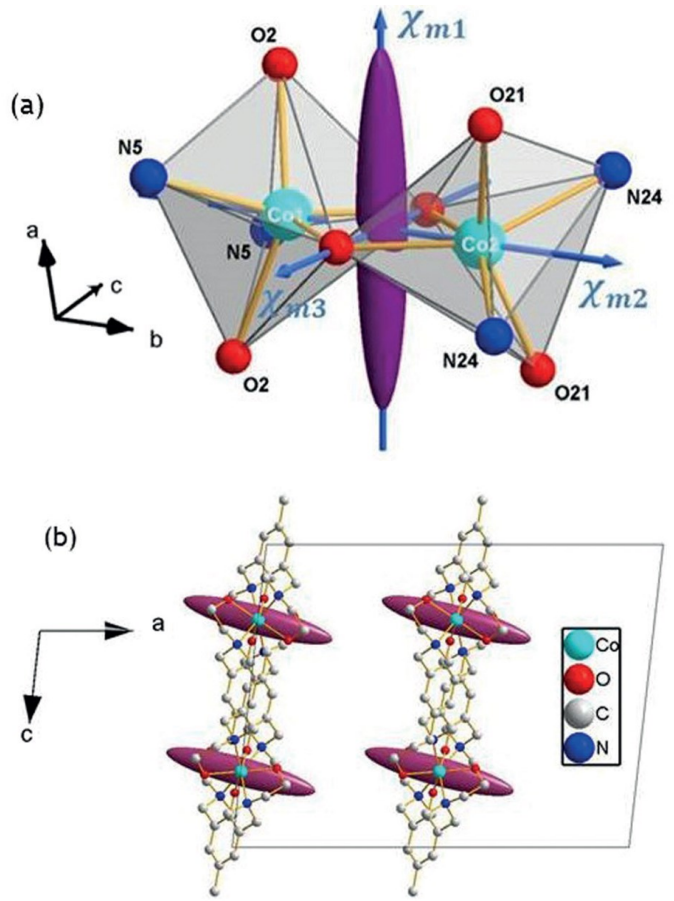

*Figure 2 : Representation of the molecular magnetic susceptibility ellipsoid obtained for complex 2 at 2 K from SQUID measurements. (a) For one molecule in perspective view with the magnetic principal directions c_{m1}, c_{m2}, and c_{m3} indicated by blue arrows. (b) For the four dimers in the unit cell in projection along the **b** axis.*

mation on magneto-structural relationships and applied this technique for the first time to the study of the magnetic anisotropy of two Co(II)-based molecular compounds : one with a single metal center per molecule (1 - Figure 1) and the other with two centers (2 - Figure 2).

In both cases, PND allowed a direct determination of the magnetic anisotropy of the molecule. For complex 1, the study clearly reveals the correlation between magnetic anisotropy and the environment of the CoII ion. For complex 2, the study showed how the magnetic anisotropy of the two cobalt (II) ions deviates from that of the isolated ion under the effect of their exchange interaction. This type of magnetic characterization at the atomic scale could not have been obtained by other experimental techniques. The generalization of the method to other molecular systems should contribute to a better understanding of the molecular magnetic anisotropy necessary for the optimization and designed of SMMs.

References

*[1] K. Ridier [LLB PhD thesis 2014], B. Gillon, A. Gukasov, G. Chaboussant, A. Cousson, D. Luneau, A. Borta, J.-F. Jacquot, R. Checa, Y. Chiba, H. Sakiyama and M. Mikuriya, "Polarized Neutron Diffraction as a Tool for Mapping Molecular Magnetic Anisotropy: Local Susceptibility Tensors in Co^{II} Complexes", Chemistry - A European Journal **22**, 724 (2016).*

*[2] F-S Guo et al, Angew. Chem. Int. Ed. **56**, 11445 (2017); C.A.P. Goodwin et al, Nature **548**, 439 (2017).*

Real-time observation of the isothermal crystallization kinetics in a deeply supercooled liquid

Below the melting temperature Tm, crystals are the stable phase of typical elemental or molecular systems. However, liquids can be supercooled well below Tm, eventually forming a glass below the glass transition temperature Tg. Despite their long lifetimes, supercooled liquids and glasses are intrinsically metastable states and prone to crystallize. We investigated the kinetics of the isothermal crystallization of the strong glassformer GeO2 in the deep supercooled liquid at 1100 K, about half-way between Tm and Tg. The crystallization process has been observed through time-resolved neutron diffraction for about three days. Data show a continuous reorganization of the amorphous structure towards the α-quartz phase, and the final material is composed by crystalline domains plunged into a, low-density, residual amorphous matrix. The time evolution of the relative fractions of crystal and amorphous was interpreted by means of a predator-prey-like mechanism between crystal and amorphous, where the density variation acts as a blocking barrier.

M. Zanatta[1], L. Cormier[2], L. Hennet[3], C. Petrillo[4], F. Sacchetti[4]

[1] Dipartimento di Informatica, Università di Verona, I-37134 Verona, Italy

[2] Institut de Minéralogie, de Physique des Matériaux, et de Cosmochimie (IMPMC), Sorbonne Universités, UPMC Université Paris 06, CNRS UMR 7590, Muséum National d'Histoire Naturelle, IRD UMR 206, F-75005 Paris, France

[3] Conditions Extrêmes et Matériaux: Haute Température et Irradiation, CEMHTI-CNRS, Université d'Orléans, F-45071 Orléans, France and Laboratoire Léon Brillouin, CEA-CNRS, CEA Saclay, F-91191 Gif sur Yvette, France

[4] Dipartimento di Fisica e Geologia, Università di Perugia, I-06123 Perugia, Italy and IOM-CNR c/o Dipartimento di Fisica e Geologia, Università di Perugia, I-06123 Perugia, Italy

marco.zanatta@univr.it

Crystallization of amorphous systems is a very common process whose relevance goes well beyond fundamental condensed matter physics and derives from the universality of glasses and supercooled liquids in everyday life. Typical examples span from geology to material science, including also biophysics and pharmacology. Crystallization can be described by the combination of two processes: nucleation and growth. Spontaneous fluctuations in the amorphous system trigger the formation of small crystallites that in certain conditions can grow, leading to a macroscopic crystallization of the amorphous system.

Here we focused on the kinetics of the isothermal crystallization process in the deep supercooled liquid, namely at a temperature $T \ll T_m$. In this regime, the viscosity is so high that the system is macroscopically solid and structural rearrangements are so slow that atoms can be thought as frozen. Nevertheless, the structure of an amorphous solid is never really frozen, and local non diffusive relaxations can lead to crystallization.

As a benchmark system, we choose vitreous germania v-GeO_2, a prototypical strong glass with a structure based on corner-sharing tetrahedral, T_m = 1388 K and $T_g \simeq$ 818 K. Starting from the glass, we approached the supercooled liquid by heating the system up to T_{exp} = 1100 K. In this condition, GeO_2 still has dynamical and structural properties very similar to those of the glass. However, with time going on the system begins to crystallize, and we have observed the kinetics of this process by collecting a set of static structure factors for about 67 h (see Figure 1a). The crystallization process is summarized in Figure 1b that shows a com-

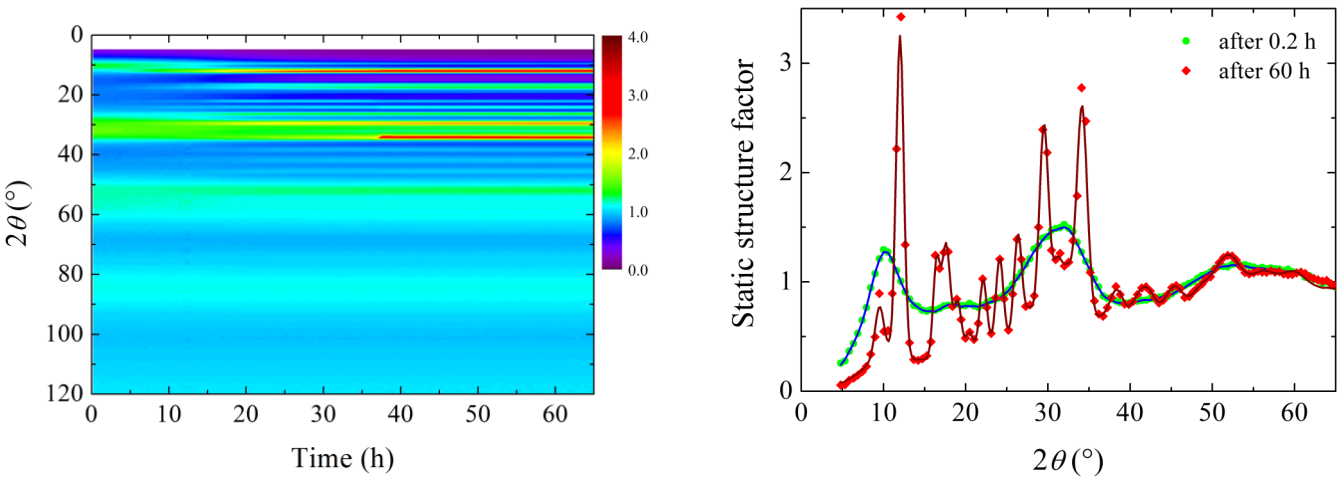

Figure 1: (left) Time evolution of the static structure factor of GeO_2 at T_{exp} = 1100 K. Time increases from left to right. The color map shows the emergence of the crystalline pattern. (right) Static structure factor S(2θ) measured after 0.2 h (green circles) and after 60.0 h (red diamonds) showing the emergence of a GeO_2 α-quartz-like structure ($P3_221$). The solid lines represent the fit used to determine the fraction of atoms in the crystalline and amorphous phases.

parison between the fully amorphous $S(2\theta)$ measured at T_{exp} and one acquired after 60 h.

The position of the Bragg peaks observed in the latter is compatible with that of the α-quartz, and no traces of other crystalline structures are visible. This implies that the crystallization process preserves the chemical composition without any appreciable phase separation.

The fraction of atoms in the crystalline (A_c) and amorphous (A_a) phase was extracted (see Figure 2). Crystallization becomes appreciable after 4 h, and then it rapidly develops by subtracting material from the amorphous phase. After about 30 h, the crystallization rate slows down leading to a final material where 77% of the atoms is organized in the α-quartz structure, whereas the remaining 23% still shows amorphous features.

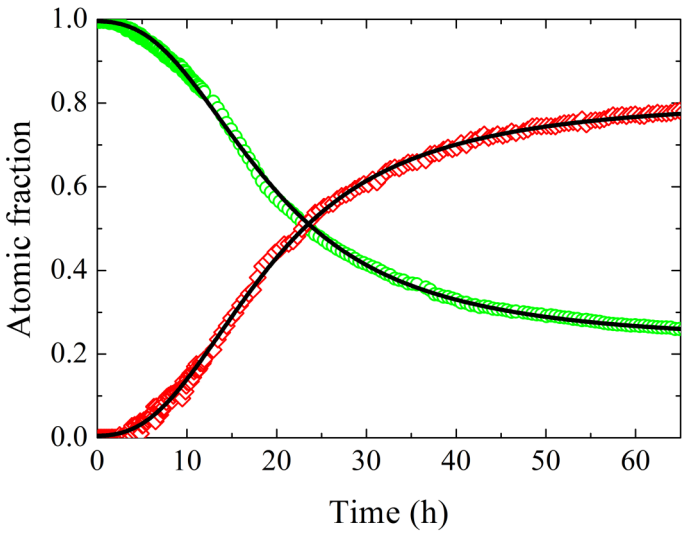

Figure 2: Time evolution of the crystalline and amorphous fractions, A_c and A_a, red open diamonds and green open circles respectively. The solid line represents the fit with the model, as described in the text.

The standard framework to describe the time evolution of the fraction of transformed material during isothermal crystallization is the Johnson-Mehl-Avrami-Kolmogorov (JMAK) model. This approach is based on the nucleation and growth processes, and it assumes that the nucleation occurs randomly with a large number of spherical transforming regions. Growth is the same for all these regions and it stops at points of impingement, continuing elsewhere. This results in a complete crystallization of the starting material, which is in contrast with the results shown in Fig. 2. Thus, the JMAK model fails in describing the observed long-time behavior.

To describe our data, we developed an empirical model for the kinetics of this crystallization process allowing for a non-complete transformation of one phase into the other. We took into account the density difference between the amorphous and the crystal phases, which causes a rarefaction in the amorphous medium around the crystal during its growth. In absence of diffusion, these depleted interfaces act as a barrier for a further growth. The same mechanism involves also the nucleation that becomes less probable as the population of nuclei increases. The density difference between the amorphous and crystalline phases can be considered as a feedback mechanism that controls the growth of the crystal. The so-established predator-prey equilibrium inhibits further growth at a given crystallite size. In particular, this process introduces a slowing down of the growth function at short time with respect to the simple case where diffusion provides material to the nucleating phase. This short time behavior is already evident from the $S(2\theta)$ data of Fig. 1, and it is well described by the model, as shown in Fig. 2 (solid lines). The model can be further extended accounting for the effect of the diffusion. In fact, even though the diffusion contribution seems negligible over the observed timescale, it could give rise to long-time effects that are expected to become dominant as T_m is approached.

References

M. Zanatta, L. Cormier, L. Hennet, C. Petrillo & F. Sacchetti, Scientific Reports | 7:43671

Macromolecules

Article

pubs.acs.org/Macromolecules

Thermoresponsive Toughening in LCST-Type Hydrogels with Opposite Topology: From Structure to Fracture Properties

Hui Guo,[†,‡] Cécile Mussault,[†,‡] Annie Brûlet,[§] Alba Marcellan,*[,†,‡] Dominique Hourdet,*[,†,‡] and Nicolas Sanson*[,†,‡]

[†]École Supérieure de Physique et de Chimie Industrielles de la Ville de Paris (ESPCI), ParisTech, PSL Research University, Sciences et Ingénierie de la Matière Molle, CNRS UMR 7615, 10 rue Vauquelin, F-75231, Paris cedex 05, France

[‡]Sorbonne-Universités, UPMC Université Paris 06, SIMM, 10 rue Vauquelin, F-75231 Paris cedex 05, France

[§]Laboratoire Léon Brillouin (UMR 12 CEA CNRS), CEA Saclay, F-91191 Gif-sur-Yvette Cedex, France

Supporting Information

ABSTRACT: The challenge of this work was to investigate the role of topology in LCST hydrogels that strongly and reversibly thermo-reinforce their mechanical strength under isochoric conditions. To achieve this, two different hydrogels with opposite topologies were designed on the basis of grafted architectures using equal amounts of water-soluble chains (poly(*N*,*N*-dimethylacrylamide) = PDMA) and LCST polymer chains (poly(*N*-isopropylacrylamide) = PNIPA). By working under isochoric conditions, with almost 85 wt % of water in the whole temperature range (20−60 °C), we were able to clearly highlight the impact of the phase transition of PNIPA on the mechanical reinforcement of the gel without any interference of the volume transition. These graft hydrogels, designed with PNIPA in the backbone (GPN-D) or as pendant chains (GPD-N), have been studied more specifically by tensile tests and 2D neutron scattering at rest and under deformation. From these complementary techniques, we show that PNIPA side-chains in GPD-N self-assemble above their transition temperature into a micellar network greatly interfering with the covalent PDMA frame. While the elastic modulus increases reversibly more than ten times throughout the phase transition, other properties like elongation at break and fracture resistance are greatly enhanced with temperature. At high temperature and under extension, SANS data highlight the affine deformation of PNIPA domains. By comparison, the opposite topology with PNIPA forming the cross-linked backbone undergoes a similar phase separation with temperature and gives rise to a bicontinuous structure that aligns under loading. The collapsed phase being topologically defined as the load bearing phase, GPN-D displays remarkable fracture toughening with crack bifurcation at high temperature whereas GPD-N gels fracture in a more conventional way.

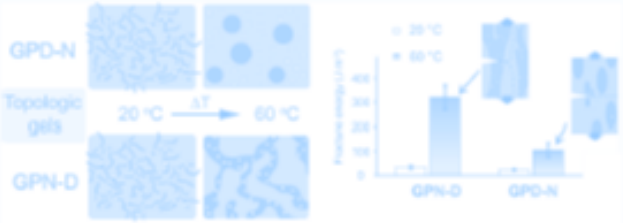

Thermo-Toughening of Hydrogels under Isochoric Condition

INTRODUCTION

During the last few decades, covalent hydrogels have received considerable attention due to their important potential as biological containers or mechanical transducers. They are actually used in many bioapplications[1−4] such as superabsorbents, contact lenses, drug delivery systems, or scaffolds for tissue engineering, but they intrinsically suffer from their poor mechanical strength. More recently, new challenges have emerged in this field such as the reinforcement of the mechanical properties in order to elaborate smart and innovative polymer-based materials. On one hand, one can find original covalent architectures like double networks,[5] slide-ring gels,[6] or tetra-PEG gels,[7] which have been shown to strongly improve the mechanical properties in terms of stiffness, fracture toughness or stretchability. On the other hand, a more versatile approach consists in introducing physical interactions into the covalent network. In this case, the reinforcement of mechanical properties has been nicely demonstrated with nanocomposite[8] and hybrid networks,[9] which develop reversible interactions between the polymer matrix and inorganic nanofillers like clay platelets or silica nanoparticles. In these examples, hybrid hydrogels showed improved mechanical response with an increase of modulus, dissipation, and fracture properties. This idea to mix both reversible and covalent cross-links within the same structure to get tough hydrogels has been extended afterward to other physical interactions. We can mention for instance hydrophobically modified hydrogels,[10−12] which show a large increase of their extensibility and resistance to crack propagation due to a "costly" deformation of hydrophobic associations under stress, or other mixed systems involving complex formation like calcium alginates embedded in a cross-linked polyacrylamide network[13] or polyampholyte hydrogels.[14] With these examples, it is clearly shown that the mechanical

Received: April 16, 2016
Revised: May 18, 2016
Published: May 26, 2016

DOI: 10.1021/acs.macromol.6b00798
Macromolecules 2016, 49, 4295−4306

Soft complex matter and biophysics

The axis "Soft Matter and Biophysics" deals with systems made of individual building blocks (molecular systems, colloidal nanoparticles, polymers, surfactants, proteins and phospholipids) whose characteristic sizes lay in the 0.1–10 nm range. In such systems, the delicate balance of interactions (of the order of kBT) can lead to the formation of large self-assembled complex architectures showing specific dynamics, kinetics or lifetime. Understanding the underlying mechanisms of their self-assembly and dynamics is then the key to control and tune the very specific properties of inert, functional or biological matter at the nanometer scale (1-100 nm). In this framework, the neutron scattering techniques combined with H/D isotopic labeling are a unique tool to characterize the systems at the relevant spatial and temporal scales of the systems. In particular, they make it possible to get a refined picture of the behavior of thermoresponsive Toughening in Grafted or Semi-interpenetrated network (Guo et al), of the mechanisms of formation of electrostatic complexes of polyelectrolytes and nanoparticles of opposite charges (Shi et al) and of the formation of rod-like supramolecular polymers based on mixture of bis-urea stickers (Ressouche et al). They also enable to get an insight on modification of properties of liquids that occur in confined geometries, in particular the specific phase transitions undergone by water in 2D confinement (Zanotti et al) or the existence of a micro-phase-separated state of binary fluids confined in nanometric channels (Abdel Hamid et al).

- **Thermoresponsive Toughening in Grafted or Semi-interpenetrated network of LCST-Type Hydrogels**

  H. Guo, C. Mussault, A. Brûlet, D. Hourdet, A. Marcellan, N. Sanson

- **Role of the ratio of biopolyelectrolyte persistence length to nanoparticle size in the structural tuning of electrostatic complexes**

  Li Shi, Florent Carn, François Boué, Eric Buhler

- **Competing coexisting phases in two-dimensional water**

  Jean-Marc Zanotti, Patrick Judeinstein, Simona Dalla-Bernardina, Gaëlle Creff, Jean-Blaise Brubach, Pascale Roy, Marco Bonetti, Jacques Ollivier, Dimitrios Sakellariou, Marie-Claire Bellissent-Funel

- **Neutrons reveal the micro-phase-separated state of confined binary fluids**

  A. R. Abdel Hamid, C. Alba-Simionesco, S. Dutta, B. Frick, A. Ghoufi, R. Lefort, R. Mhanna, D. Morineau, L. Noirez, F. Porcher

- **Two-component self-assemblies: investigation of a synergy between bis-urea stickers**

  E. Ressouche, S. Pensec, B. Isare, J. Jestin, L. Bouteiller

Thermoresponsive Toughening in Grafted or Semi-interpenetrated network of LCST-Type Hydrogels

Thermo-responsive hydrogels were designed using equal amounts of water-soluble chains (poly(N,N-dimethylacrylamide) = PDMA) and LCST polymer chains (poly(N-isopropylacrylamide) = PNIPA) and a large amount of water (85 wt%). On the basis of grafted architectures, two opposite topologies were prepared: grafted gels either with PNIPA as the backbone, or its opposite, i.e. with PNIPA as pendant chains. From a comprehensive investigation performed under isochoric conditions by coupling mechanical tests and small-angle neutron scattering (SANS) we show that both topologies demonstrate a large mechanical reinforcement driven by the phase separation of PNIPA above its LCST. Nanostructures of hydrogels determined at rest upon scanning the temperature and upon deformation at high temperature allow understanding the specificity of each topology in the thermo-toughening mechanism.

H. Guo[1,2], C. Mussault[1,2], A. Brûlet[3], D. Hourdet[1,2], A. Marcellan[1,2], N. Sanson[1,2]

[1] École Supérieure de Physique et de Chimie Industrielles de la Ville de Paris (ESPCI), ParisTech, PSL Research University, CNRS UMR 7615, 10 rue Vauquelin, F-75231, Paris cedex 05, France

[2] Sorbonne-Universités, UPMC Université Paris 06, SIMM, 10 rue Vauquelin, F-75231 Paris cedex 05, France

[3] Laboratoire Léon Brillouin, CEA, CNRS, Université Paris-Saclay, CEA Saclay, 91191 Gif-sur-Yvette, France

dominique.hourdet@espci.fr

Polymer hydrogels, which are three-dimensional networks swollen in water, have received considerable attention during the past decades due to their high potential as soft materials, water containers, texture modifiers, or mechanical transducers. In the aim of bio-applications, many efforts are made to reinforce the mechanical properties of these soft and wet materials, which are intrinsically weak. Two different approaches are generally envisaged to improve their properties: either to homogenize the stress distribution within the network or to develop dissipation mechanisms by introducing sacrificial bonds (covalent or physical). Although physical interactions are reversible in nature, they are generally not finely controlled and the preparation of hydrogels containing large amount of hydrophobic groups also requires several steps of synthesis and/or solvent exchange.

Recently, we propose to tune these secondary interactions within the hydrogel by playing with the thermodynamic properties of polymers in aqueous media. For that purpose, we selected poly(N-isopropylacrylamide) (PNIPA) for its well-known LCST behavior around 32°C, and we introduced a hydrophilic counterpart, a poly(N,N-dimethylacrylamide) (PDMA), in order to maintain a high level of swelling for the hydrogel in the segregated regime of PNIPA.

Tuning the properties of hydrogels via thermodynamic of polymers in water has been successfully demonstrated with grafted architectures prepared with equal weight fractions of PNIPA and PDMA and a high amount of water, almost 85 wt % [1-2]. Comparison between hydrogels of opposite topologies, a cross-linked PNIPA grafted with PDMA pendant chains and a cross-linked PDMA grafted with PNIPA pendant chains (named GPN-D and GPD-N, respectively) is made. By scanning the temperature up to 60 °C, it was shown that grafted hydrogels were able to keep their high original swelling in the whole range of temperature and to develop in isochoric conditions a strong and reversible thermo-toughening with a 10-fold increase of the elastic modulus above the phase transition of PNIPA [2]. Small-angle neutron scattering (SANS) experiments were performed at rest upon scanning the temperature up to above the phase transition of PNIPA, and under uniaxial stretching in order to determine the structures and their evolution upon loading. Two different structures were deduced from the scattered intensity profiles at rest for the opposite grafted topologies (see Figure 1): a micellar morphology in GPD-N gels (with PNIPA as pendant chains) and a bi-continuous phase structure in the GPN-D gels (PNIPA as cross-linked backbone).

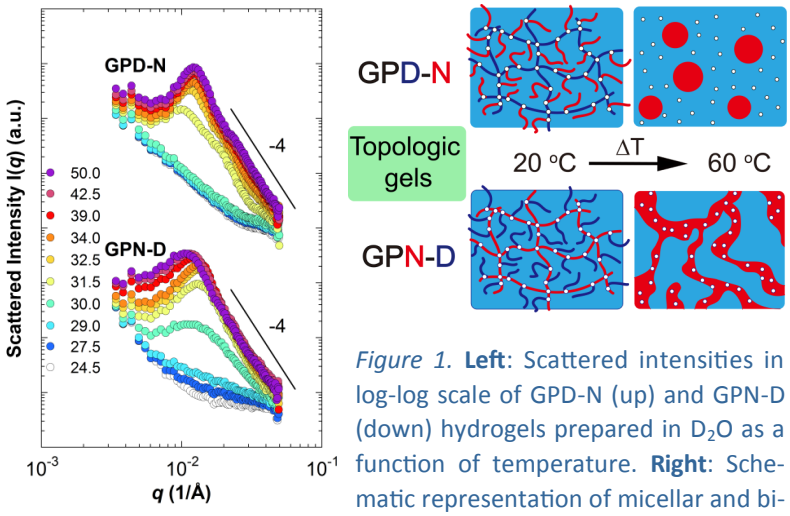

Figure 1. **Left**: Scattered intensities in log-log scale of GPD-N (up) and GPN-D (down) hydrogels prepared in D_2O as a function of temperature. **Right**: Schematic representation of micellar and bi-continuous structures developed at high temperature by GPD-N and GPN-D, respectively. *PNIPA-rich domains (red), PDMA swollen phase (blue) and chemical cross-linkers (white dots) [2].*

Under stretching, the diffraction rings observed for both GPD-N and GPN-D hydrogels corresponding to the mean distances between PNIPA micro-domains are deformed (see Figure 2). For intermediate stretching ratio (λ = 1.75), the

pattern of GPD-N (Figure 2a) changes to a rather uniform elliptically shaped correlation band qualitatively showing that PNIPA micro-domains move apart in the stretching direction while they get closer in the perpendicular direction due to the transverse compression. At higher deformation, the 2D spectrum turns to a non-uniform azimuthal intensity distribution, effectively showing up diffraction arcs and then spots for λ ≥ 2 in the perpendicular direction. This threshold value of λ corresponds to the initiation of irreversible macroscopic processes (see Figure 2c), suggesting damage phenomenon within the network. At very high deformation (λ = 2.5–3), four additional spots are clearly observed: they highlight some reorganization within the microstructure that is originated from the disruption of elongated micro-domains occurring above some critical stress. In comparison, the isotropic circular pattern of GPN-D rapidly turns into an elliptically shaped correlation band with a non-uniform azimuthal intensity distribution with two diffraction spots above λ = 2 in the perpendicular direction (see Figure 2d). In this case, the structural changes are highly recoverable, up to λ = 4, as shown in Figure 2c. The GPN-D topology is capable to maintain 94% of its initial modulus with a negligible residual strain. At higher deformation (λ = 3–5), the anisotropy becomes even more important. Qualitatively, this means that the inter-domains distance in GPN-D is preserved in the perpendicular direction during the process of domains deformation. The stress–strain mechanical response highlights the formation of PNIPA-rich domains that strongly enhances the stiffness of the mechanical response (i.e., the initial modulus is increased by 1 order of magnitude), independently of the gels topologies (see Figure 2b). Interestingly, both stiffness and elongation at break are simultaneously enhanced. Moreover, by introducing an initial edge notch on the gel, a clear distinction between toughening mechanisms at play in GPD-N and GPN-D topologies can be drawn. As shown in Figure 2e, the fracture resistance is greatly improved at 60 °C for both microphase-separated gels, but the thermo-toughening mechanism operates differently for the two opposite gel topologies; the GPN-D structure with PNIPA forming the cross-linked network being more efficient and exhibiting a systematic crack bifurcation although the crack proceeds straightly in GPD-N.

Complementary experiments were performed with semi-interpenetrated networks of similar composition (PDMA/PNIPA 50/50): a linear PNIPA embedded into a cross-linked PDMA matrix or the opposite, clearly emphasize the impact of the topology with a more efficient thermo-toughening behavior when the concentrated PNIPA phase percolates within the hydrogel [3].

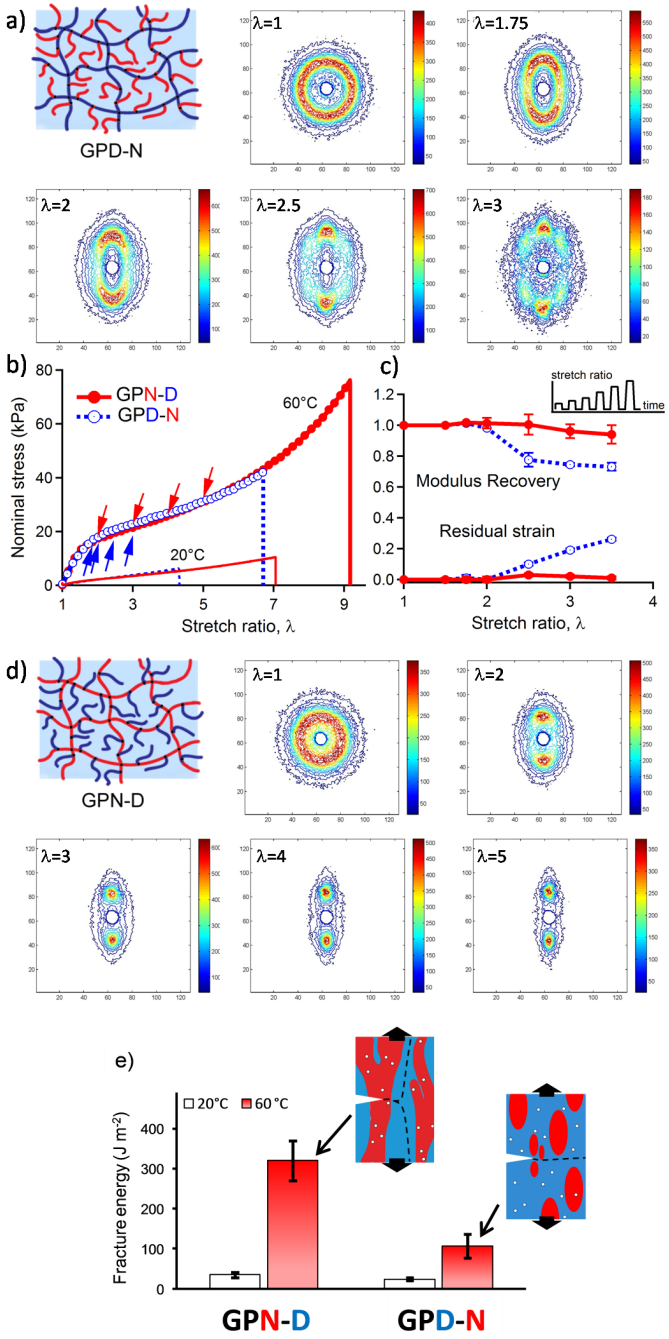

Figure 2. Structure and properties of GPD-N and GPN-D under deformation. (a and d) Primary structure of GPD-N and GPN-D, respectively, along with their iso-intensity SANS patterns obtained after a step-by-step loading at 60 °C. The direction of the uniaxial deformation is along the horizontal axis. (b) Uniaxial tensile stress–strain curves of GPN-D (red continuous line) and GPD-N (blue dashed line) hydrogels at 20 and 60 °C. The arrows refer to the elongation ratio studied by SANS. (c) Modulus recovery and residual strain at 60 °C for GPN-D (red continuous line) and GPD-N (blue dashed line) after a series of loading/unloading steps up to different maximal stretch ratio. (e) Fracture energies obtained at 20 and 60 °C with a schematic representation of the reinforcing mechanisms at microscale ..

References

[1]. Hui Guo, Nicolas Sanson, Dominique Hourdet, Alba Marcellan Advanced Materials. 2016,28, pp5857- 5864

[2]. Hui Guo, Cécile Mussault, Annie Brûlet, Alba Marcellan, Dominique Hourdet, and Nicolas Sanson, Macromolecules, **2016,** *49* (11), pp 4295–4306.

[3]. Hui Guo, Alba Marcellan and Dominique Hourdet, Macromolecules, **2016**, *49* (24), pp 9568–9577.

Role of the ratio of biopolyelectrolyte persistence length to nanoparticle size in the structural tuning of electrostatic complexes

Aggregation of nanoparticles of given size R induced by addition of a polymer strongly depends on its degree of rigidity (persistence length). This is shown here on a large variety of silica nanoparticle self-assemblies obtained by electrostatic complexation with carefully selected oppositely charged biopolyelectrolytes of different rigidity. SANS evidences the fractal aggregates; Df varies from 1 (linear) to 2.8 (compact).

Li Shi [1,2], Florent Carn [1] François Boué [2,3] and Eric Buhler [1,2]

[1] Matière et Systèmes Complexes (MSC) Laboratory, UMR CNRS 7057, University Paris Diderot-Paris 7, Sorbonne Paris Cité, Bâtiment Condorcet, 75205 Paris Cedex 13, France

[2] Laboratoire Léon Brillouin, CEA, CNRS, Université Paris-Saclay, CEA Saclay, 91191 Gif-sur-Yvette, France

[3] GMPA, UMR INRA 782-AgroParisTech-UPSay, 1 avenue Lucien Brétignières, 78850 Thiverval-Grignon, France

francois.boue@inra.fr, eric.buhler@univ-paris-diderot.fr

The effective rigidity is quantified by the total persistence length L_T representing the sum of the intrinsic (Lp) and electrostatic (Le) polyelectrolyte persistence length, which depends on the screening, i.e., on ionic strength due to counterions and external salt concentrations. We experimentally show that the ratio L_T/R is the main tuning parameter that controls the fractal dimension Df of the nanoparticles self-assemblies, which is determined using small-angle neutron scattering:

(i) For $L_T/R < 0.3$ (with flexible poly-L-lysine in the presence of an excess of salt), chain flexibility promotes, by easy wrapping around nanoparticles in excess, ramified structures ($D_f \sim 2$).

(ii) For $0.3 < L_T/R < 1$ (semiflexible Chitosan or Hyaluronan complexes), chain stiffness induces one-dimensional nanorods (in excess of nanoparticles), in agreement with simulations.

(iii) For $L_T/R > 1$, Le is strongly increased due to the absence of salt and repulsions between nanoparticles cannot be compensated for by the polyelectrolyte wrapping, which allows a spacing between nanoparticles and the formation of one-dimensional pearl necklace complexes.

(iv) Finally, electrostatic screening, i.e., ionic strength, turned out to be a reliable way of controlling Df and the phase diagram behaviour. It finely tunes the short-range inter-particle potential, resulting in larger fractal dimensions at higher ionic strength.

Hence, a universal account of ionic strength I through the

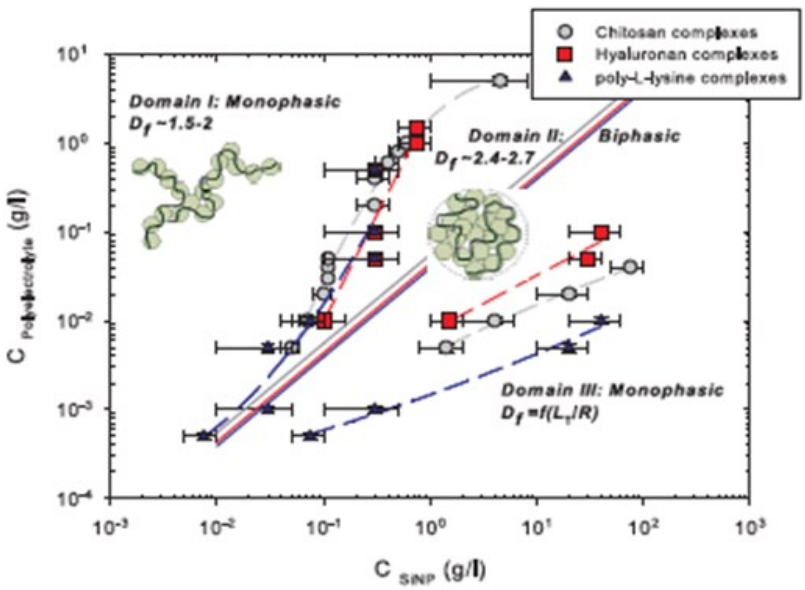

Figure 1. Sequence of phase behaviours in the PEL-SiNP concentration plane at T = 20 ◦C and high ionic strength. For Chitosan, Hyaluronan, and PLL systems, mixtures are prepared in H2O in the presence of 0.2 M CH3COONa, 0.1 M NaCl, and 0.2 M KBr, respectively. The continuous gray, red, and blue lines indicate the stoichiometric thresholds corresponding to a charge ratio [+]/[–] = 1 for chitosan, HA, and PLL complexes, respectively.

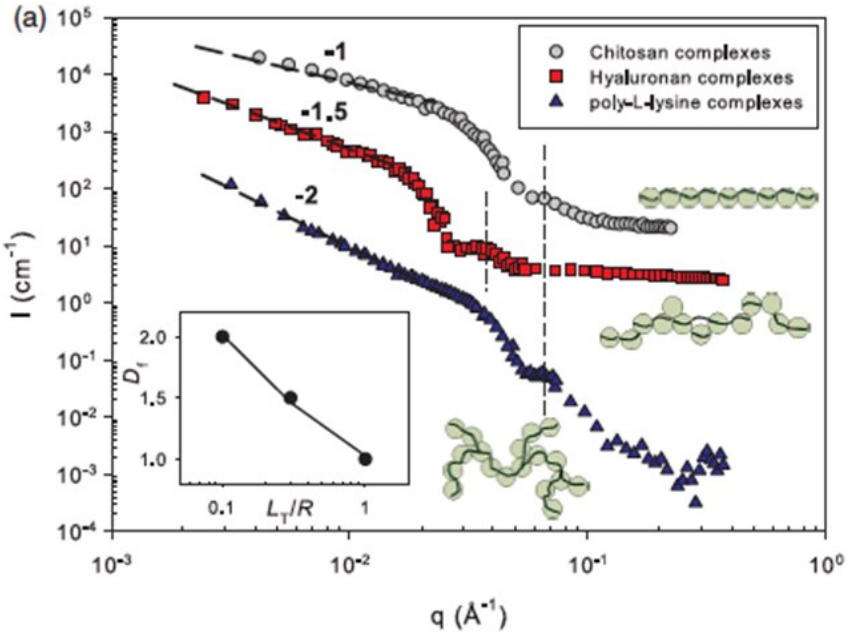

Figure 2. SANS profiles collected at high ionic strength, I, and 20 °C, of the three PEL complexes: 0.01 g/l chitosan-10 g/l SiNP, 0.01 g/l HA–2 g/l SiNP, and 0.01 g/l PLL–10 g/l SiNP (monophasic and representative of domain III in D2O) solutions are prepared in the presence of 0.2 M CH3COONa, 0.1 M NaCl, and 0.2 M KBr, respectively. For clarity, Hyaluronan and Chitosan complexes spectra have been shifted by two and three log units along the y axis with respect to that of PLL complexes, respectively. All curves exhibit the first oscillation associated with the form factor of the SiNPs cross-section occurring around 6.5 × 10−2 °A−1 (9.2 nm SiNP−) or 3.5 × 10−2 °A−1 (17 nm SiNP+) for Chitosan and PLL or Hyaluronan complexes, respectively (see dashed lines and Appendix). The inset represents the variation of Df with the characteristic ratio L_T/R (in presence of 0.1 or 0.2 M external salt, L_T = Lp).

total persistence length L_T is obtained. Low-dimensional NP assemblies, such as well-defined compact nanorods obtained for $L_T/R \sim 1$, open routes toward alternative applications such as a plasmon-based waveguide, biosensors, nano-rulers, theragnostic materials, or cancer cell therapy (e.g., with gold nanoparticles). Opposite to elaborate procedures, such as rod-like nanocrystals syntheses, this basic approach of self-assembly of preformed spherical NPs leads to nanorods with well-defined length, determined by the PEL contour length, and monodisperse cross section (the cross-section radius and polydispersity values are similar to those of free NPs). On the other hand, pearl necklace nanorods obtained for $L_T/R > 1$ at low I could have strong interest by tuning the distance between NPs and hence some electromagnetic properties. One may thus foresee that our approach can be applied to a variety of developments involving other types of nanoparticles—such as gold and metallic ones, proteins, or viruses—covering a wide range of applications in materials as well as in the biological sciences.

References

This paper : Li Shi, F. Carn, F. Boué, E. Buhler, Physical Review E 2016, E 94, 032504

Optimized synthesis of cationic gold nanoparticles and their self-assembly with a flexible polyelectrolyte, Li Shi, F. Boué, E. Buhler, F. Carn, Langmuir 2015, 31, 5731-5737

Control over the electrostatic self-assembly of nanoparticle semiflexible biopolyelectrolyte complexes, Li Shi, F. Carn, F. Boué, G. Mosser and Eric Buhler, Soft Matter 2013, 9, 5004-5015

Nanorods of well-defined length and monodisperse cross-section from stable electrostatic complexation of nanoparticles and semiflexible biopolymers F. Carn, L. Shi, F. Boué, E. Buhler, ACS Macroletters 2012 1 (7), 857–861

Competing coexisting phases in two-dimensional water

The properties of bulk water come from a delicate balance of interactions on length scales encompassing several orders of magnitudes: i) the Hydrogen Bond (HBond) at the molecular scale and ii) the extension of this HBond network up to the macroscopic level. We have addressed the physics of water when the three dimensional extension of the HBond network is frustrated, so that the water molecules are forced to organize in only two dimensions. We account for the large scale fluctuating HBond network by an analytical mean-field percolation model. This approach provides a coherent interpretation of the different events experimentally (calorimetry, neutron, NMR, near and far infra-red spectroscopies) detected in interfacial water at 160, 220 and 250 K. Starting from an amorphous state of water at low temperature, these transitions are respectively interpreted as the onset of creation of transient high density patches of 4-HBonded molecules at 160 K, the percolation of these domains at 220 K and finally the total invasion of the surface by them at 250 K. The source of this surprising behavior in 2D is the frustration of the natural bulk tetrahedral local geometry and the underlying very significant increase in entropy of the interfacial water molecules.

Jean-Marc Zanotti[1], Patrick Judeinstein[1,2], Simona Dalla-Bernardina[3], Gaëlle Creff[3], Jean-Blaise Brubach[3], Pascale Roy[3], Marco Bonetti[4], Jacques Ollivier[5], Dimitrios Sakellariou[6] and Marie-Claire Bellissent-Funel[1]

[1] Laboratoire Léon Brillouin, CEA, CNRS, Université Paris-Saclay, CEA Saclay, 91191 Gif-sur-Yvette Cedex, France.

[2] ICMMO, (UMR CNRS 8182), Univ. Paris-Sud, Université Paris-Saclay, 91405 Orsay, France.

[3] Synchrotron SOLEIL, L'Orme des Merisiers, BP 48, Gif-sur-Yvette Cedex F-91192, France.

[4] SPEC, CEA, CNRS, Université Paris-Saclay, CEA Saclay, 91191 Gif-sur-Yvette Cedex, France.

[5] Institut Laue Langevin, *38042 Grenoble CEDEX,* France.

[6] NIMBE, CEA, CNRS, Université Paris-Saclay, CEA Saclay, 91191 Gif-sur-Yvette Cedex, France

Jean-marc.zanotti@cea;fr

In bulk water, local energetics and long-range connectivity come along with a very specific local three-dimensional (3D) tetrahedral organization of the Hydrogen Bond (HBond) network (Fig.1a). Altogether these properties drive the numerous so-called "water anomalies", for example the apparent power-law divergence of thermodynamical (thermal expansivity, specific heat) and dynamical (self-diffusion coefficient) quantities toward a singular region of the phase diagram at $T_s \approx 228$ K and $P_s \approx 100$ MPa.

Recently[1], we have explored deeper the physics of a HBond network to observe what happens when its three dimensional extension is frustrated, so that the water molecules are forced to organize in only two dimensions (2D).

A striking hint that this situation might be interesting is provided by calorimetry. Compared to bulk hexagonal ice, interfacial water shows a large specific-heat suggesting specific dynamical modes at low temperature. And indeed, Synchrotron-based far and near Infra-Red spectroscopy evidences phases and/or dynamical transitions in the 160, 220 and 250 K regions. Solid-state Quadrupolar NMR reveals a strong dynamical heterogeneity of this interfacial water due to the coexistence of a liquid-like and a solid-like phase. The temperature dependence of those two phases can be directly inferred from the NMR spectra.

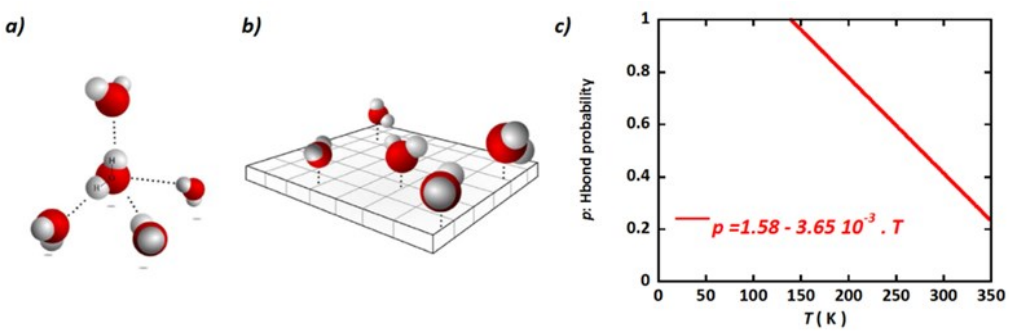

Figure 1. In two-dimensions on a hydrophilic silica surface, the ideal tetrahedral organization of the bulk HBond network (a) is frustrated (b): a water molecule may only engage three "classical" HBonds with neighboring molecules lying on the surface and a much more long-lived/ stable one with a Si-OH group of the surface. (c) Temperature dependence of the probability, p, to form a HBond. This quantity is directly derived from time-of-flight quasi-elastic data (Fig.2a)

On a more theoretical ground, we show[1] that, while simple, a purely analytical mean-field percolation model is robust enough to account in a coherent manner of this whole set of experimental structural, dynamical and thermody-

namical data on an extended temperature range from 150 to 300 K.

Following Stanley and Teixeira[2], the essence of our approach is to point-out that the local density around a given water molecule is ruled by the number of short-lived HBonds this molecule experiences. Two extreme situations can be described: the presence of a molecule engaged in four HBonds induces a local *ice-like* low density, while the density is maximum if the molecule is transiently "free" *i.e.* not bound to any neighbouring molecule. As the HBond is a transient interaction (typically a few ps at room temperature), an assembly of water molecules experiences constant density, hence entropy, fluctuations. The basic building block of the model is *p*, the probability, to form a hydrogen bond. To tune *p (T),* the temperature dependence of *p*, we measure D_s, the translational self-diffusion coefficient of interfacial water as inferred at the local scale by QENS (Fig.2a):

$D_S(T) = C.ln(3p(T) - 3p(T)^2 + p(T)^3)$ where *C* is a constant.

What do we learn? At very low temperatures all water molecules are frozen within a low density amorphous ice phase. As the temperature increases, several transitions are observed (Fig.2b). Starting at temperatures as low as 160 K water molecules are found capable of breaking hydrogen bonds. These mobile and liquid-like molecules have a strong tendency to cluster into transient patches.

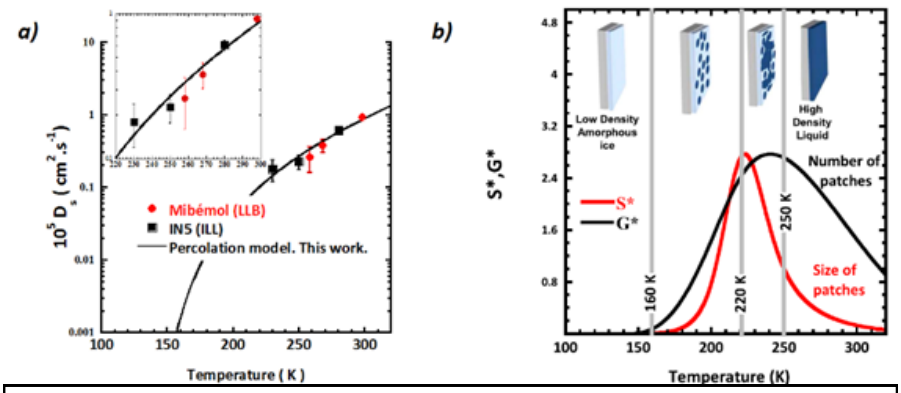

Figure 2. (a) To tune, p, the probability to form a HBond, we use the temperature dependence of the self-diffusion coefficient of a monolayer of water as measured by QENS (Spectrometers Mibémol at LLB, Saclay and IN5 at ILL, Grenoble). (b) Two-dimensional water is a heterogeneous system where a low-density (light blue) and a high-density phase (dark blue) coexist. This system shows unexpected physical properties: a glass transition at 165 K, a dynamic transition at 220 K and a liquid-liquid transition at 250 K.

These patches grow and at 220 K percolate, i.e. they form a connected surface. In the end a single patch emerges that covers the whole surface. The source of this particular water behavior in two dimensions is the frustration of the natural bulk tetrahedral local geometry and the underlying very significant increase in entropy of the water molecules: ΔS = 48 J/mol/K in 2D *vs* 21.6 J/mol/K in bulk.

The results of this study on the surprising structural and dynamic properties of interfacial water have relevance in all areas where water is in monolayer situation such as in the fields of biophysics[3], food industry[4] or in materials[5] and nuclear science[6] (storage of long-lived waste).

References

[1]. Zanotti, J.-M. et al. Competing coexisting phases in 2D water. Sci. Rep. ***6,*** *(2016).*

[2]. Stanley, H. E. & Teixeira, J. Interpretation of the unusual behavior of H2O and D2O at low temperatures: Tests of a percolation model. J. Chem. Phys. ***73,*** *3404 (1980).*

[3]. Combet, S. & Zanotti, J.-M. Further evidence that interfacial water is the main 'driving force' of protein dynamics: a neutron scattering study on perdeuterated C-phycocyanin. Phys. Chem. Chem. Phys. ***14,*** *4927 (2012).*

[4]. Champion, D., Loupiac, C., Russo, D., Simatos, D. & Zanotti, J. M. Dynamic and sub-ambient thermal transition relationships in water–sucrose solutions: Differential scanning calorimetry and neutron scattering analysis. J. Therm. Anal. Calorim. ***104,*** *365–374 (2011).*

[5]. Malikova, N. et al. Signature of Low-Dimensional Diffusion in Complex Systems. Phys. Rev. Lett. ***101,*** *265901 (2008).*

[6].. Briman, I. M. et al. Impact of Pore Size and Pore Surface Composition on the Dynamics of Confined Water in Highly Ordered Porous Silica. J. Phys. Chem. C ***116,*** *7021–7028 (2012).*

Neutrons reveal the micro-phase-separated state of confined binary fluids

The properties of liquids confined in nanometric cavities can be very different from their bulk counterparts, which raises exciting new questions for basic condensed matter physics. Among many fascinating confinement effects, we focused on the formation of new liquid structures of glassforming binary systems confined in nanochannels. We report here how this topic went one step further, with the observation of confinement induced micro-phase separation of fully miscible low-molecular-weight binary mixtures confined in different types of straight and mono-disperse channels of mesoporous silicates. It also highlights the strength of neutron scattering method with isotopic substitution, which is a unique experimental approach to reveal this phenomenon.

A. R. Abdel Hamid[a], C. Alba-Simionesco[b], S. Dutta[a], B. Frick[c], A. Ghoufi[a], R. Lefort[a], R. Mhanna[a,c], D. Morineau[a], L. Noirez[b], F. Porcher[b]

[a] Institute of Physics of Rennes, CNRS-University of Rennes 1, UMR 6251, Rennes, France

[b] Laboratoire Léon Brillouin, CEA-CNRS ,UMR 12, Gif-sur-Yvette, France

[c] Institut Laue-Langevin, Grenoble, France

denis.morineau@univ-rennes1.fr

Shrinking objects down to the nanometer scale tends to reveal new properties of matter that have no equivalent bulk counterpart. This is the foremost motivation of many current research studies on nanomaterials, which revealed fascinating new phenomena especially for hard solid materials. It inspired us to explore the validity of our knowledge about the fundamental properties of fluids confined into ever-smaller capillary tubes and it turns out it needs to be reconsidered.

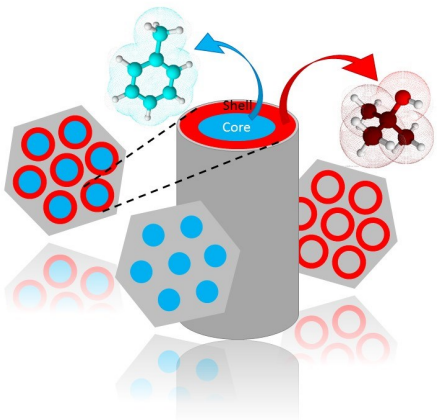

***Figure 1**: Sketch of the core-shell structure formed by the binary liquids confined in the triangular array of cylindrical pores.*

We reported a peculiar state of miscible fluids contained within nanochannels. It corresponds to a well-ordered concentric arrangement of two co-existing liquid regions of different composition (cf. Figure 1). One region forms a shell, surrounding a second liquid core, both of them having radial thickness of only one-to-four molecular sizes [1,2,3]. The phenomenon has been entitled microphase-separation, because it does not imply that the constituents of the two liquid regions would indeed phase-separate: they actually form a unique homogeneous liquid phase under normal conditions. In fact, this hidden tendency of binary fluids to form spontaneous supramolecular ordered structures is revealed only under confinement on a microscopic scale.

The phenomenon was first observed during a neutron scattering experiment performed at the Laboratory Léon Brillouin (LLB) [3]. The study was further developed at the LLB in collaboration with the Institute Laue-Langevin (ILL) [2,4]. We investigated the structure of Tert-Butanol (TBA)-Toluene (TOL) mixtures confined in the straight and mono-dispersed cylindrical nanochannels of MCM-41 and SBA-15 mesoporous silicates (pore size D = 3.6, 8.3 nm). These synthetic porous solid materials exhibit a honeycomb-like crystalline arrangement of parallel channels, which can be viewed as a bunch of nanometer-sized test-tubes. The 2D-crystalline structure of the empty materials was resolved by neutron diffraction from the analysis of specific Bragg reflections on the cold source diffractometer G6.1 and the SANS instrument PAXY for MCM-41 and SBA-15 materials, respectively (cf. Figure 2).

Then, neutron diffraction experiments on samples filled with different H/D isotopic compositions were performed to systematically vary the scattering length density of the differ-

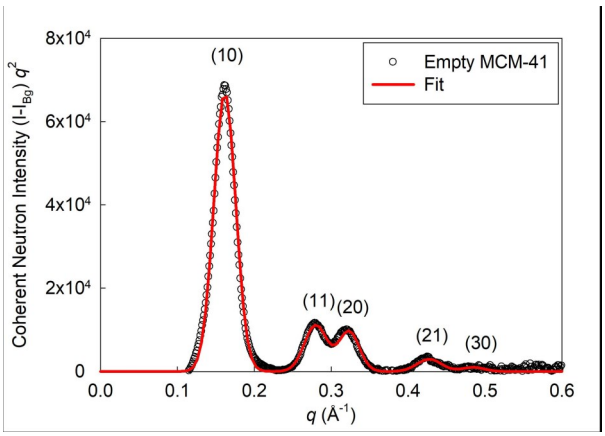

***Figure 2**: Neutron diffraction intensity of empty MCM-41. The five Bragg peaks are labelled by Miller indexes.*

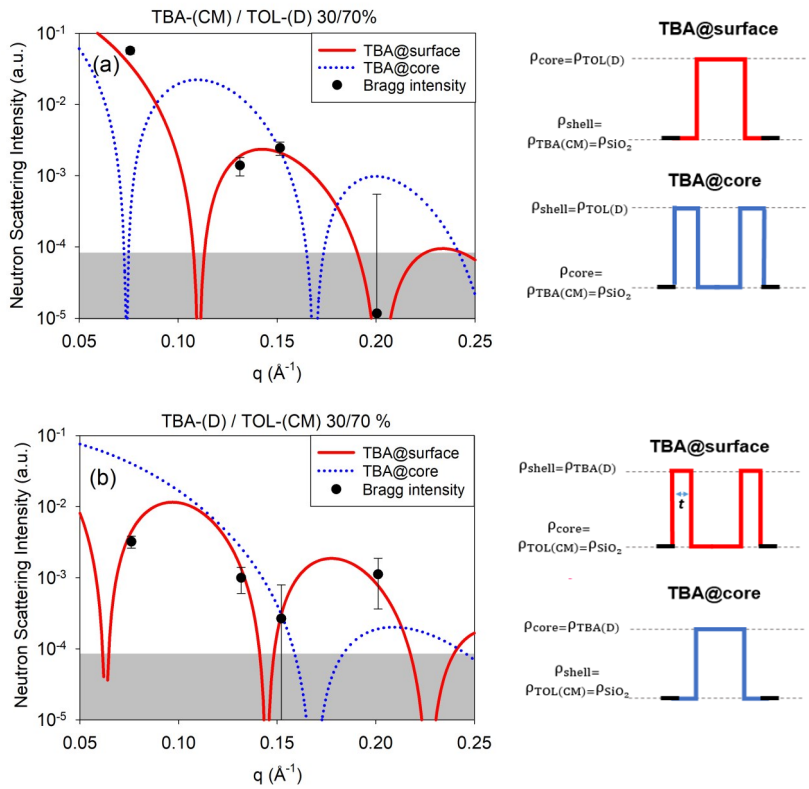

***Figure 3**: Experimental value of the integrated intensity of the four Bragg peaks of SBA-15 filled with two binary liquids having the same chemical composition but specifically designed isotopic compositions The different lines are the predicted results from two models (cf. text). Right panel: Sketch of the scattering length density profile across the pore.*

ent compounds and assess the radial concentration profile of the confined phases.

We first demonstrated that under contrast-matching condition, the measured scattered intensity is actually cancelled for unary liquids. However, the surprising observation was obtained for some confined binary liquids, where the expected extinction of the scattered intensity was not observed, but the signal was even higher than ever.

This observed apparently anomalous variation of the intensity of the Bragg peaks of the porous matrices after filling demonstrates without further analysis that the liquid mixture must be inhomogeneous at the nanoscale.

We later conducted a series of carefully designed experiments, comprising methods to label specifically one or the other component of the binary liquids in order to localize it. Combined with the development of a computational model, that shows excellent agreements with the present experiments, we provided a handy method to assess the original self-organisation of fluids imbibed in nanometer-scale environments. Figure 3 shows the resulting modulation of the Bragg reflections for one typical case, compared with the predictions from different core-shell models. Here, the two binary liquids have the same chemical composition with a TBA/TOL volume fraction composition 30/70% but different isotope labelling, comprising a fully deuterated component mixed with its contrast matching (CM) counterpart (Fig. 3 a: contrast matching Tert-Butanol mixed with deuterated Toluene and Fig. 3b: deuterated Tert-Butanol mixed with contrast matching Toluene). The lines are the predicted results, which allowed making an unambiguous distinction between the two models with either TBA or TOL at the surface (i.e. TBA@surface and TBA@core).

Strikingly, the thermal behaviour (diffraction and specific heat) shows that the molecules forming the two regions never crystallize but indeed exhibit two distinct glass transition temperatures [5]. Recent diffraction experiments performed on G6.1 on further H-bonding binary solvents suggest that this core-shell phenomenon is probably more general. We believe it is related to different interfacial interactions that we have quantified by Dynamical Vapor Sorption experiments: a situation which is expected for a variety of other complex fluids in nanopores [6]. Our experiments also highlight the strength of neutron scattering method with isotopic substitution, which is a unique experimental approach for understanding this phenomenon.

References

[1]. Press release of the American Institute of Physics, January 10th (2017): https://publishing.aip.org/publishing/journal-highlights/zeroing-true-nature-fluids-within-nanocapillaries

[2]. Ramona Mhanna, Abdel Razzak Abdel Hamid, Sujeet Dutta, Ronan Lefort, Laurence Noirez, Bernhard Frick, and Denis Morineau, 2017, J. Chem. Phys. 146, 024501

[3]. Abdel Razzak Abdel Hamid, Ramona Mhanna, Ronan Lefort, Aziz Ghoufi, Christiane Alba-Simionesco, Bernhard Frick, and Denis Morineau, 2016, J. Phys. Chem. C, 120, 9245

[4]. Ramona Mhanna, 2015, ILL-PhD, University of Rennes 1

[5]. Abdel Razzak Abdel Hamid, Ramona Mhanna, Pierre Catrou, Yann Bulteau, Ronan Lefort, and Denis Morineau, 2016, J. Phys. Chem. C, 120 (20), pp.11049

[6]. Sujeet Dutta, Ronan Lefort, Denis Morineau, Ramona Mhanna, Odile Merdrignac-Conanec, Arnaud Saint-Jalmes and Théo Leclercq, 2016, Phys. Chem. Chem. Phys., 18, 24361

Two-component self-assemblies: investigation of a synergy between bis-urea stickers

It is of interest to develop two-component systems for added flexibility in the design of supramolecular polymers, nanofibers or organogels. Bis-ureas are known to self-assemble by hydrogen bonding into long supramolecular objects. We show here that mixing aromatic bis-ureas with slightly different structures can yield surprisingly large synergistic effects. A strong increase in viscosity is observed when a bis-urea with the sterically demanding 2,4,6-trimethylbenzene spacer is combined with a bis-urea bearing no methyl group in position 2 of the aromatic spacer (i.e. 4,6-dimethylbenzene). This effect is the consequence of a change in supramolecular assembly triggered by the composition of the mixture. SANS experiments show that the mixture of complementary bis-ureas forms rod-like objects that are thicker than the rod-like objects formed by both parent systems.

E. Ressouche[1], S. Pensec[1], B. Isare[1], J. Jestin[2], L. Bouteiller[1]

[1] Sorbonne Universités, UPMC Univ Paris 06, CNRS, Institut Parisien de Chimie Moléculaire, Equipe Chimie des Polymères, 4 Place Jussieu, F-75005 Paris, France

[2] Laboratoire Léon Brillouin, UMR 12 CNRS-CEA, 91191 Gif-sur-Yvette Cedex, France

laurent.bouteiller@upmc.fr

Self-assembly of small molecules into large objects of various topologies is of interest in many fields. For instance, self-assembled 1D objects (supramolecular polymers, nanofibres, organogels) are often developed for their rheological properties or as templates in material science. While some of these systems may involve a single component bearing a self-complementary sticker that is designed to self-assemble into large objects, it is of interest to develop two-component systems for added flexibility in the design of the properties and to be able to trigger the assembly at will.[1,2] Usually the complementarity between stickers is obvious from their molecular structure, as in the case of metal/ligand, host/guest, acid/base, donor/acceptor or complementary hydrogen bonded systems. In contrast, we report the fact that bis-ureas $\mathbf{X_{PIB}}$ and **M** (Figure 1) form 1D hydrogen bonded co-assemblies that are more stable than each homo-assembly.[3]

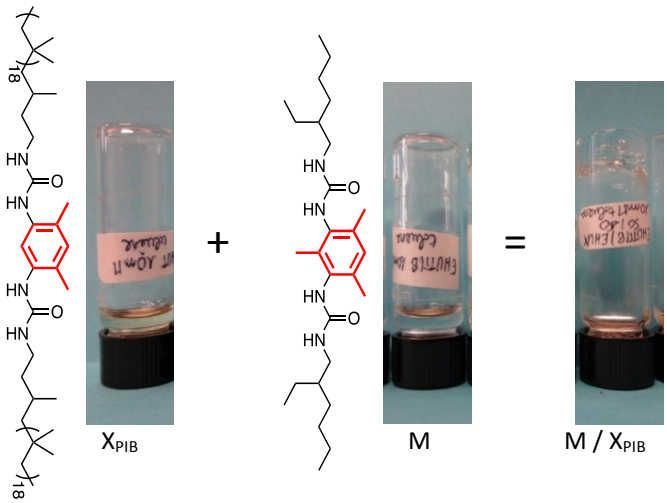

Figure 1. Bis-urea structures. Appearance of their solutions (ca 4 g/L in toluene) and their 1/1 mixture.

In this case, the origin of the complementarity between the stickers is not obvious because they are both composed of similar urea moieties, but results from subtle steric effects.[4] We employed these complementary bis-urea stickers for the rational design of two-component gels,[5] and the aim of the present work is to characterize the structure and the stability of these co-assemblies.

The structure of the assemblies was probed by Small Angle Neutron Scattering (SANS) to prove the transition between two supramolecular structures. Figure 2 shows the scattered intensity for various $\mathbf{M/X_{PIB}}$ compositions at 20 °C. All curves are characterized at low angles by a q^{-1} dependence of the scattered intensity over one decade. This feature is typical of long and rigid objects. In addition, at larger angles, the systems that contain at least 10% of $\mathbf{X_{PIB}}$ show a q^{-2} dependence of the scattered intensity that is typical of solvated polymer chains. The combination of the q^{-1} dependence at low q and the q^{-2} dependence at large q is a signature for the presence of rod-like objects that are decorated with solvated chains, i.e., hairy rods. Importantly, the fact that the scattered intensity for the mixtures containing 25% or 50% **M** is higher than the intensities for both pure solutions proves that **M** and $\mathbf{X_{PIB}}$ co-assemble into a different and thicker structure than the pure components. Indeed, the scattered intensity in the q^{-1} region depends only on the contrast and on the mass per unit length of the rods. Since the contrast of the mixture is the average of the contrast for the pure components, only a change in mass per unit length of the objects can explain the experimental data.

At the concentration of the experiment (6 g/L), the inter-

actions between objects can be neglected. Therefore, the fit of the data was attempted with various form factors of rigid cylinders. The simplest one that can describe the whole data set is the form factor for a rigid cylinder with an elliptical cross-section and a uniform contrast. Only three parameters were adjusted for each curve: the length of the cylinder and the minor and major radii of the elliptical cross-section. The other parameters (the scattering length densities and the volume fraction) were a priori evaluated from the known composition. The fit confirms that the cross-section of the objects is larger for some intermediate compositions (25 and 50 mol% of M) than for the pure systems. This feature can only be explained if the structure of the assembly at the molecular scale changes with the composition. Based on these and on complementary spectroscopic data, we propose that the pure systems are assembled into filament structures that contain a single molecule in the cross-section. In contrast, the 50/50 mixed system is assembled into a thicker structure that contains three molecules in the cross-section.

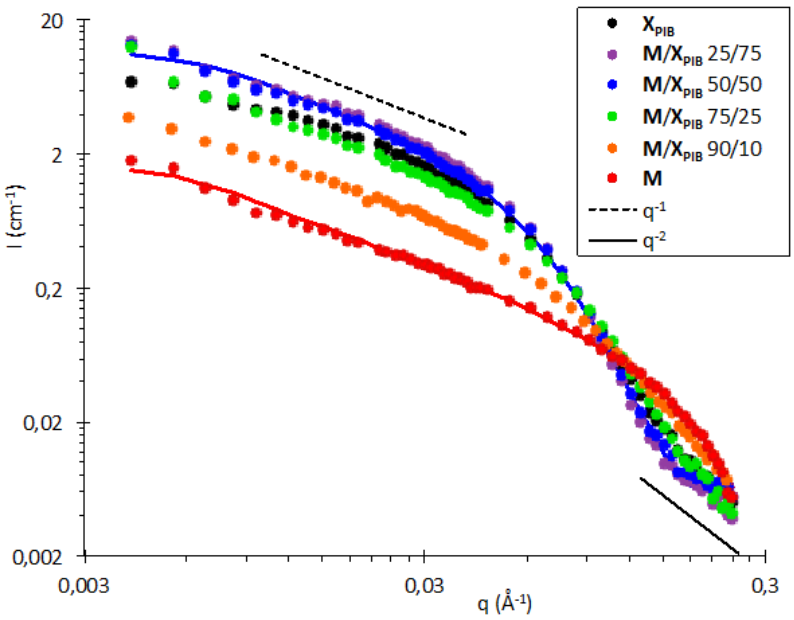

*Figure 2. SANS intensity (I) versus scattering vector (q) for solutions of **M** or X_{PIB} at a concentration of 6 g/L in toluene-d_8 and for their mixtures (molar fraction) (20 °C). The continuous lines are fits according to the form factor of a rod-like cylinder with an elliptical cross-section and homogeneous contrast.*

References

[1]. Hirst, A. R.; Smith, D. K. Two-Component Gel-Phase Materials - Highly Tunable Self-Assembling Systems. Chem. - Eur. J. 2005, 11, 5496–5508.

[2]. Buerkle, L. E.; Rowan, S. J. Supramolecular Gels Formed from Multi-Component Low Molecular Weight Species. Chem. Soc. Rev. 2012, 41, 6089–6102.

[3]. Ressouche, E.; Pensec, S.; Isare, B.; Jestin, J.; Bouteiller, L. Two-Component Self-Assemblies: Investigation of a Synergy between Bisurea Stickers. Langmuir 2016, 32, 11664–11671.

[4]. Isare, B.; Linares, M.; Lazzaroni, R.; Bouteiller, L. Engineering the Cavity of Self-Assembled Dynamic Nanotubes. J. Phys. Chem. B 2009, 113, 3360–3364.

[5]. Ressouche, E.; Pensec, S.; Isare, B.; Ducouret, G.; Bouteiller, L. Rational Design of Urea-Based Two-Component Organogelators. ACS Macro Lett. 2016, 5, 244–247.

Publications

1 Abdelmoulahi, H., Ghalla, H., Nasr, S., Bahri, M. & **Bellissent-Funel, M. C.** Hydrogen-bond network in liquid ethylene glycol as studied by neutron scattering and DFT calculations. *Journal of Molecular Liquids* **220**, 527-539, (2016).

2 Abdelmoulahi, H., Ghalla, H., Nasr, S., **Darpentigny, J.** & **Bellissent-Funel, M. C.** Intermolecular associations in an equimolar formamide-water solution based on neutron scattering and DFT calculations. *Journal of Chemical Physics* **145**, (2016).

3 Alekseev, P. A., **Mignot, J. M.**, Savchenkov, P. S. & Lazukov, V. N. First evidence for a Sm3+-type contribution to the magnetic form factor in the quasielastic spectral response of intermediate valence SmB6. *Jetp Letters* **103**, 636-642, (2016).

4 Amann-Winkel, K., **Bellissent-Funel, M. C.**, Bove, L. E., Loerting, T., Nilsson, A., Paciaroni, A., Schlesinger, D. & Skinner, L. X-ray and Neutron Scattering of Water. *Chemical Reviews* **116**, 7570-7589, (2016).

5 Anagnostopoulou, E., Grindi, B., Lacroix, L. M., **Ott, F.**, Panagiotopoulos, I. & Viau, G. Dense arrays of cobalt nanorods as rare-earth free permanent magnets. *Nanoscale* **8**, 4020-4029, (2016).

6 Andrieu, S., Neggache, A., Hauet, T., Devolder, T., Hallal, A., Chshiev, M., **Bataille, A. M.**, Le Fevre, P. & Bertran, F. Direct evidence for minority spin gap in the Co2MnSi Heusler compound. *Physical Review B* **93**, (2016).

7 Aoun, B. & Russo, D. Nano-confinement of biomolecules: Hydrophilic confinement promotes structural order and enhances mobility of water molecules. *Nano Research* **9**, 273-281, (2016).

8 Balima, F., Le Floch, S., Adessi, C., Cerqueira, T. F. T., Blanchard, N., Arenal, R., **Brulet, A.**, Marques, M. A. L., Botti, S. & San-Miguel, A. Radial collapse of carbon nanotubes for conductivity optimized polymer composites. *Carbon* **106**, 64-73, (2016).

9 Baran, S., Szytula, A., Kaczorowski, D. & **Damay, F.**

Magnetic structures in TmPdIn and TmAgSn. *Journal of Alloys and Compounds* **662**, 11-15, (2016).

10 Baran, S., Szytula, A., Kaczorowski, D. & **Damay, F.** Complex magnetic ordering in Tm3Cu4Si4. *Journal of Alloys and Compounds* **688**, 577-584, (2016).

11 **Bellissent-Funel, M. C.**, Kaneko, K., Ohba, T., Appavou, M. S., Soininen, A. J. & Wuttke, J. Crossover from localized to diffusive water dynamics in carbon nanohorns: A comprehensive quasielastic neutron-scattering analysis. *Physical Review E* **93**, (2016).

12 Ben Abdellah, A., Grosdidier, B., Osman, S. M., Rahman, S. M. M., Mayoufi, M., Ataati, J. & Gasser, J. G. Spin-state dependence of electrical resistivity and thermoelectric power of molten Al-Mn alloys: Experiment and theory. *Journal of Alloys and Compounds* **658**, 1010-1019, (2016).

13 Benavent, V., Frizon, F. & Poulesquen, A. Effect of composition and aging on the porous structure of metakaolin-based geopolymers. *Journal of Applied Crystallography* **49**, 2116-2128, (2016).

14 Bernardina, S. D., Paineau, E., Brubach, J. B., **Judeinstein, P.**, Rouziere, S., Launois, P. & Roy, P. Water in Carbon Nanotubes: The Peculiar Hydrogen Bond Network Revealed by Infrared Spectroscopy. *Journal of the American Chemical Society* **138**, 10437-10443, (2016).

15 Berriaud, C., Aubert, G., **Bataille, A. M.**, Bredy, P., Dael, A., **Klimko, S.**, **Lavie, P.**, **Meuriot, J. L.**, Nunio, F., Peugeot, A., Rifflet, J. M., **Robillard, T.** & Simon, D. Development of an Innovative Wide Aperture Vector Magnet: WAVE. *Ieee Transactions on Applied Superconductivity* **26**, (2016).

16 **Berrod, Q.**, **Ferdeghini, F.**, **Judeinstein, P.**, Genevaz, N., Ramos, R., Fournier, A., Dijon, J., Ollivier, J., Rols, S., Yu, D., Mole, R. A. & Zanotti, J. M. Enhanced ionic liquid mobility induced by confinement in 1D CNT membranes. *Nanoscale* **8**, 7845-7848, (2016).

17 Bonetti, M. & **Zanotti, J. M.** A simple AC calorimeter for specific heat measurement of liquids confined in porous materials: A study of hydrated Vycor. *Review of Scientific Instruments* **87**, (2016).

18 Bonville, P., **Guitteny, S.**, **Gukasov, A.**, **Mirebeau, I.**, **Petit, S.**, Decorse, C., Hatnean, M. C. & Balakrishnan, G. Magnetic properties and crystal field in Pr2Zr2O7. *Physical Review B* **94**, (2016).

19 Bottari, C., Crisci, G. M., Crupi, V., Ignazzitto, V., La Russa, M. F., Majolino, D., Ricca, M., Rossi, B., Ruffolo, S. A., **Teixeira, J.** & Venuti, V. SANS investigation of the salt-crystallization- and surface-treatment-induced degradation on limestones of historic-artistic interest. *Applied Physics a-Materials Science & Processing* **122**, (2016).

20 **Boue, F.**, Combet, J., Deme, B., Heinrich, M., Zilliox, J. G. & Rawiso, M. SANS from Salt-Free Aqueous Solutions of Hydrophilic and Highly Charged Star-Branched Polyelectrolytes. *Polymers* **8**, (2016).

21 Bouty, A., Petitjean, L., Chatard, J., Matmour, R., Degrandcourt, C., Schweins, R., Meneau, F., Kwasniewski, P., Boue, F., Couty, M. & **Jestin, J.** Interplay between polymer chain conformation and nanoparticle assembly in model industrial silica/rubber nanocomposites. *Faraday discussions* **186**, 325-343, (2016).

22 **Burkhardt, M.**, **Noirez, L.** & **Gradzielski, M.** Organogels based on 12-hydroxy stearic acid as a leitmotif: Dependence of gelation properties on chemical modifications. *Journal of Colloid and Interface Science* **466**, 369-376, (2016).

23 Cedervall, J., Beran, P., Vennstrom, M., Danielsson, T., Ronneteg, S., Hoglin, V., Lindell, D., Eriksson, O., **Andre, G.**, Andersson, Y., Nordblad, P. & Sahlberg, M. Low temperature magneto-structural transitions in Mn3Ni20P6. *Journal of Solid State Chemistry* **237**, 343-348, (2016).

24 Ceretti, M., Corallini, S. & Paulus, W. Influence of Phase Transformations on Crystal Growth of Stoichiometric Brownmillerite Oxides: Sr2ScGaO5 and Ca2Fe2O5. *Crystals* **6**, (2016).

25 Chaix, L., Ballou, R., Cano, A., **Petit, S.**, de Brion, S., Ollivier, J., Regnault, L. P., Ressouche, E., Constable, E., Colin, C. V., Zorko, A., Scagnoli, V., Balay, J., Lejay, P. & Simonet, V. Helical bunching and symmetry lowering inducing multiferroicity in Fe langasites. *Physical Review B* **93**, (2016).

26 Chan, M. K., Dorow, C. J., **Mangin-Thro, L.**, Tang, Y., Ge, Y., Veit, M. J., Yu, G., Zhao, X., Christianson, A. D., Park, J. T., **Sidis, Y.**, Steffens, P., Abernathy, D. L., **Bourges, P.** & Greven, M. Commensurate antiferromagnetic excitations as a signature of the pseudogap in the tetragonal high-T-c cuprate HgBa2CuO4+delta. *Nature Communications* **7**, (2016).

27 Chan, M. K., Tang, Y., Dorow, C. J., **Jeong, J.**, **Mangin-Thro, L.**, Veit, M. J., Ge, Y., Abernathy, D. L., **Sidis, Y.**, **Bourges, P.** & Greven, M. Hourglass Dispersion and Resonance of Magnetic Excitations in the Superconducting State of the Single-Layer Cuprate HgBa2CuO4+delta Near Optimal Doping. *Physical Review Letters* **117**, (2016).

28 Chappard, C., **Andre, G.**, Daudon, M. & Bazin, D. Analysis of hydroxyapatite of subchondral bone in osteoarthritis of the hip by Fourier transform infrared and

powder neutron diffraction methods. *European Journal of Clinical Investigation* **46**, 112-112, (2016).

29 Chattopadhyay, S., Baledent, V., **Damay, F.**, **Gukasov, A.**, Moshopoulou, E., Auban-Senzier, P., Pasquier, C., Andre, G., Porcher, F., Elkaim, E., Doubrovsky, C., Greenblatt, M. & Foury-Leylekian, P. Evidence of multiferroicity in NdMn2O5. *Physical Review B* **93**, (2016).

30 **Chenneviere, A.**, **Cousin, F.**, Boue, F., Drockenmuller, E., Shull, K. R., Leger, L. & Restagno, F. Direct Molecular Evidence of the Origin of Slip of Polymer Melts on Grafted Brushes. *Macromolecules* **49**, 2348-2353, (2016).

31 Cherhal, F., **Cousin, F.** & Capron, I. Structural Description of the Interface of Pickering Emulsions Stabilized by Cellulose Nanocrystals. *Biomacromolecules* **17**, 496-502, (2016).

32 Chiappisi, L., **Noirez, L.** & Gradzielski, M. A journey through the phase diagram of a pharmaceutically relevant microemulsion system. *Journal of Colloid and Interface Science* **473**, 52-59, (2016).

33 Coursault, D., Zappone, B., Coati, A., Boulaoued, A., Pelliser, L., Limagne, D., Boudet, N., Ibrahim, B. H., de Martino, A., **Alba, M.**, Goldmann, M., Garreau, Y., Gallas, B. & Lacaze, E. Self-organized arrays of dislocations in thin smectic liquid crystal films. *Soft Matter* **12**, 678-688, (2016).

34 Coz, E., Thery, J., Boillat, P., Faucheux, V., Alincant, D., Capron, P. & Gebel, G. Water management in a planar air-breathing fuel cell array using operando neutron imaging. *Journal of Power Sources* **331**, 535-543, (2016).

35 Dalle-Ferrier, C., Kisliuk, A., Hong, L., Carini, G., Carini, G., D'Angelo, G., **Alba-Simionesco, C.**, Novikov, V. N. & Sokolov, A. P. Why many polymers are so fragile: A new perspective. *Journal of Chemical Physics* **145**, (2016).

36 **Damay, F.**, **Petit, S.**, Rols, S., Braendlein, M., Daou, R., Elkaim, E., Fauth, F., Gascoin, F., Martin, C. & Maignan, A. Localised Ag+ vibrations at the origin of ultralow thermal conductivity in layered thermoelectric AgCrSe2. *Scientific Reports* **6**, (2016).

37 Danyliv, O., Iojoiu, C., Lyonnard, S., Sergent, N., Planes, E. & Sanchez, J. Y. Highly Phase Separated Aromatic Ionomers Bearing Perfluorosulfonic Acids by Bottom-up Synthesis: Effect of Cation on Membrane Morphology and Functional Properties. *Macromolecules* **49**, 4164 -4177, (2016).

38 Daudon, M., Letavernier, E., Weil, R., Veron, E., Matzen, G., **Andre, G.** & Bazin, D. Type 2 diabetes and uric acid stones: a powder neutron diffraction investigation. *European Journal of Clinical Investigation* **46**, 119-119, (2016).

39 Desmarchelier, A., Alvarenga, B. G., Caumes, X., Dubreucq, L., Troufflard, C., Tessier, M., Vanthuyne, N., Ide, J., Maistriaux, T., Beljonne, D., Brocorens, P., Lazzaroni, R., Raynal, M. & Bouteiller, L. Tuning the nature and stability of self-assemblies formed by ester benzene 1,3,5-tricarboxamides: the crucial role played by the substituents. *Soft Matter* **12**, 7824-7838, (2016).

40 Desmarchelier, A., Caumes, X., Raynal, M., Vidal-Ferran, A., van Leeuwen, P. & Bouteiller, L. Correlation between the Selectivity and the Structure of an Asymmetric Catalyst Built on a Chirally Amplified Supramolecular Helical Scaffold. *Journal of the American Chemical Society* **138**, 4908-4916, (2016).

41 Diou, O., **Brulet, A.**, Pehau-Arnaudet, G., Morvan, E., Berti, R., Astafyeva, K., Taulier, N., Fattal, E. & Tsapis, N. PEGylated nanocapsules of perfluorooctyl bromide: Mechanism of formation, influence of polymer concentration on morphology and mechanical properties. *Colloids and Surfaces B-Biointerfaces* **146**, 762-769, (2016).

42 Dos Santos, L., Marechal, M., Guillermo, A., Lyonnard, S., Moldovan, S., Ersen, O., Sel, O., Perrot, H. & Laberty-Robert, C. Proton Transport in Electrospun Hybrid Organic-Inorganic Membranes: An Illuminating Paradox. *Advanced Functional Materials* **26**, 594-604, (2016).

43 Dos Santos, L., Rose, S., Sel, O., Marechal, M., Perrot, H. & Laberty-Robert, C. Electrospinning a versatile tool for designing hybrid proton conductive membrane. *Journal of Membrane Science* **513**, 12-19, (2016).

44 Douliez, J. P., Houssou, B. H., Fameau, A. L., Navailles, L., Nallet, F., Grelard, A., Dufourc, E. J. & Gaillard, C. Self-Assembly of Bilayer Vesicles Made of Saturated Long Chain Fatty Acids. *Langmuir* **32**, 401-410, (2016).

45 Dubarle-Offner, J., Moussa, J., Amouri, H., Jouvelet, B., Bouteiller, L. & Raynal, M. Induced Circular Dichroism in Phosphine Gold(I) Aryl Acetylide Urea Complexes through Hydrogen-Bonded Chiral Co-Assemblies. *Chemistry-a European Journal* **22**, 3985-3990, (2016).

46 Escale, P., Save, M., Billon, L., Ruokolainen, J. & Rubatat, L. When block copolymer self-assembly in hierarchically ordered honeycomb films depicts the breath figure process. *Soft Matter* **12**, 790-797, (2016).

47 Fabian, M. & Araczki, C. Basic network structure of SiO2 -B2O3-Na2O glasses from diffraction and reverse Monte Carlo simulation. *Physica Scripta* **91**, (2016).

48 Fabian, M. & Svab, E. Formation of Mixed Bond-Angle Linkages in Zinc Boromolybdate Glasses, *Journal of the American Ceramic Society* Vol. 99 2292-2299 (2016).

49 **Fabreges, X.**, **Gukasov, A.**, Bonville, P., Maurya, A., Thamizhavel, A. & Dhar, S. K. Exploring metamagnetism of single crystalline EuNiGe3 by neutron scattering. *Physical Review B* **93**, (2016).

50 Favvas, E. P., Stefanopoulos, K. L., Stefopoulos, A. A., Nitodas, S. F., Mitropoulos, A. C. & **Lairez, D.** Phenol functionalized MWCNTs: A dispersion study into polar solvents by small angle neutron scattering. *Colloid Surf. A-Physicochem. Eng. Asp.* **496**, 94-99, (2016).

51 Fernandez-Castanon, J., Bomboi, F., Rovigatti, L., Zanatta, M., Paciaroni, A., Comez, L., Porcar, L., Jafta, C. J., **Fadda, G. C.**, Bellini, T. & Sciortino, F. Small-angle neutron scattering and molecular dynamics structural study of gelling DNA nanostars. *The Journal of chemical physics* **145**, 084910, (2016).

52 Fernandez-Posada, C. M., Castro, A., **Kiat, J. M.**, **Porcher, F.**, Pena, O., Alguero, M. & Amorin, H. A novel perovskite oxide chemically designed to show multiferroic phase boundary with room-temperature magnetoelectricity. *Nature Communications* **7**, (2016).

53 Fillaux, F. & **Cousson, A.** Quantum interferences revealed by neutron diffraction accord with a macroscopic-scale quantum-theory of ferroelectrics KH2(1-rho)D2 rho PO4. *European Physical Journal B* **89**, (2016).

54 Fillaux, F. & **Cousson, A.** A neutron diffraction study of the crystal of benzoic acid from 6 to 293 K and a macroscopic-scale quantum theory of the lattice of hydrogen-bonded dimers. *Chemical Physics* **479**, 26-35, (2016).

55 Gal, F., Challier, L., **Cousin, F.**, Perez, H., Noel, V. & Carrot, G. Electrocatalytic (Bio)Nanostructures Based on Polymer-Grafted Platinum Nanoparticles for Analytical Purpose. *Acs Applied Materials & Interfaces* **8**, 14747-14755, (2016).

56 Geneste, G., Bellaiche, L. & **Kiat, J. M.** Simulating the Radio-Frequency Dielectric Response of Relaxor Ferroelectrics: Combination of Coarse-Grained Hamiltonians and Kinetic Monte Carlo Simulations. *Physical Review Letters* **116**, (2016).

57 Genix, A. C., Baeza, G. P. & Oberdisse, J. Recent advances in structural and dynamical properties of simplified industrial nanocomposites. *Eur. Polym. J.* **85**, 605-619, (2016).

58 Gloaguen, D., Girault, B., Fajoui, J., **Klosek, V.** & Moya, M. J. In situ lattice strains analysis in titanium during a uniaxial tensile test. *Materials Science and Engineering a -Structural Materials Properties Microstructure and Processing* **662**, 395-403, (2016).

59 Gomez-Perez, A., Azcondo, M. T., Yuste, M., Perez-Flores, J. C., Bonanos, N., **Porcher, F.**, Munoz-Noval, A., Hoelzel, M., Garcia-Alvarado, F. & Amador, U. The A-cation deficient perovskite series La2-xCoTiO6-delta (0 <= x <= 0.20): new components for potential SOFC composite cathodes. *Journal of Materials Chemistry A* **4**, 3386-3397, (2016).

60 Gorbunov, D. I., Henriques, M. S., Andreev, A. V., Eigner, V., **Gukasov, A.**, **Fabreges, X.**, Skourski, Y., Petricek, V. & Wosnitza, J. Magnetic anisotropy and reduced neodymium magnetic moments in Nd 3Ru 4Al 12. *Physical Review B* **93**, 024407 (024411 pp.)-024407 (024411 pp.), (2016).

61 Goujon, A., Du, G. Y., Moulin, E., Fuks, G., Maaloum, M., Buhler, E. & Giuseppone, N. Hierarchical Self-Assembly of Supramolecular Muscle-Like Fibers. *Angewandte Chemie-International Edition* **55**, 703-707, (2016).

62 Gras, P., Rey, C., **Andre, G.**, Charvillat, C., Sarda, S. & Combes, C. Crystal structure of monoclinic calcium pyrophosphate dihydrate (m-CPPD) involved in inflammatory reactions and osteoarthritis. *Acta Crystallographica Section B-Structural Science Crystal Engineering and Materials* **72**, 96-101, (2016).

63 **Guenet, H.**, Davranche, M., Vantelon, D., Pedrot, M., Al-Sid-Cheikh, M., Dia, A. & **Jestin, J.** Evidence of organic matter control on As oxidation by iron oxides in riparian wetlands. *Chemical Geology* **439**, 161-172, (2016).

64 **Guennouni, Z.**, **Cousin, F.**, Faure, M. C., Perrin, P., Limagne, D., Konovalov, O. & Goklmann, M. Self-Organization of Polystyrene-b-polyacrylic Acid (PS-b-PAA) Monolayer at the Air/Water Interface: A Process Driven by the Release of the Solvent Spreading. *Langmuir* **32**, 1971-1980, (2016).

65 Guo, H., Mussault, C., **Brulet, A.**, Marcellan, A., Hourdet, D. & Sanson, N. Thermoresponsive Toughening in LCST -Type Hydrogels with Opposite Topology: From Structure to Fracture Properties. *Macromolecules* **49**, 4295-4306, (2016).

66 Guo, H., Sanson, N., Marcellan, A. & Hourdet, D. Thermoresponsive Toughening in LCST-Type Hydrogels: Comparison between Semi-Interpenetrated and Grafted Networks. *Macromolecules* **49**, 9568-9577, (2016).

67 **Hamid, A. R. A.**, Mhanna, R., Catrou, P., Bulteau, Y., Lefort, R. & Morineau, D. Multiple Glass Transitions of Microphase Separed Binary Liquids Confined in MCM-41. *Journal of Physical Chemistry C* **120**, 11049-11053, (2016).

68 Hamid, A. R. A., Mhanna, R., Lefort, R., Ghoufi, A., **Alba-Simionesco, C.**, Frick, B. & Morineau, D. Microphase Separation of Binary Liquids Confined in Cylindrical Pores. *Journal of Physical Chemistry C* **120**, 9245-9252, (2016).

69 Hardy, V., Payen, C., **Damay, F.**, Meddar, L., Josse, M. & **Andre, G.** Phase transitions and magnetic structures in MnW1-xMoxO4 compounds (x <= 0.2). *Journal of Physics-Condensed Matter* **28**, (2016).

70 Herfurth, C., Laschewsky, A., **Noirez, L.**, von Lospichl, B. & Gradzielski, M. Thermoresponsive (star) block copolymers from one-pot sequential RAFT polymerizations and their self-assembly in aqueous solution. *Polymer* **107**, 422-433, (2016).

71 Holbein, S., Ackermann, M., Chapon, L., Steffens, P., **Gukasov, A.**, Sazonov, A., Breunig, O., Sanders, Y., Becker, P., Bohaty, L., Lorenz, T. & Braden, M. Strong magnetoelastic coupling at the transition from harmonic to anharmonic order in NaFe(WO4)(2) with 3d(5) configuration. *Physical Review B* **94**, (2016).

72 Ivanov, S. A., Bush, A. A., Hudl, M., Stash, A. I., **Andre, G.**, Tellgren, R., Cherepanov, V. M., Stepanov, A. V., Kamentsev, K. E., Tokunaga, Y., Taguchi, Y., Tokura, Y., Nordblad, P. & Mathieu, R. Spin and dipole order in geometrically frustrated mixed-valence manganite Pb3Mn7O15. *Journal of Materials Science-Materials in Electronics* **27**, 12562-12573, (2016).

73 Jarry, A., Joubert, O., Suard, E., **Zanotti, J. M.** & Quarez, E. Location of deuterium sites at operating temperature from neutron diffraction of BaIn0.6Ti0.2Yb0.2O2.6-n (OH)(2n), an electrolyte for proton-solid oxide fuel cells. *Physical Chemistry Chemical Physics* **18**, 15751-15759, (2016).

74 Jolly, W., Toffolon-Masclet, C., Joubert, J. M., Marini, B., **Porcher, F.**, **Andre, G.**, Cortial, F., Petit, P. & Ringeval, S. In situ monitoring of isothermal phase transformation in two Nb stabilized austenitic stainless steels (316Nb) by neutron diffraction. *Journal of Alloys and Compounds* **688**, 695-702, (2016).

75 Jouault, N., Crawford, M. K., Chi, C. Z., Smalley, R. J., Wood, B., **Jestin, J.**, Melnichenko, Y. B., He, L. L., Guise, W. E. & Kumar, S. K. Polymer Chain Behavior in Polymer Nanocomposites with Attractive Interactions. *Acs Macro Letters* **5**, 523-527, (2016).

76 Jouault, N. & **Jestin, J.** Intra- and Interchain Correlations in Polymer Nanocomposites: A Small-Angle Neutron Scattering Extrapolation Method. *Acs Macro Letters* **5**, 1095-1099, (2016).

77 Jovari, P., Lucas, P., Yang, Z. Y., Bureau, B., Kaban, I., **Beuneu, B.**, Pantalei, C. & Bednarcik, J. On the structure of Ge-As-Te-Cu glasses. *Journal of Non-Crystalline Solids* **433**, 1-5, (2016).

78 **Kahl, P.**, **Baroni, P.** & **Noirez, L.** Bringing to Light Hidden Elasticity in the Liquid State Using In-Situ Pretransitional Liquid Crystal Swarms. *Plos One* **11**, (2016).

79 Kaurova, I. A., Kuz'micheva, G. M., Brykovskiy, A. A., Rybakov, V. B., Gorobets, Y. N., Shekhovtsov, A. N. & **Cousson, A.** Influence of growth conditions on structural parameters of scheelite PbTO4 (T = Mo, W) crystals. *Materials & Design* **97**, 56-63, (2016).

80 Kawaguchi, S., Ishibashi, H., Nishihara, S., Mori, S., Campo, J., **Porcher, F.**, Fabelo, O., Sugimoto, K., Kim, J., Kato, K., Takata, M., Nakao, H. & Kubota, Y. Orthorhombic distortion and orbital order in the vanadium spinel FeV2O4. *Physical Review B* **93**, (2016).

81 **Kiat, J. M.**, Hehlen, B., Anoufa, M., Bogicevic, C., Curfs, C., Boyer, B., Al-Sabbagh, M., **Porcher, F.** & Al-Zein, A. Lowering of ground state induced by core-shell structure in strontium titanate. *Physical Review B* **93**, (2016).

82 Klotz, S., Strassle, T., Lebert, B., d'Astuto, M. & Hansen, T. High pressure neutron diffraction to beyond 20 GPa and below 1.8 K using Paris-Edinburgh load frames. *High Pressure Research* **36**, 73-78, (2016).

83 Kozhevnikov, S. V., **Ott, F.** & Radu, F. Neutron methods for the direct determination of the magnetic induction in thick films. *Journal of Magnetism and Magnetic Materials* **402**, 83-93, (2016).

84 Kuz'micheva, G. M., Ivleva, L. I., Kaurova, I. A., Rybakov, V. B. & **Cousson, A.** Structure and real composition of undoped and Cr- and Ni-doped Sr0.61Ba0.39Nb2O6 single crystals. *Structural Chemistry* **27**, 1623-1634, (2016).

85 Kuz'micheva, G. M., Kaurova, I. A., Brykovskiy, A. A., Rybakov, V. B., Gorobets, Y. N., Shekhovtsov, A. N. & **Cousson, A.** Structural investigation of Pb(Mo xW 1-x) O 4 solid solutions via X-ray and neutron diffraction. *Materials Research Bulletin* **78**, 134-140, (2016).

86 **Lairez, D.**, Clochard, M. C. & Wegrowe, J. E. The concept of entropic rectifier facing experiments. *Scientific Reports* **6**, (2016).

87 Lazukov, V. N., Alekseev, P. A., Shitsevalova, N. Y. & Philippov, V. B. Thermal evolution of magnetic-excitation spectrum of PrB6. *Physics of Metals and Metallography* **117**, 460-465, (2016).

88 Lee, C. H., Kihou, K., Park, J. T., Horigane, K., Fujita, K., Wasser, F., Qureshi, N., **Sidis, Y.**, Akimitsu, J. & Braden, M. Suppression of spin-exciton state in hole overdoped iron-based superconductors. *Scientific Reports* **6**, (2016).

89 Lefrancois, E., Pradipto, A. M., Sala, M. M., Chapon, L. C., Simonet, V., Picozzi, S., Lejay, P., **Petit, S.** & Ballou, R. Anisotropic interactions opposing magnetocrystalline anisotropy in Sr3NiIrO6. *Physical Review B* **93**, (2016).

90 Lefrancois, E., **Songvilay, M.**, Robert, J., Nataf, G., Jor-

dan, E., Chaix, L., Colin, C. V., Lejay, P., Hadj-Azzem, A., Ballou, R. & Simonet, V. Magnetic properties of the honeycomb oxide Na2Co2TeO6. *Physical Review B* **94**, (2016).

91 Letoublon, A., Paofai, S., Ruffle, B., **Bourges, P.**, Hehlen, B., Michel, T., Ecolivet, C., Durand, O., Cordier, S., Katan, C. & Even, J. Elastic Constants, Optical Phonons, and Molecular Relaxations in the High Temperature Plastic Phase of the CH3NH3PbBr3 Hybrid Perovskite. *Journal of Physical Chemistry Letters* **7**, 3776-3784, (2016).

92 Levieil, B., Bridier, F., Doudard, C., Thevenet, D. & Calloch, S. User Influence on Two Complementary Residual Stress Determination Methods: Contour Method and Incremental X-Ray Diffraction. *Experimental Mechanics* **56**, 1641-1652, (2016).

93 Li, Z. W., Drees, Y., Kuo, C. Y., Guo, H., Ricci, A., **Lamago, D.**, Sobolev, O., Rutt, U., Gutowski, O., Pi, T. W., Piovano, A., Schmidt, W., Mogare, K., Hu, Z., Tjeng, L. H. & Komarek, A. C. Incommensurate spin correlations in highly oxidized cobaltates La2-xSrxCoO4. *Scientific Reports* **6**, (2016).

94 Li, Z. W., Drees, Y., Ricci, A., **Lamago, D.**, Piovano, A., Rotter, M., Schmidt, W., Sobolev, O., Rutt, U., Gutowski, O., Sprung, M., Castellan, J. P., Tjeng, L. H. & Komarek, A. C. Electronic and Magnetic Nano Phase Separation in Cobaltates La2-x Sr (x) CoO4. *Journal of Superconductivity and Novel Magnetism* **29**, 727-731, (2016).

95 Louisfrema, W., Paillaud, J. L., **Porcher, F.**, Perrin, E., Onfroy, T., Massiani, P., Boutin, A. & Rotenberg, B. Cation Migration and Structural Deformations upon Dehydration of Nickel-Exchanged NaY Zeolite: A Combined Neutron Diffraction and Monte Carlo Study. *Journal of Physical Chemistry C* **120**, 18115-18125, (2016).

96 **Martin, N.**, Deutsch, M., Bert, F., Andreica, D., Amato, A., Bonfa, P., De Renzi, R., Rossler, U. K., Bonville, P., Fomicheva, L. N., Tsvyashchenko, A. V. & **Mirebeau, I.** Magnetic ground state and spin fluctuations in MnGe chiral magnet as studied by muon spin rotation. *Physical Review B* **93**, (2016).

97 **Martin, N.**, Deutsch, M., Itie, J. P., Rueff, J. P., Rossler, U. K., Koepernik, K., Fomicheva, L. N., Tsvyashchenko, A. V. & **Mirebeau, I.** Magnetovolume effect, macroscopic hysteresis, and moment collapse in the paramagnetic state of cubic MnGe under pressure. *Physical Review B* **93**, (2016).

98 Martineau, C., Allix, M., Suchomel, M. R., **Porcher, F.**, Vivet, F., Legein, C., Body, M., Massiot, D., Taulelle, F. & Fayon, F. Structure determination of Ba5AlF13 by coupling electron, synchrotron and neutron powder diffraction, solid-state NMR and ab initio calculations. *Dalton Transactions* **45**, 15565-15574, (2016).

99 Maschek, M., **Lamago, D.**, **Castellan, J. P.**, Bosak, A., Reznik, D. & Weber, F. Polaronic metal phases in La0.7Sr0.3MnO3 uncovered by inelastic neutron and x-ray scattering. *Physical Review B* **93**, (2016).

100 Meinnel, J., Latouche, C., Ghanemi, S., Boucekkine, A., Barone, V., Moreac, A. & Boudjada, A. Anharmonic Computations Meet Experiments (IR, Raman, Neutron Diffraction) for Explaining the Behavior of 1,3,5-Tribromo-2,4,6-trimethylbenzene. *Journal of Physical Chemistry A* **120**, 1127-1132, (2016).

101 Meyer, M., Viau, L., Mehdi, A., Monge, S., **Judeinstein, P**. & Vioux, A. What use for polysilsesquioxane lithium salts in lithium batteries? *New Journal of Chemistry* **40**, 7657-7662, (2016).

102 Mhanna, R., Lefort, R., **Noirez, L.** & Morineau, D. Microstructure and concentration fluctuations in alcohol-Toluene and alcohol-Cyclohexane binary liquids: A small angle neutron scattering study. *Journal of Molecular Liquids* **218**, 198-207, (2016).

103 Morfin, I., Spagnoli, S., Rambaud, C., **Longeville, S.** & Plazanet, M. Behaviour of a solvent trapped in a physical molecular gel. *Philosophical Magazine* **96**, 809-815, (2016).

104 Moussa, W., Colombani, O., Benyahia, L., Nicolai, T. & Chassenieux, C. Structure of a self-assembled network made of polymeric worm-like micelles. *Polymer Bulletin* **73**, 2689-2705, (2016).

105 Nemkovski, K. S., Kozlenko, D. P., Alekseev, P. A., **Mignot, J. M**., Menushenkov, A. P., Yaroslavtsev, A. A., Clementyev, E. S., Ivanov, A. S., Rols, S., Klobes, B., Hermann, R. P. & Gribanov, A. V. Europium mixed-valence, long-range magnetic order, and dynamic magnetic response in EuCu2(SixGe1-x)(2). *Physical Review B* **94**, (2016).

106 Noirjean, C., Testard, F., Dejugnat, C., **Jestin, J.** & Carriere, D. Molten fatty acid based microemulsions. *Physical Chemistry Chemical Physics* **18**, 15911-15918, (2016).

107 Ondrejkovic, P., Kempa, M., Savinov, M., Bednyakov, P., Kulda, J., **Bourges, P.**, Dec, J. & Hlinka, J. Electric-field influence on the neutron diffuse scattering near the ferroelectric transition of Sr0.61Ba0.39Nb2O6. *Phase Transitions* **89**, 808-815, (2016).

108 Pachoud, E., **Damay, F.**, Martin, C., Mordvinova, N. E., Lebedev, O. I. & Maignan, A. Robustness of Antiferromagnetism and Pyroelectricity in AgCr1-xRhxS2. *Chemistry of Materials* **28**, 1816-1822, (2016).

109 Papamihail, K., Mergia, K., **Ott, F.**, Serruys, Y., Speliotis,

T., Apostolopoulos, G. & Messoloras, S. Magnetic effects induced by self-ion irradiation of Fe films. *Physical Review B* **93**, (2016).

110 Park, K., Oh, J., Leiner, J. C., **Jeong, J.**, Rule, K. C., Le, M. D. & Park, J. G. Magnon-phonon coupling and two-magnon continuum in the two-dimensional triangular antiferromagnet CuCrO2. *Physical Review B* **94**, (2016).

111 Paul-Boncour, V., Filipek, S. M., Crivello, J. C., Couturas, F. & Morawski, A. Properties of ZrNi5 deuteride synthesized under high pressure studied by neutron diffraction and first principles calculations. *International Journal of Hydrogen Energy* **41**, 17408-17420, (2016).

112 Pauly, C. S., Genix, A. C., Alauzun, J. G., **Jestin, J.**, Sztucki, M., Mutin, P. H. & Oberdisse, J. Structure of alumina-silica nanoparticles grafted with alkylphosphonic acids in poly(ethylacrylate) nanocomposites. *Polymer* **97**, 138-146, (2016).

113 Pavlosiuk, O., Kaczorowski, D., **Fabreges, X.**, **Gukasov, A.** & Wisniewski, P. Antiferromagnetism and superconductivity in the half-Heusler semimetal HoPdBi. *Scientific Reports* **6**, (2016).

114 Pethes, I., Kaban, I., Stoica, M., **Beuneu, B.** & Jovari, P. Chemical ordering in Pd81Ge19 metallic glass studied by reverse Monte-Carlo modelling of XRD, ND and EXAFS experimental data. *Physica Scripta* **91**, (2016).

115 **Petit, S.**, Lhotel, E., Canals, B., Hatnean, M. C., Ollivier, J., Mutka, H., Ressouche, E., Wildes, A. R., Lees, M. R. & Balakrishnan, G. Observation of magnetic fragmentation in spin ice. *Nature Physics* **12**, 746-750, (2016).

116 **Petit, S.**, Lhotel, E., **Guitteny, S.**, Florea, O., Robert, J., Bonville, P., **Mirebeau, I.**, Ollivier, J., Mutka, H., Ressouche, E., Decorse, C., Hatnean, M. C. & Balakrishnan, G. Antiferroquadrupolar correlations in the quantum spin ice candidate Pr2Zr2O7. *Physical Review B* **94**, (2016).

117 **Porcher, F.**, Paillaud, J. L., Gaberova, L., **Andre, G.**, Casale, S. & Massiani, P. Monitoring by in situ neutron diffraction of simultaneous dehydration and Ni2+ mobility in partially exchanged NaY zeolites. *New Journal of Chemistry* **40**, 4228-4235, (2016).

118 Portnichenko, P. Y., Paschen, S., Prokofiev, A., Vojta, M., Cameron, A. S., **Mignot, J. M.**, Ivanov, A. & Inosov, D. S. Incommensurate short-range multipolar order parameter of phase II in Ce3Pd20Si6. *Physical Review B* **94**, (2016).

119 Pospisil, J., Opletal, P., Valiska, M., Tokunaga, Y., Stunault, A., Haga, Y., Tateiwa, N., **Gillon, B.**, Honda, F., Yamamura, T., Niznansky, V., Yamamoto, E. & Aoki, D. Properties and Collapse of the Ferromagnetism in UCo1-xRuxAl Studied in Single Crystals. *Journal of the Physical Society of Japan* **85**, (2016).

120 Raneri, S., Barone, G., Mazzoleni, P. & **Rabot, E.** Visualization and quantification of weathering effects on capillary water uptake of natural building stones by using neutron imaging. *Applied Physics a-Materials Science & Processing* **122**, (2016).

121 Rau, J. G., **Petit, S.** & Gingras, M. J. P. Order by virtual crystal field fluctuations in pyrochlore XY antiferromagnets. *Physical Review B* **93**, (2016).

122 Ressouche, E., Pensec, S., Isare, B., **Jestin, J.** & Bouteiller, L. Two-Component Self-Assemblies: Investigation of a Synergy between Bisurea Stickers. *Langmuir* **32**, 11664-11671, (2016).

123 **Ridier, K.**, **Gillon, B.**, **Gukasov, A.**, **Chaboussant, G.**, **Cousson, A.**, Luneau, D., Borta, A., Jacquot, J. F., Checa, R., Chiba, Y., Sakiyama, H. & Mikuriya, M. Polarized Neutron Diffraction as a Tool for Mapping Molecular Magnetic Anisotropy: Local Susceptibility Tensors in Co -II Complexes. *Chemistry-a European Journal* **22**, 724-735, (2016).

124 **Ridier, K.**, Mondal, A., Boilleau, C., Cador, O., **Gillon, B.**, **Chaboussant, G.**, Le Guennic, B., Costuas, K. & Lescouezec, R. Polarized Neutron Diffraction to Probe Local Magnetic Anisotropy of a Low-Spin Fe(III) Complex. *Angewandte Chemie (International ed. in English)* **55**, 3963-3967, (2016).

125 Rousse, G., Radtke, G., Klein, Y. & Ahouari, H. Long-range antiferromagnetic order in malonate-based compounds Na2M(H2C3O4)(2)center dot 2H(2)O (M = Mn, Fe, Co, Ni). *Dalton Transactions* **45**, 2536-2548, (2016).

126 Royappa, A. T., Royappa, A. D., Moral, R. F., Rheingold, A. L., **Papoular, R. J.**, Blum, D. M., Duong, T. Q., Stepherson, J. R., Vu, O. D., Chen, B. H., Suchomel, M. R., Golen, J. A., Andre, G., Kourkoumelis, N., Mercer, A. D., Pekarek, A. M. & Kelly, D. C. Copper(I) oxalate complexes: Synthesis, structures and surprises. *Polyhedron* **119**, 563-574, (2016).

127 Rueff, J. M., Poienar, M., Guesdon, A., Martin, C., Maignan, A. & Jaffres, P. A. Hydrothermal synthesis for new multifunctional materials: A few examples of phosphates and phosphonate-based hybrid materials. *Journal of Solid State Chemistry* **236**, 236-245, (2016).

128 Russo, D., Plazanet, M., **Teixeira, J.**, Moulin, M., Hartlein, M., Wurm, F. R. & Steinbach, T. Investigation into the Relaxation Dynamics of Polymer-Protein Conjugates Reveals Surprising Role of Polymer Solvation on Inherent Protein Flexibility. *Biomacromolecules* **17**, 141-147, (2016).

129 Scussat, S., **Ott, F.**, **Helary, A.**, **Desert, S.**, Cayot, P. &

Loupiac, C. Neutron Imaging of Meat during Cooking. *Food Biophysics* **11**, 207-212, (2016).

130 Shi, L., Carn, F., **Boue, F.** & Buhler, E. Role of the ratio of biopolyelectrolyte persistence length to nanoparticle size in the structural tuning of electrostatic complexes. *Physical Review E* **94**, (2016).

131 Soininen, A. J., Appavou, M. S., Frykstrand, S., Welch, K., Khaneft, M., Kriele, A., **Bellissent-Funel, M. C.**, Stromme, M. & Wuttke, J. Dynamics of water confined in mesoporous magnesium carbonate. *Journal of Chemical Physics* **145**, (2016).

132 Szuszkiewicz, W., **Ott, F.**, Kisielewski, J., Sveklo, I., Dynowska, E., Minikayev, R., Kurant, Z., Kuna, R., Jakubowski, M., Wawro, A., Sobierajski, R. & Maziewski, A. Polarized neutron reflectivity and X-ray scattering measurements as tools to study properties of Pt/Co/Pt ultrathin layers irradiated by femtosecond laser pulses. *Phase Transitions* **89**, 328-340, (2016).

133 Tao, F. Q., Genevois, C., Lu, F. Q., Kuang, X. J., **Porcher, F.**, Li, L. J., Rang, T., Li, W. B., Zhou, D. & Ailix, M. First 14 -Layer Twinned Hexagonal Perovskite Ba14Mn1.75Ta10.5O42: Atomic-Scale Imaging of Cation Ordering. *Chemistry of Materials* **28**, 4686-4696, (2016).

134 Toulouse, J., Iolin, E., **Hennion, B.**, **Petitgrand, D.** & Erwin, R. Resonance damping of the terahertz-frequency transverse acoustic phonon in the relaxor ferroelectric KTa1-xNbxO3. *Physical Review B* **94**, (2016).

135 van der Maarel, J. R. C., Guttula, D., **Arluison, V.**, Egelhaaf, S. U., Grillo, I. & Forsyth, V. T. Structure of the H-NS-DNA nucleoprotein complex. *Soft Matter* **12**, 3636-3642, (2016).

136 Wagner, A., Bergner, F., Chaouadi, R., Hein, H., Hernandez-Mayoral, M., Serrano, M., Ulbricht, A. & Altstadt, E. Effect of neutron flux on the characteristics of irradiation-induced nanofeatures and hardening in pressure vessel steels. *Acta Materialia* **104**, 131-142, (2016).

137 Wang, Q. S., Shen, Y., Pan, B. Y., Hao, Y. Q., Ma, M. W., Zhou, F., Steffens, P., Schmalzl, K., Forrest, T. R., Abdel-Hafiez, M., Chen, X. J., Chareev, D. A., Vasiliev, A. N., **Bourges, P.**, **Sidis, Y.**, Cao, H. B. & Zhao, J. Strong interplay between stripe spin fluctuations, nematicity and superconductivity in FeSe. *Nature Materials* **15**, 159-+, (2016).

138 **Zanotti, J. M.**, **Judeinstein, P.**, Dalla-Bernardina, S., Creff, G., Brubach, J. B., Roy, P., Bonetti, M., Ollivier, J., Sakellariou, D. & **Bellissent-Funel, M. C.** Competing coexisting phases in 2D water. *Scientific Reports* **6**, (2016).

139 Zhang, L., Mikhailovskaya, A., Constantin, D., Foffi, G., Tavacoli, J., Schmitt, J., **Muller, F.**, Rochas, C., Wang, N., Langevin, D. & Salonen, A. Varying the counter ion changes the kinetics, but not the final structure of colloidal gels. *Journal of Colloid and Interface Science* **463**, 137-144, (2016).

140 Zhao, D., Di Nicola, M., Khani, M. M., **Jestin, J.**, Benicewicz, B. C. & Kumar, S. K. Self-Assembly of Monodisperse versus Bidisperse Polymer-Grafted Nanoparticles. *Acs Macro Letters* **5**, 790-795, (2016).

141 Zhao, D., Di Nicola, M., Khani, M. M., **Jestin, J.**, Benicewicz, B. C. & Kumar, S. K. Role of block copolymer adsorption versus bimodal grafting on nanoparticle self-assembly in polymer nanocomposites. *Soft Matter* **12**, 7241-7247, (2016).

142 Zhong, S. Y., **Klosek, V.**, de Carlan, Y. & **Mathon, M. H.** Modeling of structural hardening in oxide dispersion-strengthened (ODS) ferritic alloys. *Journal of Materials Science* **51**, 2540-2549, (2016).

143 Zhou, Z., Bouwman, W. G., Schut, H., **Desert, S.**, **Jestin, J.**, Hartmann, S. & Pappas, C. From nanopores to macropores: Fractal morphology of graphite. *Carbon* **96**, 541-547, (2016).

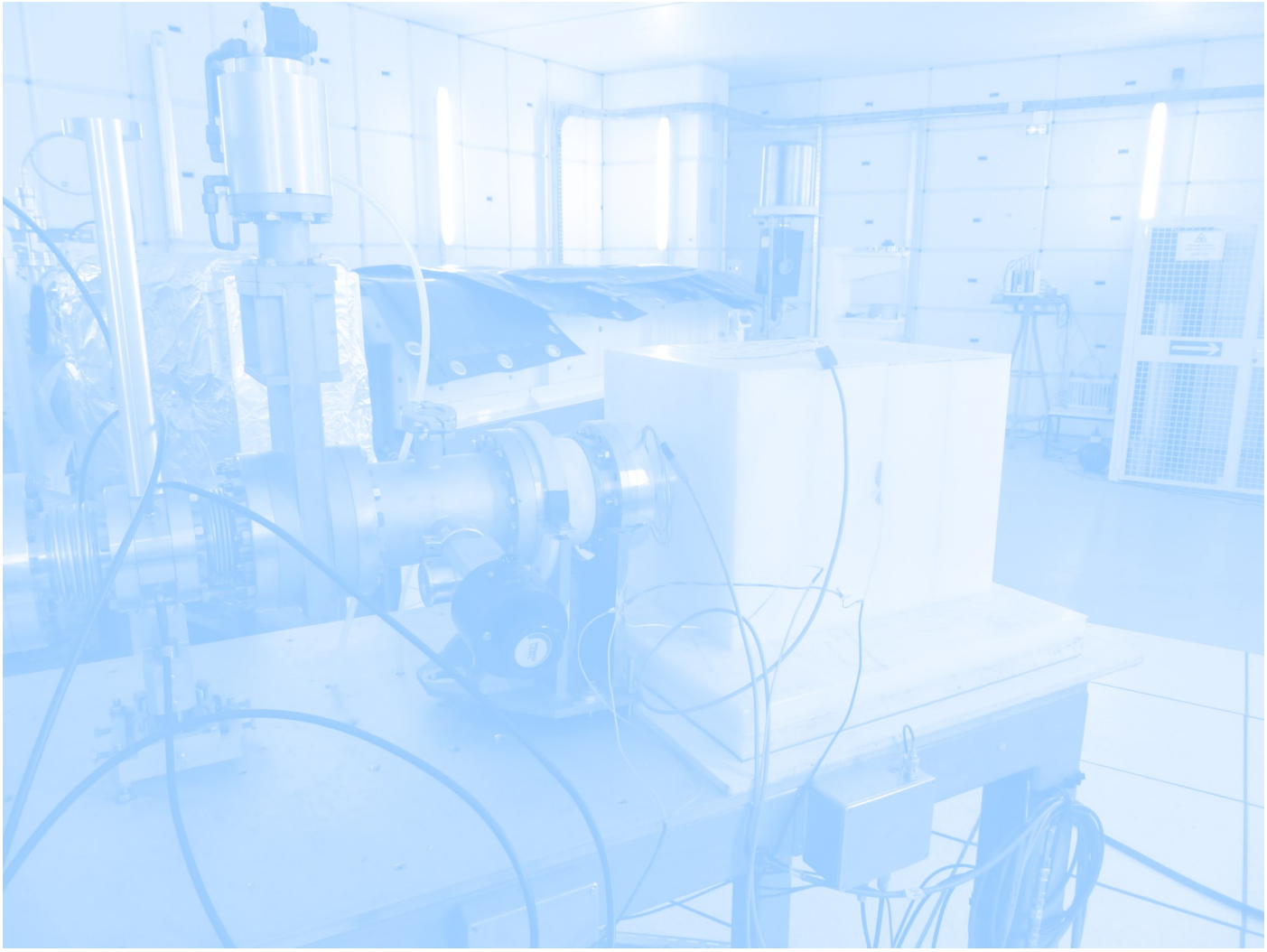

SONATE COMPACT NEUTRON SOURCE

Neutrons production on the IPHI accelerator for the validation of the design of the compact neutron source SONATE

We aim at building an accelerator based compact neutron source which would provide a thermal neutron flux on the order of 4x1012 n.s-1.cm-2.sr-1. Such a brilliance would put compact neutron sources on par with existing medium flux neutron research reactors. We performed the first neutron production tests on the IPHI proton accelerator at Saclay. The neutron flux were measured using gold foil activation and 3He detectors. The measured flux were compared with MCNP and GEANT4 Monte Carlo simulations in which the whole experimental setup was modelled. There is a good agreement between the experimental measurements and the Monte-Carlo simulations. The available modelling tools will allow us to optimize the whole Target Moderator Reflector assembly together with the neutron scattering spectrometer geometries.

F. Ott[1], A. Menelle[1], F. Prunes[1], B. Homatter[1], B. Annighöfer[1], F. Porcher[1], N. Chauvin[2], J. Schwindling[2], A. Letourneau[3], A. Marchix[3], N.H. Tran[3]

[1] Laboratoire Léon Brillouin, CEA, CNRS, Université Paris-Saclay, CEA Saclay 91191 Gif sur Yvette France
[2] IRFU/DACM, Université Paris-Saclay, CEA Saclay 91191 Gif sur Yvette France
[3] IRFU/DPhN, CEA, CNRS, Université Paris-Saclay, CEA Saclay 91191 Gif sur Yvette France

Frederic.Ott@cea.fr

There is currently an interest in developing compact neutron sources (CNS) based on low energy proton accelerators (10-100 MeV) [1]. Such sources could serve as neutron sources for neutron scattering to replace small ageing nuclear reactors [2]. There are already several projects of CNS on-going around the world. The currently most advanced is LENS Low Energy Neutron Source at Indiana University [3]. The CNS operating or under construction have gathered into the UCANS, Union for Compact Accelerator-driven Neutron Sources [4].

At Saclay we are considering the possible construction of a high end CANS source. Our first aim has been to experimentally validate the neutron production and moderation obtained by Monte Carlo simulations using MCNP and GEANT4. Once reliable simulation tools are available we shall be able to estimate the performances of a CNS for neutron scattering experiments (from the source to the spectrometer) and compare its performances to existing facilities (reactor or spallation based).

The experiments have been performed on the 3 MeV IPHI proton accelerator which is based at CEA Saclay, France. The accelerator is designed to operate in continuous mode with proton currents up to 100 mA which corresponds to a total power of 300 kW. For the current experiments dedicated to validations of neutron production and moderator Monte Carlo simulations we operated the accelerator at a very low power of about 10 W, both to avoid any target damage and for radioprotection issues. The accelerator was operated in pulsed mode with proton pulses of length 100 µs and with a repetition rate of 1 Hz and a peak current of 30 mA. Rather narrow thermal neutron pulses are thus obtained so that precise time-of-flight measurements can be performed.

In order to produce neutrons we opted for a beryllium target of thickness 0.5mm (99.0%) which stopped all incident protons. The target was installed in a polyethylene (PE) moderator box (300x300x400 mm3) so as to cool down the neutron to thermal energies (around 26meV). A 20 mm diameter hole was drilled through the moderator from the position where the thermal neutron density was expected to be the highest to the outside of the PE box. In order to change the moderator geometry, it was possible to insert PE plugs inside the exit hole so as to fill more or less the neutron extraction channel.

Polyethylene moderator (white cube) containing à Be target on which protons of energy 3MeV are sent. The Time of flight detector is set in the back, 8m away from the moderator.

In order to validate the Monte-Carlo simulations inside the moderators, gold disks were positioned at various positions inside the moderator. These gold activation

measurements provide a simple and quantitative way of measuring the thermal neutron flux. The measured activation values have then been compared with the calculated activation values (see Figure 2). The experimental values are in good agreement with the calculated values.

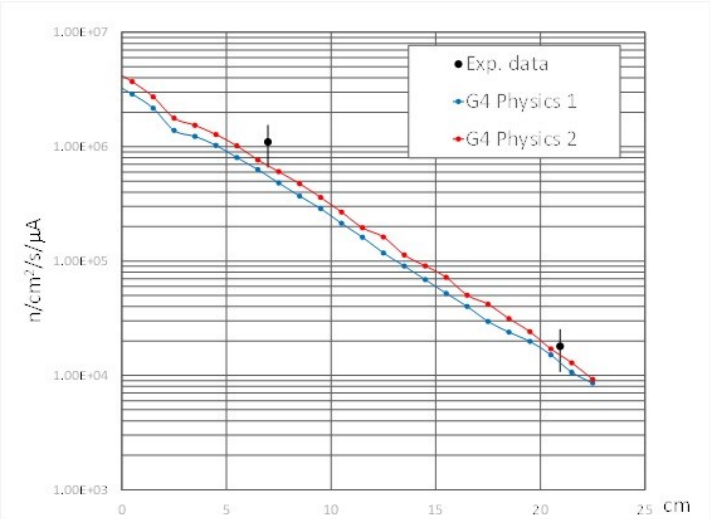

Comparison of the flux measurement (black dots) with two GEANT4 simulations along the neutron beam axis inside the moderator.

In order to measure the neutron pulse shape and the time-of-flight parameters, we used a graphite single crystal. We performed the measurement in a diffraction geometry with the crystal set at 45° with respect to the incident neutron beam. The crystal was installed at 8.4 meters from the source and the detector was set at 90° from the incident neutron beam. Hence it was possible to perform a Time-of-flight diffraction experiment on the (00l) graphite diffraction peaks. Due to the 90° position of the detector, the background noise was significantly reduced compared to a transmission geometry .

The IPHI accelerator was operated for the first time to produce thermal neutrons. Further experiments will be performed to test fast neutron yields and emission anisotropies as well as various thermal and cold moderator geometries. We have already achieved confidence in the Monte-Carlo simulations so that rather reliable new designs can be proposed on the basis on numerical simulations.

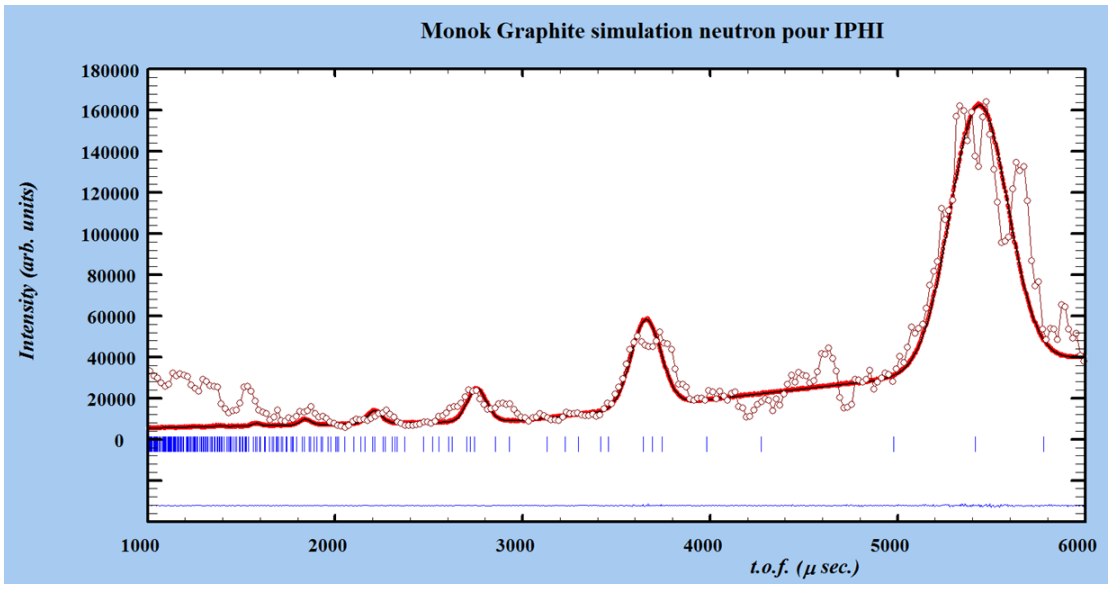

Raw time-of-flight spectra measured on a graphite single crystal and FullProf fit. The pattern was measured at a power of 10W for 15 minutes with a single ^{3}He detector

References

[1] C. Andreani, C-K. Loong and G. Prete, Eur. Phys. J. Plus 131 (2016) 217. DOI: 10.1140/epjp/i2016-16217-1

[2] U. Rücker, T. Cronert, J. Voigt, et al, Eur. Phys. J. Plus 131:19 (2016).DOI 10.1140/epjp/i2016-16019-5

[3] C.M. Lavelle et al, NIM A 587 (2008) 324-341

[4] UCANS, www.ucans.org/facilities.html

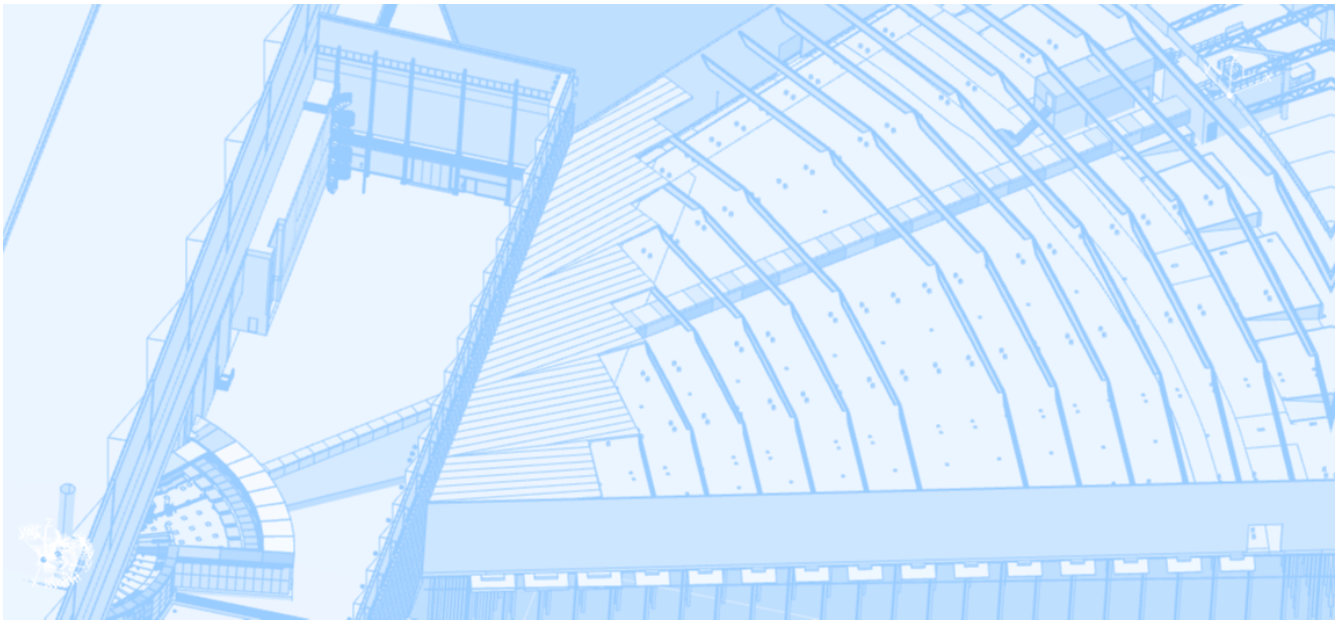

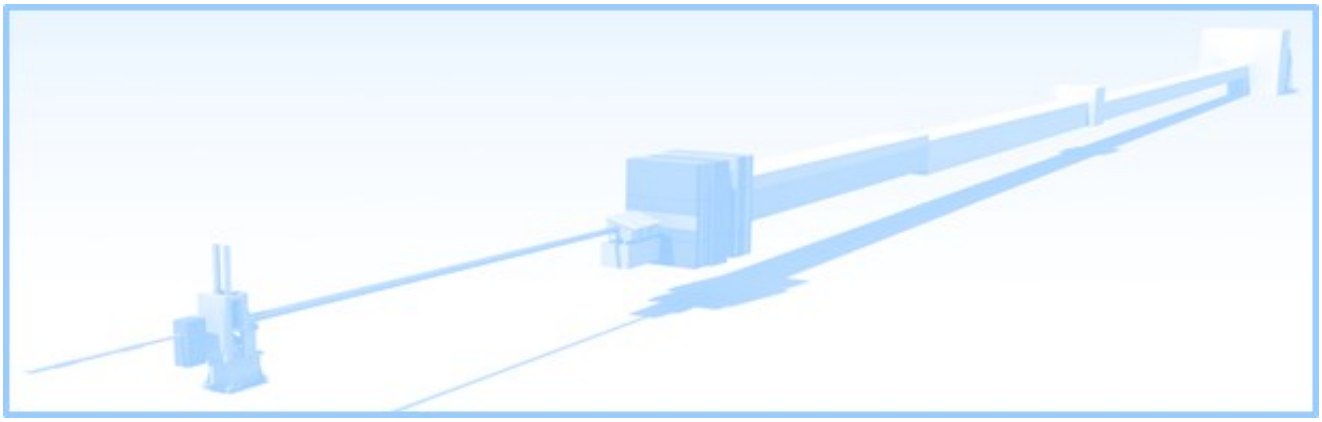

ESS PROJECTS

Instruments construction at the ESS

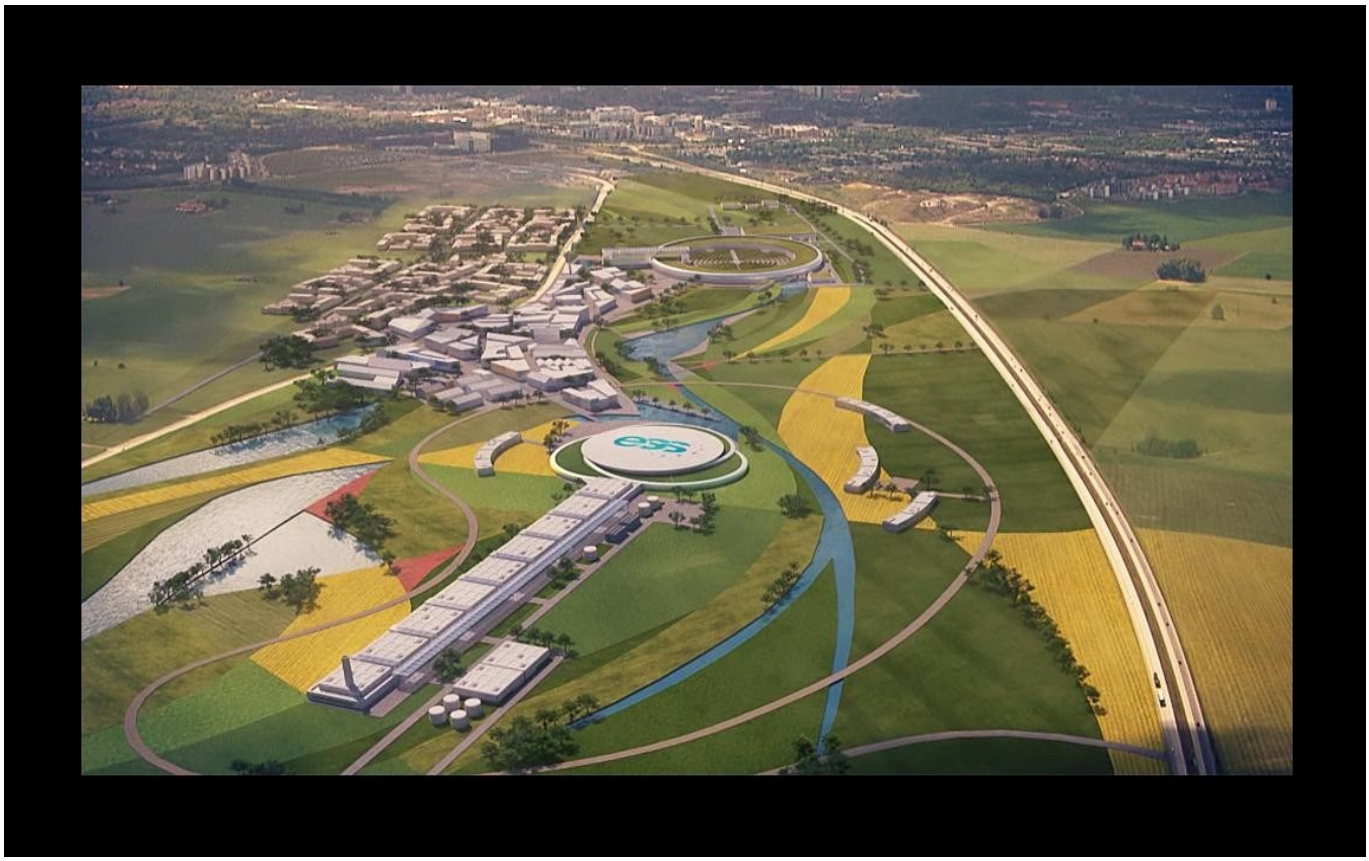

The European Spallation Source (ESS) is currently under construction in the city of Lund, situated in south Sweden just facing the city of Copenhagen. Unlike most of the current European sources, that are based on nuclear reactors (with the notable exception of ISIS and PSI) the ESS uses Spallation for neutron production. A beam of protons is accelerated to high energies (nominally 2 Gev) and sends on a heavy metal target made of tungsten. The proton beam loses its energy in the target, producing a large number of neutrons at each collision. Whereas the previous spallation sources over the world use short proton pulses of ~100 ms at frequencies of ~50Hz, the ESS is a long pulse source (2.86 ms / 14 Hz). The time structure of the neutron flux—combined with innovative instrumentation—should generate dramatic performance gains of several orders of magnitude with respect to existing sources.

The instruments are constructed by the different partners of the ESS through in-kind contributions. The first 15 instruments were selected in 2014-2015 followed by a preliminary design phase (Phase 1) that lead to a common agreement of the instrument definition and costs (Scope Setting Meeting) in 2016 (see table).

For the NSS part (Neutron Science System) of the ESS construction, the ~35 M€ French contribution is managed by the LLB. This contribution is split over the construction of:

- Three diffractometers: SKADI (small angle diffractometer), MAGIC (polarized single-crystal diffractometer, LLB lead partner of the project), DREAM (powder diffractometer);
- Two spectrometers: BIFROST (indirect geometry time-of-flight cold spectrometer) and C-SPEC (direct geometry time of flight cold spectrometer);
- A sample environment package covering the needs of the early ESS suite.

These instruments are all constructed in collaboration with European partner institutes and will be part of the very first instruments completed at ESS. As of today, the first neutrons are expected on the instruments in 2021/2022 corresponding to the switch into the hot commissioning phase. This phase is the last step before opening the instrument to the external user program. Until then, a phased process will take place for design, procurement and installation. The ESS and a board of worldwide scientific and technical experts will review each phase.

	Consortium and fraction	Scope Setting Meeting	Hot Comm. date
SKADI	JCNS (50%), LLB (50%)	06/2016	01/2023
MAGIC	LLB (60% , JCNS (24 %), PSI (16%)	10/2016	02/2022
DREAM	JCNS (75%), LLB (25%)	09/2016	06/2021
BIFROST	KDU/DTU (29.8%), PSI (27.2%), LLB (19.7%), IFE (20.8%), WIGNER (2.5%)	10/2016	06/2022
C-SPEC	TUM (50%), LLB (50%)	10/2016	11/2021

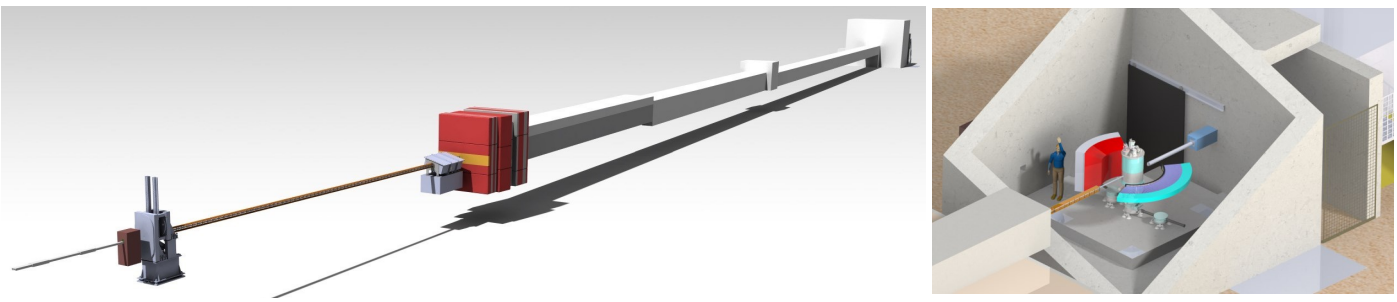

CAD drawing of the preliminary design of diffractometer MAGIC from the first chopper (6 m from the moderator) to the cave (left), one can see in red the bunker wall (28 m) from the moderator in the west hall, and experimental area (right).

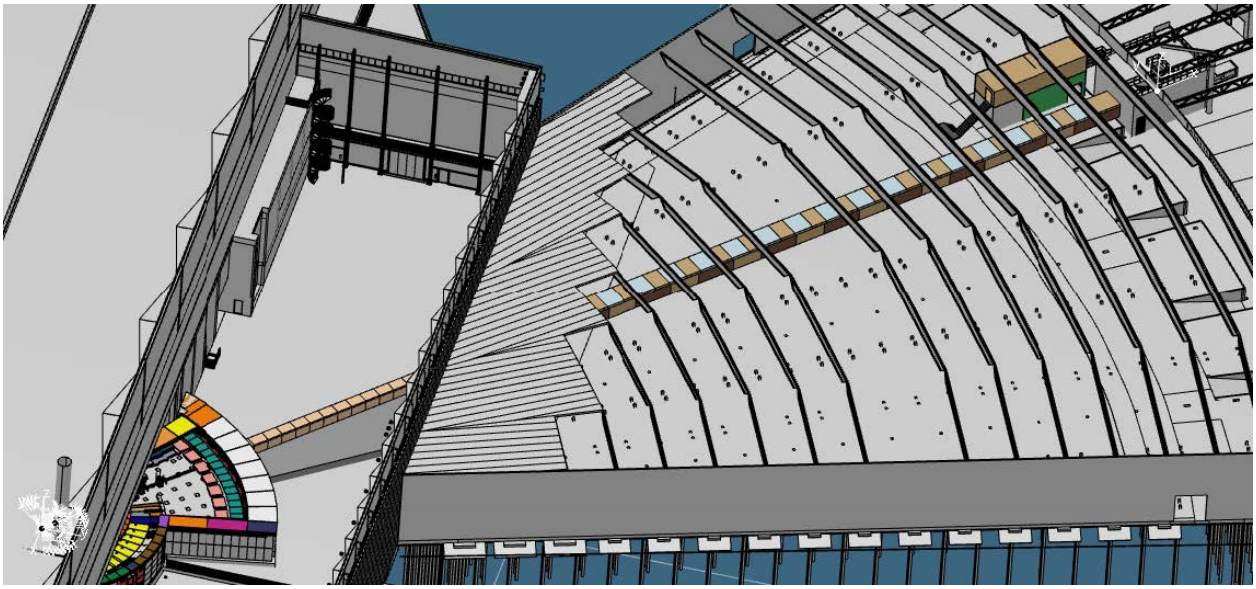

CAD drawing of the complete C-SPEC implantation (west sector W3). Total length of the spectrometer: 160 m from moderator to sample

Acronyms

Acronyms: ESS - European Spallation Source (Lund Sweden), NSS - Neutron Science Systems, JCNS - Juelich Center for Neutron Science (Jülich – Germany), PSI - Paul Sherrer Institute (Villigen Switzerland), KDU - Kolej Damansara Utama (Denmark), DTU - Denmark Technical University (Denmark), TUM - Technical University München


Federation | CNRS | CEA | Contact | Help
phoenix
Neutronics French federation Web portal
Email
Password
Log in
Create an account.
Forgot password?
Copyright © 2016 Laboratoire Léon Brillouin.
Credits | Legals

SOFTWARE DEVELOPMENT

PHOENIX

French Federation for Neutron Scattering web portal

Phoenix application is an online system dedicated to management of proposals on French federation instruments. Developed and established by Laboratoire Léon Brillouin (LLB), Phoenix is intended to centralize the proposals submissions and the on-site reception of scientists. The aim is to gather information related to beam time request on available spectrometers and to guide through administrative steps.

G. Exil, E. Jorgji, E.Eliot, A.Menelle, A.Touze, P. Jégou

Laboratoire Léon Brillouin, CEA, CNRS, Université Paris-Saclay, CEA Saclay 91191 Gif sur Yvette France

Phoenix on-line application is a joint initiative of CEA and CNRS to push forward a single portal aiming at offering open common access to spectrometers implanted in different laboratories.

Phoenix manages presently 26 instruments that are available on Saclay and Grenoble, 21 of which are operated by LLB, powered by reactor Orphée beam-lines and 5 in ILL manage by INAC, LIPHy and Neel Institute.

Main features of Phoenix:

- Experiment proposal management
- Declaration and follow-up of the samples for experiments.
- Users reception management
- Selection committees management
- Proposal calendar
- Instrument calendar
- Users notification system
- Statistics and data export from database

Development of PHOENIX:

The requirement specifications were defined by the LLB direction and the development of PHOENIX was realized with the collaboration of IPSIS, a company member of the IT Link Group. The project was implemented by using the Agile software development method that includes Iterative functional testing with tools like Git and Jira .

Life of the project and staff:

142 working days, 3 months of technical assistance.
Contractor : IPSIS
2 developers + 1 chargé d'affaires
Project management : LLB
2 software engineers
1 system administrator

PHOENIX homepage, https://phoenix.cea.fr

Technologies used

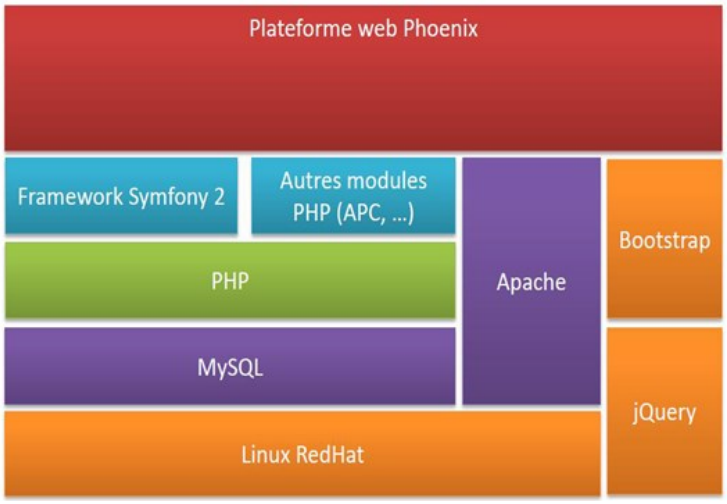

Multiplatform

Windows Linux Mac

Responsive

Suitable for mobile devices

With these technologies, Phoenix provides a modern and robust European web portal for scientists around the world.

The CEA partner platform

CEA offers a platform for webhosting of open internet sites. Phoenix is the second project to use this platform. This ensures the compliance with the French data protection authority demands (CNIL). The security of the entire website is provided by the CEA.

1st deployment for Windows : 27/10/2016

INTERNET opening : 03/03/2017

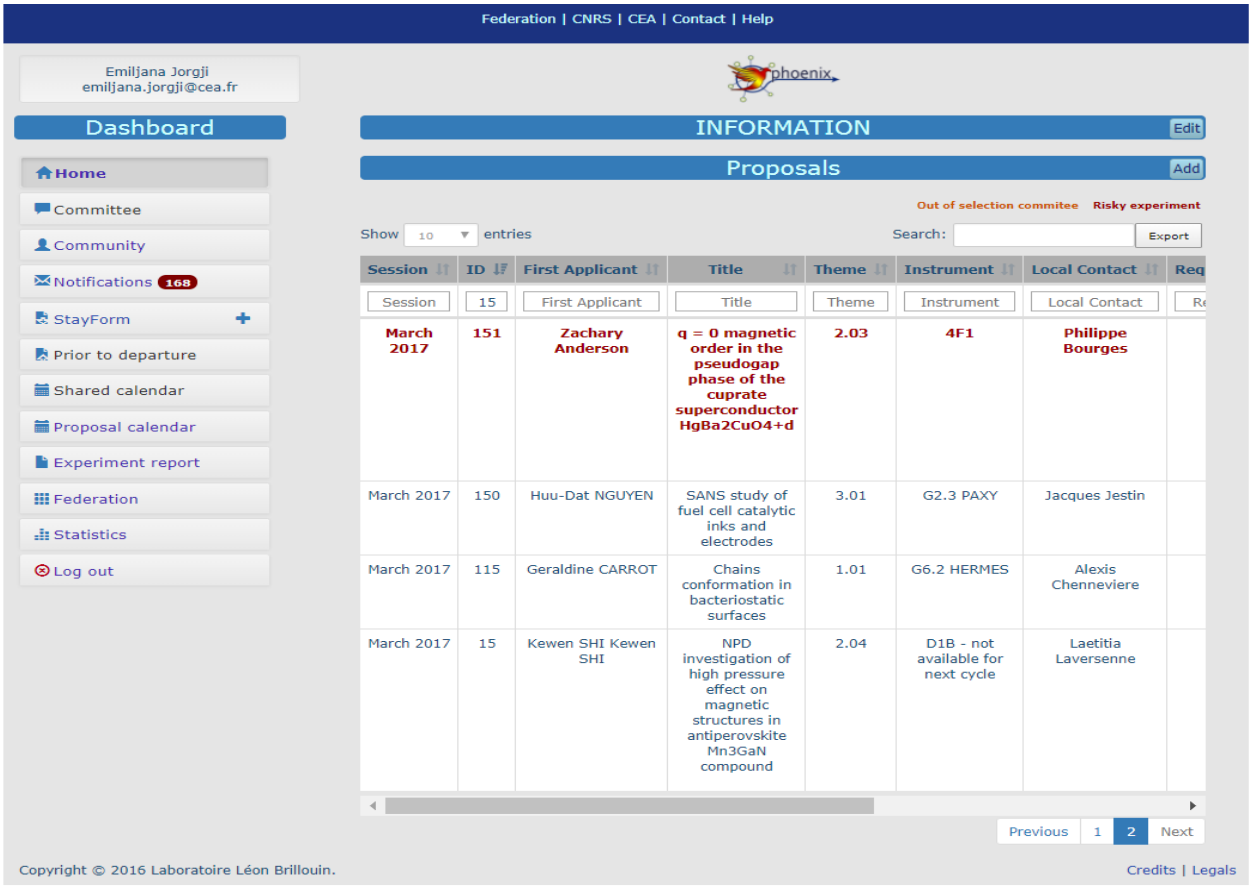

PHOENIX dashboard, proposal management view

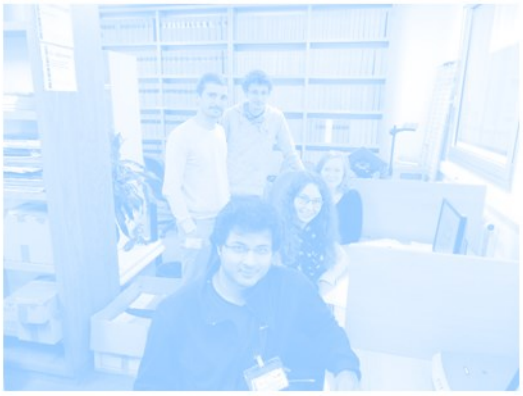

TEACHING AND EDUCATION

FAN of LLB

28th of November

1st of December

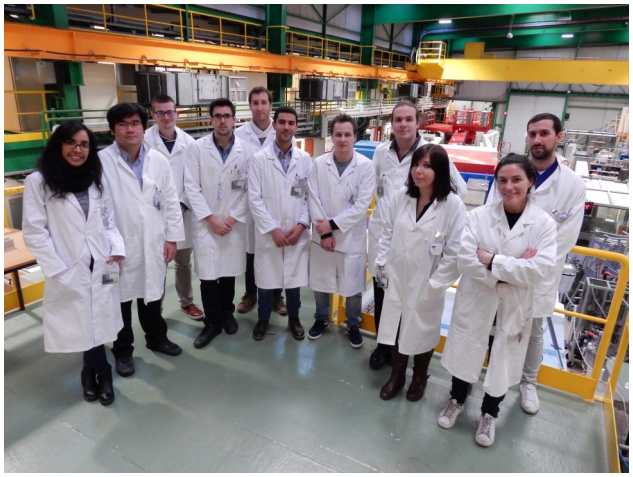

PhDs day the 27th of October

10 PhDs and 4 post-docs have presented their work to the staff of LLB and collaborating researchers during the annual day dedicated to them.

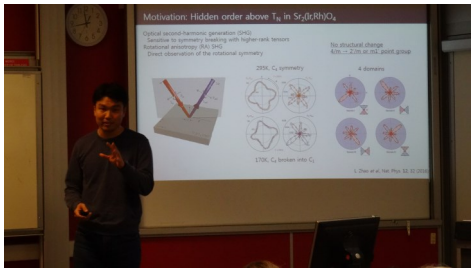

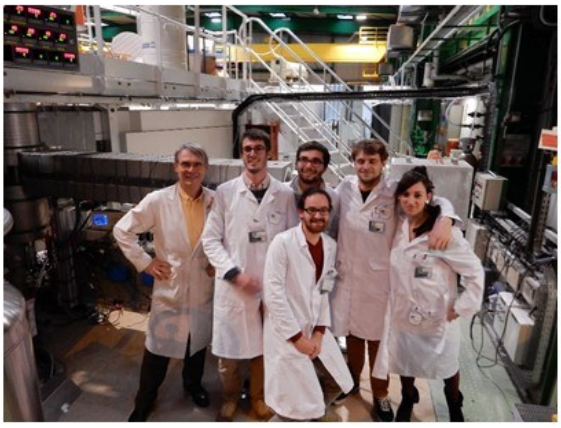

Bordeaux University practical training

Thesis defended in 2016

BLOUZON Camille – 06 January 2016

"Etude des propriétés photoélectriques et magnétiques des parois de domaines multiferroïques"

Directeur de thèse : M. Viret (SPEC) / F. Ott (Material and nanosciences, fundamental studies and applications)

SCUSSAT Simone – 29 April 2016

« Identification des marqueurs repérables par des capteurs spectroscopiques et significatifs des étapes clefs de la cuisson de viande et de poisson »

Directeur de thèse : Philippe CAYOT / Camille LOUPIAC (LLB/Soleil) (soft complex matter and biophysics)

KAHL Philipp- 11 January 2016

« Identification of long range solid correlation in liquids abd role of the fluid/substrate interaction »

Directeur de thèse : L. Noirez (Material and nanosciences, fundamental studies and applications)

SONGVILAY Manila- 29 September 2016

Directeur de thèse : F. Damay-Rowe (Material and nanosciences, fundamental studies and applications)

Beam Time Access

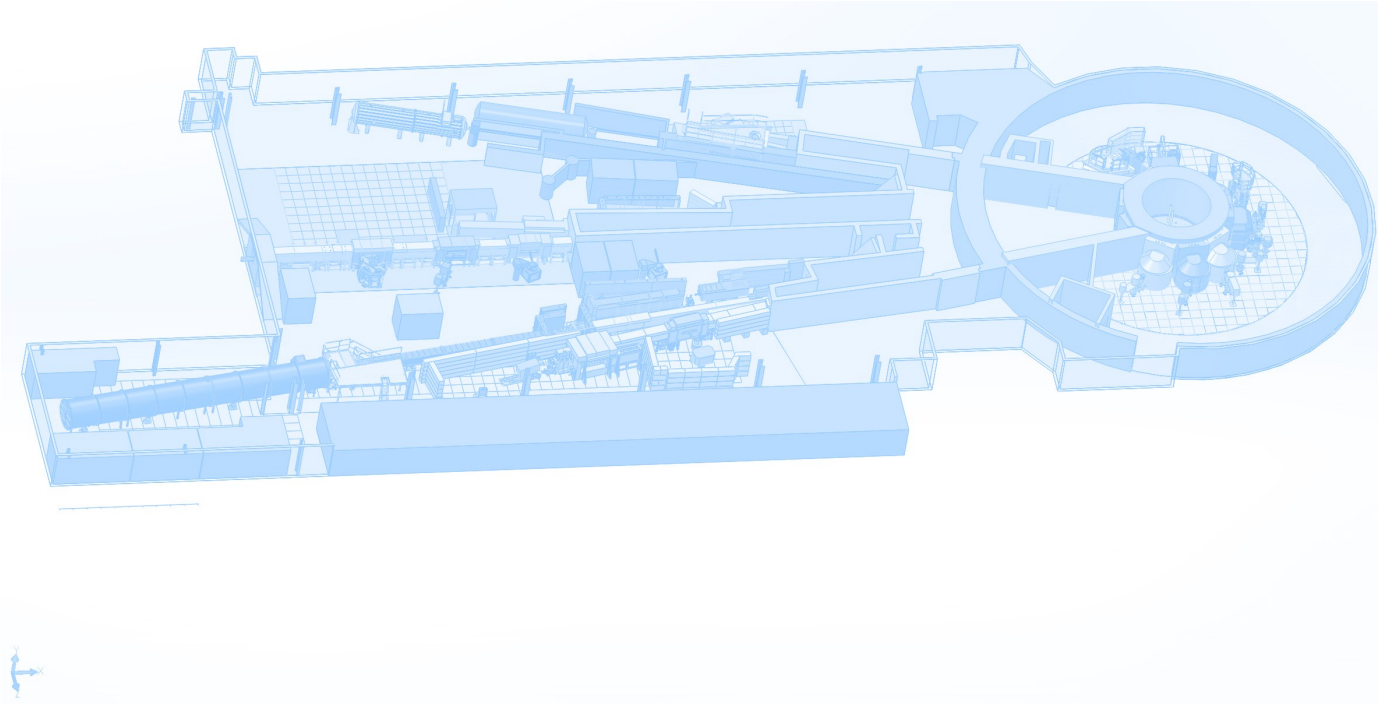

General layout of the spectrometers

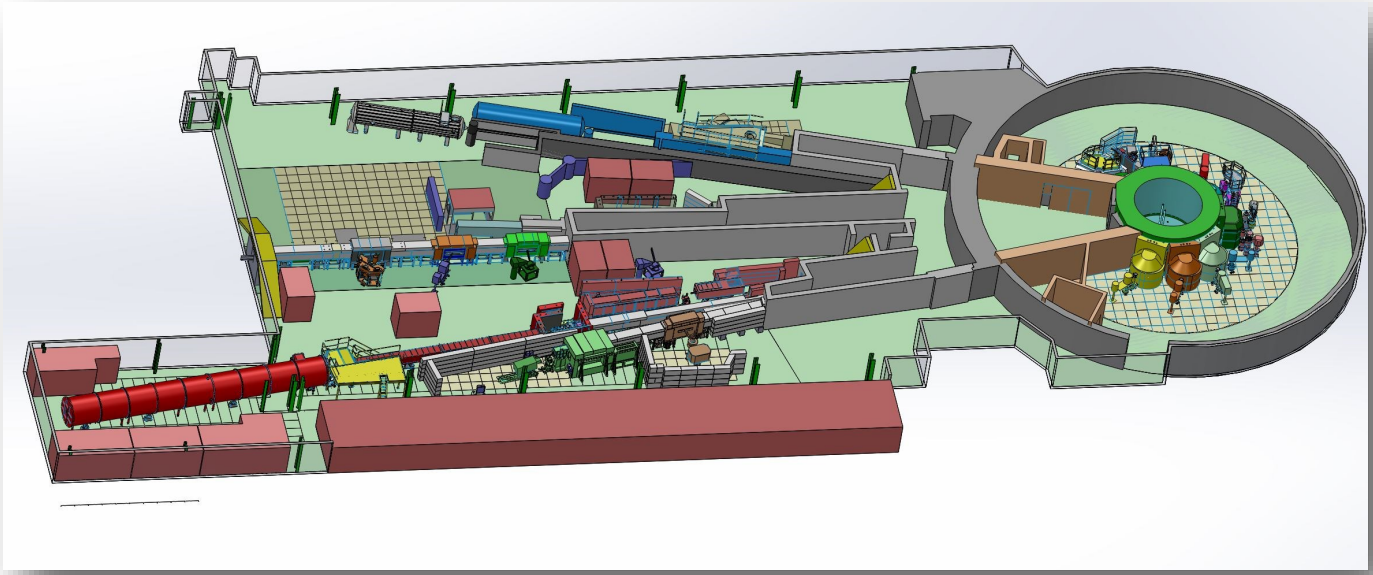

	SPECTROMETERS OPEN TO USERS	CONTACTS
	Powder diffractometers	
3T2	Florence Porcher	florence.porcher@cea.fr
G4.1	Françoise Damay	francoise.damay@cea.fr
G4.4 PHR	Florence Porcher	florence.porcher@cea.fr
G6.1	Florence Porcher	florence.porcher@cea.fr
	Single crystal diffractometers	
5C1 - VIP	Béatrice Gillon	beatrice.gillon@cea.fr
5C2	Alexandre Bataille	alexandre.bataille@cea.fr
Super 6T2	Arsen Goukassov	arsen.goukassov@cea.fr
	Diffuse scattering instrument	
7C2	Jacques Darpentigny	jacques.darpentigny@cea.fr
	Small-angle scattering instruments	
G2.3 - PAXY	Fabrice Cousin	fabrice.cousin@cea.fr
G5.1 - PA20	Gregory Chaboussant	gregory.chaboussant@cea.fr
G5bis - TPA	Annie Brûlet	annie.brulet@cea.fr
	Diffractometers for material science studies	
6T1	Sébastien Gautrot	sebastien.gautrot@cea.fr
	Reflectometers	
G6.2 - HERMES	Didier Lairez / Lay-Theng Lee	didier.lairez@cea.fr / lay-theng.lee@cea.fr
G2.4 - PRISM	Frédéric Ott	frederic.ott@cea.fr
	Triple-axis instruments	
1T	John Paul Castellan (CRG Instrument Karlsruhe/LLB)	john-paul.castellan@cea.fr
2T	Philippe Bourges	philippe.bourges@cea.fr
4F1	Sylvain Petit	sylvain.petit@cea.fr
4F2	Yvan Sidis	yvan.sidis@cea.fr
	Quasi-elastic instruments	
G1bis - MUSES	Stéphane Longeville	stephane.longeville@cea.fr
	Neutron radiography	
G3bis - IMAGINE	Frédéric Ott	frederic.ott@cea.fr

The LLB neutron scattering and imaging instruments

Powder diffractometers

3T2 "Thermal neutrons" 2-axis (50 detectors) high resolution, mainly for nuclear structure determination.

G4.1 "Cold neutrons" 2-axis (multidetector 800 cells) high flux, mainly for magnetic structure determination.

G4.4 "Cold neutrons" 2-axis (70 detectors) high resolution, for structure determination on polycrystalline samples with large unit cell.

G6.1 "Cold neutrons" 2-axis, flat 2D detector with long wavelength and high flux for long period magnetic systems and liquids (Available with limited support) .

Single crystal diffractometers

5C1 "Hot neutrons" 2-axis with lifting arm, polarized neutrons, magnetic field (8 Tesla) for spin-density maps determination

5C2 "Hot neutrons" 4-circle for nuclear structure determination.

6T2 "Thermal neutrons" 2-axis, lifting arm and 4-circles, mainly for magnetic structure determination. 12 Tesla magnetic field available, 2D detector.

Diffuse scattering instruments

7C2 "Hot neutrons" 2-axis (multidetector 640 cells) for local order studies in liquid or amorphous systems. Cryostat and furnace available (1.2K to 1300°C). (Available with limited support)

Small-angle scattering instruments

G2.3 "Cold neutrons" (X-Y detector, 128x128 cells) for study of large scale structures (10 to 500 Å) in anisotropic systems (polymers under stress, metallurgical samples, vortex in superconductors).

G5.1 "Cold neutrons" (X-Y detector, 128x128 cells) for study of large scale structures (10 to 500 Å) in anisotropic systems (polymers under stress, metallurgical samples, vortex in superconductors). PA20.

G5bis Very Small Angle Neutrons Scattering spectrometer

Diffractometers for material science studies

G4.2 "Cold neutrons" 2-axis for internal strain determination in bulk samples . (Available with limited support)

Reflectometers

G6.2 "Cold neutrons" reflectometer operating in time-of-flight mode for multipurpose surface studies.

G2.4 "Cold neutrons" reflectometer with polarized neutrons and polarization analysis for the study of magnetic layers.

Triple-axis instruments

1T "Thermal neutrons" high-flux 3-axis instrument with focussing monochromator and analyser, mainly devoted to phonon dispersion curves measurements. High pressure cells (100 Kbar) available. CRG Instrument operated in collaboration with the KIT Karlsruhe

2T "Thermal neutrons" high-flux spectrometer with focussing monochromator and analyser, mainly devoted to spin-waves and magnetic excitations studies (1.5 to 80 meV).

4F1 **4F2** "Cold neutrons" high flux 3-axis instruments with double monochromator and analyzer, mainly devoted to the study of low-energy (15µeV to 4meV) magnetic excitations. Polarized neutrons and polarization analysis option available.

G4.3 "Cold neutrons" high resolution and low background 3-axis instrument. (Available with limited support)

Quasi-elastic instruments

G1bis "Cold neutrons", high resolution and high flux spin-echo instrument. It can study, in a large Q range, slow dynamics of large molecules in biology or long relaxation times like in glassy transition (Fourier times ~ 20ns)

Imaging

G3bis IMAGINE: Imaging station mainly dedicated to soft matter.

AUXILIARY SERVICES AVAILABLE

Laboratories for sample preparation:

- Chemistry laboratory
- Biological laboratory

Technical help for:

- Cryostat, Furnace (0.1 – 2000 K)
- Medium/High pressures
- High magnetic fields (up to 10 T)
- Mechanics, Cryogenics, *Vacuum*

http://www-llb.cea.fr/fr-en/spectros_p.php

Access to beam time and selection committees

2016 was the first year using PHOENIX for selection committees and beam time access. The joint LLB - CRGs selection committee has been set up in the frame of the new French federation of neutron scattering (2FDN).

Beam time access is free of charge for any experimentalist from the French Scientific community. LLB takes in charge the expenses (travel and stay) of 2 people during the experiment.

Beam time on the open-access spectrometers can be requested by submission of:

- *An experimental application to a Selection Committee (Normal Procedure)*
  This procedure is open to any public/industrial researcher that is interested in using neutron scattering for his research. Results should be suitable for total or partial publication in a Scientific Review.
  USUAL DEADLINE FOR APPLICATION: April 1st and October 1st
  http://www-llb.cea.fr/en/fr-en/proposal.php

- *An experimental application to the Directors (Exceptional)*
  This special procedure should only be used exceptionally for hot topics, confidentiality reasons or if an anomaly in the review procedure is suspected. The delay between the acceptation decision and the realization of the experiment is shortened to the minimum.
  No deadline applies for such propositions (Application all along the year).
  http://www-llb.cea.fr/en/fr-en/proposal.php

- *A fast access application*
  This procedure allows a rapid access (1 to 2 months delay) to the spectrometers in order to perform a short experiment (1 day max.). It can be used for feasibility tests, sample characterization, obtaining complementary results…
  No deadline applies for such propositions (Application all along the year).
  http://www-llb.cea.fr/en/fr-en/prop-rap.php

CONTACT AT LABORATOIRE LEON BRILLOUIN

Laboratoire Léon Brillouin

Scientific Office

CEA SACLAY

Bâtiment 563 *F - 91191 Gif-sur-Yvette Cedex*

Tel. : 33(0) 1 69 08 60 38 *Fax : 33 (0) 1 69 08 82 61*

e-mail : experience-llb at cea.fr

Internet : http://www-llb.cea.fr

rphée
Laboratoire Léon Brillouin

LABORATOIRE LEON BRILLOUIN
UMR 12 CEA-CNRS
CEA Saclay, Bât.563
F-91191 GIF-SUR-YVETTE Cedex
France

+33 (0)1 69 08 52 41
+33 (0)1 69 08 82 61

www-llb-cea.fr